Development of Whole Body Scanning PCR, a highly sensitive method to study the biodistribution of mRNAs, noncoding RNAs and therapeutic oligonucleotides

Inauguraldissertation

zur

Erlangung der Würde eines Doktors der Philosophie

vorgelegt der

Philosophisch-Naturwissenschaftlichen Fakultät

der Universität Basel

von

Julien Alfred Jean-Paul Boos

aus

Straßburg, Elsass (FR)

Basel 2015

Genehmigt von der Philosophisch-Naturwissenschaftlischen Fakultät auf
Antrag von
Prof Dr Nancy Hynes, Dr Iwan Beuvink, Dr Helge Grosshans.

Basel, den 17. September 2013

Dekan: Prof Dr Jörg Schibler

I. Abstract

Based on RNA interference (RNAi), a mechanism regulating gene expression at the post-transcriptional level in eukaryotes, therapeutic siRNAs are slowly moving towards late phase clinical trials. The development of therapeutic oligonucleotides is however paved with many challenges, mostly regarding a mean to deliver siRNAs in a highly tissue-specific manner and to monitor their *in vivo* biodistribution. Two major axes are therefore structuring this thesis, the first one being the development of a method to assess the *in vivo* biodistribution of siRNAs, and the second one aiming at unraveling the possible use of exosomes for tissue-specific delivery.

We first developed an assay compatible with various RT-qPCR assays to assess the biodistribution of oligonucleotides biodistribution in mouse whole body sections. The RT-qPCR signals are converted into an image that represents the *in vivo* biodistribution of the analyzed oligonucleotide. This method, called Whole Body Scanning PCR (WBS-PCR), has been first validated for the detection of tissue-specific or ectopic mRNAs. We subsequently developed an assay to detect miRNAs and siRNAs by RT-qPCR, which was validated with the WBS-PCR for the detection of tissue-specific miRNAs. An *in vivo* study was then performed, aiming at determining the *in vivo* biodistribution of an unformulated siRNA in mouse whole body sections. However, since more and more chemistry is being incorporated in therapeutic oligonucleotides to provide them higher resistance towards nucleases, these oligonucleotides could not be detected anymore by our assay. We therefore designed a novel assay, allowing the detection of highly chemically modified oligonucleotides, which we called Chemical Ligation qPCR (CL-qPCR). The compatibility of CL-qPCR with WBS-PCR was assessed by performing *in vivo* studies using a fully 2'-MOE modified antagomir, an oligonucleotide targeting miR-16-5p.

Having successfully developed a method allowing the rapid determination of the *in vivo* biodistribution of therapeutic oligonucleotides, we focused in the second part of this thesis on assessing the use of exosomes as novel oligonucleotides delivery vehicles.

Although a vast majority of siRNAs in clinical trials are delivered systemically via lipidic nanoparticles (LNP), some concerns have been raised with respect to the difficulty to efficiently design and generate LNPs displaying tissue-specificity and low toxicity. An increasing amount of studies reported that naturally occurring vesicles called exosomes might be involved in inter-cellular communication via the transfer of proteins, mRNAs and miRNAs, suggesting some degree of tissue-specific delivery potential. Moreover, the fact that these exosomes are secreted by cells, and their presence in the circulation indicates that these vesicles might exhibit a low lipid-induced toxicity, made them ideal transporters candidates of therapeutic oligonucleotides. We first investigated ways to efficiently characterize exosomes isolated from cell culture supernatant. An extensive characterization of exosomes was crucial because of the subsequent *in vivo* injections, planned to demonstrate the utility of exosomes as oligonucleotides delivery vehicles. We therefore selected a series of criteria which for us accounted for the presence of exosomes in a sample. These criteria are based on exosomes hallmarks such as particle size, the detection of exosomes-enriched miRNAs, as well as the detection of exosomal proteins. We then focused on the identification of an efficient exosomes isolation method from cell culture supernatant. We therefore compared various methods described in the literature for exosomes isolation, such as the commonly used differential ultracentrifugation, or the recently commercialized ExoQuick kit. We also tested isolation methods based on either particle size segregation, or taking advantage of the virus-like characteristics of exosomes.

None of the samples prepared by using these methods did meet all criterions which could have confirmed the presence of exosomes in the purified cell culture supernatants. However, further characterization of one of the exosomes isolation methods confirmed that cells might not only secrete miRNAs encapsulated in exosomes, but also miRNAs in complex with a member of the RISC complex, namely Ago2.

Although CL-qPCR, in combination with WBS-PCR, would allow the detection and biodistribution of many kinds of unmodified, or heavily chemically modified therapeutic siRNAs, we were unable to demonstrate the use of exosomes as siRNA delivery vehicles.

II. Abbreviations

2'-MOE	2'-O-Methyl-etoxyethyl
2'-Ome	2'-O-Methyl
AD	Alzheimer's disease
ag	Attogram
Ago2	Argonaute protein 2
Alix/PDCD6IP	Programmed cell death 6 interacting protein
AMO	Anti-miRNA oligonucleotide
ASO	Antisense-based oligonucleotide
BPS	BisPhenylSulfonyl
cDNA	Complementary DNA
CL-qPCR	Chemical Ligation qPCR
CSC	Chondroitin Sulfate C
Ct	Threshold cycle
Da	Dalton
DEPC	Diethylpyrocarbonate
DLS	Dynamic Light Scattering
DNA	Deoxyribonucleic acid
ELAVL1	(Embryonic lethal, abnormal vision, Drosophila)-like 1
ESCRT	Endosome sorting complex required for transport
FCS	Fetal Calf Serum
FDA	Food and Drug Administration
fg	Femtogram
GAPDH	Glyceraldehyde-3-phosphate dehydrogenase
HBV	Hepatitis B Virus
HCT-116	Human colon carcinoma cell line
HIV	Human Immunodeficiency Virus
IGFBP1	Insulin-like Growth factor binding protein 1
ISH	In Situ Hybridization
kDA	Kilodalton
Lamp2b	Lysosome associated Protein 2b
LC-MS	Liquid Chromatography-Mass Spectrometry
LNA	Locked Nucleic Acid
LNP	Lipidic Nanoparticle
log	Logarithm
max	Maximum
MBP	Myelin Basic Protein
MHC	Major Histocompatibility Complex
Min	Minute
miRNA	MicroRNA
mL	Milliliter
MODC	Monocyte derived Dendritic Cell
mRNA	Messenger RNA
Mrp4	Multidrug resistance protein 4
MS	Mass Spectrometry
MVB	Multivesicular Body
Myh6	Myosin Heavy chain 6

n.s.	Non-significant
ng	Nanogram
nm	Nanometer
NTC	No Template Control
PBS	Phosphate Buffer Saline
PC	Pachyonichia congenita
PCR	Polymerase Chain Reaction
PEI	Polyethylenimine
pg	Picogram
PO-MOE	PO backbone MOE modified AMO
PS	Phosphorothioate
PSP	Progressive Supranuclear Palsy
PTGS	Post-Transcriptional Gene Silencing
qPCR	Quantitative Polymerase Chain Reaction
QWBA	Quantitative Whole Body Autoradiography
RISC	RNA-induced silencing complex
RNA	Ribonucleic Acid
RNAi	RNA interference
rRNA	Ribosomal RNA
RT	Reverse Transcription
RT-qPCR	Reverse Transcriptase-quantitative Polymerase Chain Reaction
RVG	Rabies Virus Glycoprotein
sem	Standard error of the mean
shRNA	Small hairpin RNA
siRNA	Small interfering RNA
SSB	Sjögren's syndrom b
STDEV	Standard deviation
TCEP	Tris(2-carboxyethyl)phosphine
TEM	Transmission Electronic Microscopy
TFF	Tangential Flow Filtration
TRS	Target Recognition Sequence
µm	Micrometer
V	Volt
WBS	Whole Body Section
WBS-PCR	Whole Body Scanning PCR

III.   Introduction

In an attempt to propose an increasing choice of therapeutic possibilities to cure various diseases, or to at least ease the life of chronically ill patients, pharmaceutical companies invest many efforts in the development of innovative therapeutic means. After the extensive and successful use of small molecule compounds, as well as the development of therapeutic antibodies, pharmaceutical companies started assessing the use of a novel class of therapeutic molecules, namely therapeutic oligonucleotides.

A.   Development of antisense therapeutic oligonucleotides

Since the first mention of the possibility to use oligonucleotides as therapeutic agents against viruses in 1978 ([1],[2]), oligonucleotides have been attributed the potential to drug targets considered as "undruggable" by small molecules ([3]). Although biological activity, intracellular uptake and especially delivery of these oligonucleotides are still major hurdles in the therapeutic oligonucleotides field, many efforts have been invested to overcome these challenges ([4]). The main interest in using oligonucleotides as therapeutic molecules is their ability to hybridize to cellular nucleic acids, being DNA or RNA and to induce nucleic acid degradation, transcriptional or translational arrests. The first class of therapeutic oligonucleotides, called antisense oligonucleotides, were single-stranded DNA molecules which were tested for their potential use in early attempts at slowing down the proliferation of HIV viruses *in vitro* by hybridizing to complementary sites on viral mRNAs ([5]). The development of techniques allowing an automated high-throughput production of oligonucleotides, such as the MerMade automated synthesizers, raised much hope for the therapeutic applicability of these antisense oligonucleotides ([6]). The development of antisense oligonucleotides resulted in early 2013 in the approval by the American Food and Drug Administration (FDA) of Kynamro™, an antisense oligonucleotide produced by Isis Therapeutics ([7]), for the intravenous treatment of inherited hypercholesterolemia. This clearly confirms the potential held by oligonucleotides based drugs, although antisense oligonucleotides are not the only class of potentially therapeutic oligonucleotides. The evidence of a silencing mechanism based on double stranded RNAs in plants ([8]) led to the unraveling of the RNA interference (RNAi) mechanism, also called Post-Transcriptional Gene Silencing (PTGS), as well as to the identification of a population of endogenous regulatory RNAs, called micro RNAs (miRNAs).

B.   MicroRNAs, key elements of the Post-Transcriptional Gene Silencing

MicroRNAs (miRNAs) are a class of endogenously expressed 20 to 25 nucleotides long double-stranded RNA molecules implied in the regulation of protein expression ([9]). The mechanism by which miRNAs have the capability to regulate gene expression is known as Post-Transcriptional Gene Silencing (PTGS) ([10]) (**Fig. 1A**). The production of active miRNAs occurs via the maturation of precursor double-stranded RNA molecules called pri-miRNAs ([11]). The pri-miRNAs are processed by the Microprocessor protein complex composed of Drosha and DGCR8 into a pre-miRNA intermediate. The pre-miRNA is guided to nuclear pores by the Exportin 5 protein and is subsequently exported to the cytoplasm where it undergoes cleavage in active miRNAs by the Dicer protein. The active strand of the miRNA is then loaded in the RNA-Induced Silencing Complex (RISC), and more specifically in the Argonaute 2 protein (Ago2). The single-stranded miRNA loaded in

this activated RISC is now able to fully or only partially bind to complementary sequences on its target messenger RNA(s) (mRNA), inducing mRNA degradation and thus reducing the production rate of the protein encoded by this mRNA.
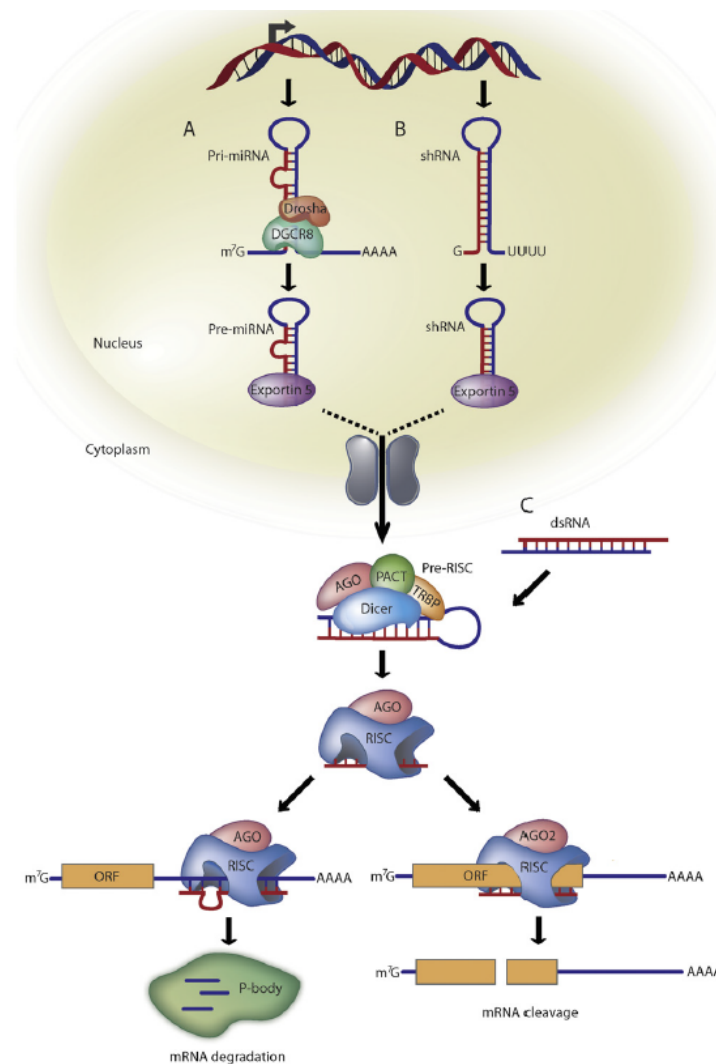
Figure 1: *Post-Transcriptional Gene Silencing (PTGS) mediated by miRNA (**A**), shRNA (**B**) and siRNA (**C**)*

Because of the central role that PTGS plays in protein expression, the deregulation of miRNAs expression can be the trigger for many diseases, such as cancer for example ([12-14]). This predominant role in the control of protein expression offers on the other hand perspectives for the development of new therapeutic compounds ([15]). It would indeed be possible, by using miRNAs mimics to act upstream of the production of a protein, instead of using a small molecule compound targeting a protein. Such a strategy could be beneficial in many disease onsets where a single or a subset of disease-related protein is produced, as in cancers, viral infection, or inherited genetic diseases for example. It has therefore been investigated whether oligonucleotides could be used as therapeutic agents.

C.   Therapeutic action of siRNAs

The first observation of RNAi-induced silencing in animal cells using short small interfering RNA molecules (siRNAs) ([16]) together with the publication of studies showing the higher potency of siRNA molecules over antisense oligonucleotides ([17]), was a trigger for the development of therapeutic siRNAs.

siRNAs, as other regulatory RNAs such as miRNAs, are loaded into the RISC complex with the potential of triggering post-translational silencing ([18]) and therefore inhibit the production of a target protein by either degrading its coding mRNA or by translational repression. siRNAs can be found in two flavors, either genomically expressed as small hairpin RNAs (shRNAs) (**Fig. 1B**) or present in the cytoplasm as functional siRNAs after systemic delivery for example (**Fig. 1C**). Although these strategies sound very appealing, it has to be noted that the non-controlled integration of shRNAs or siRNAs in cells can lead to a saturation of the miRNA machinery by shRNAs and siRNAs, a phenomenon already known for having caused mice death ([19]). The development of siRNAs as therapeutic compounds has to overcome still a few technical and biological hurdles before being able to make them commercially available ([20],[21]), the most important being tissue-specific delivery of siRNAs ([22],[23]). Despite the many challenges faced by the siRNA, several siRNA candidates have already entered clinical studies ([20],[24-27]) (**Table 1**).

Indication	Compound name	Company	Clinical Phase
Age related Macular Degeneration	AGN211745	Merck/Allergan	II
	PF-4253655	Silence Therapeutics/Pfizer/Quark	II
Anti-viral	ALN-RSV	Alnylam	II/III
	Miravirsen	Santaris	II
	ARC-520	Arrowhead Research	I
	TKM-Ebola	Tekmira	I
Diabetic Macular Oedema	PF-04523655	Silence Therapeutics/Pfizer/Quark	II
Hypercholesterolemia	ALN-PCS	Alnylam	I/II
	TKM-ApoB	Tekmira	I/II
	SPC4955	Santaris	I
Non-arteritic Anterior Ischemic Optic Neuropathy	QPI-1007	Quark Pharmaceuticals/BioSpring	I
Ocular pain	SYL1001	Sylentis	II
Oncology	FANG	Gradalis	II
	ALN-VSP	Alnylam	I/II
	Atu027	Silence Therapeutics	I/II
	CEQ508	Marina Biotech	I/II
	CALAA-01	Arrowhead Research	I
	EZN-2968	Santaris	I
	NCT00672542	Duke University	I
	siG12D LODER	Silenseed	I
	TKM-PLK1	Tekmira	I
Open Angle Glaucoma	SYL040012	Sylentis	II
Pachyonychia Congenita	TD101	Pachyonychia Congenita Project/TransDerm	I
Prevention of Delayed Graft Function	QPI-1002	Silence Therapeutics/Novartis/Quark	II
TTRmediated amyloidosis	ALN-TTR02	Alnylam	II
	ALN-TTRsc	Alnylam	I

Table 1: siRNA candidates in clinical trials

As can be seen from the different therapeutic areas targeted by the siRNAs presented in **Table 1**, a major part of the siRNA candidates aim at curing diseases such as inherited genetic diseases ([28]), or cancer ([27]). The tissue-specific delivery of these oligonucleotides

is a major hurdle in the development of this technology, but over the years, many solutions have been tested to overcome this challenge ([29]).

D. Delivery strategies for siRNAs

Although siRNA delivery based on lipidic nanoparticles seems to be the most frequently used delivery method for siRNAs ([30-32]), a variety of other delivery routes has also been investigated. These delivery methods include local injection of siRNAs, conjugation of siRNAs to targeting-peptides, as well as virus-mediated delivery, and encapsulation of siRNAs in exosomes.

D.1. Lipidic Nanoparticles (LNP) mediated delivery of siRNAs

Most of the clinical siRNA candidates are administered via small lipidic nanoparticles (LNP), which are known to allow delivery of siRNAs in tissues ([33]). LNPs are composed of a mixture of positive and neutral lipids and are able to form complexes with the negatively charged siRNAs. Care has however to be taken as to how these LNPs are formed, since LNPs displaying too many positive charges may elicit severe dose-dependent toxic effects ([34]). However, a thorough and careful design of the LNPs used for siRNA delivery, allowed to generate formulations not eliciting severe toxicities, such as the ALN-VSP siRNA from Alnylam ([35],[36]). The lipid composition of the LNPs can also impact the siRNA delivery efficiency to a given tissue, as could already be observed for liver-targeting LNPs ([37],[38]).

D.2. Local injections of siRNAs

An alternative delivery route for siRNA consists in injecting an unformulated siRNA directly in the tissues where its action is required. This strategy has been successfully used in a Phase Ib trial of the TD101 siRNA, aiming at alleviate the symptoms of a rare skin disorder, pachyonichia congenita (PC) ([39]). This siRNA has been designed to selectively target the N171K mutant of the keratin 6a mRNA, responsible for the inherited PC disorder. The scientists who developed this compound adopted a strategy well suited to increase the selectivity of their compound, namely to directly inject siRNA subcutaneously in the callus, an area of thickened skin and accumulation of keratin, characteristic of this disease. The rationale of this strategy is to circumvent the difficulties caused by systemic delivery by injecting the siRNA only where its action is required. Furthermore, in the case of a systemic escape of the siRNA, the absence of any chemical modifications makes it highly sensitive to degradation by nucleases in the circulation ([40]). One pitfall of this delivery method is however the necessity to perform frequent injections, which can furthermore be extremely painful for the patients. Solutions to this problem can however be found, such as applying the siRNA in a nanopatch, an apparently painless way of injection ([41]).
The global applicability of such a strategy is therefore restricted to only a few diseases where subcutaneous injection might be employed.

D.3. siRNAs conjugated to cell-penetrating peptides

Another way of delivering siRNAs to specific sites resides in their coupling to or co-injection with cell penetrating peptides. For the treatment of Hepatitis B virus infection, it was reported that HBV-siRNAs, when coinjected with an hepatocyte-targeting peptide, could successfully reduce the amount of HBV mRNA specifically in hepatocytes ([42]). The use of such peptides has the advantage of being fully biodegradable, lowering any

adverse effects that could occur because of systemic administration. However, these peptides present the disadvantage of potentially raising immune responses ([43]). Another disadvantage of using this kind of delivery vehicle is that the siRNA is fully exposed to the plasma nucleases, requiring to chemically modify the injected siRNA to confer elevated resistance towards nucleases ([40]).

The possibility to design small peptides binding specifically to a tissue-specific receptor, allowing a tissue-specific uptake into only a limited amount of cells, offers many possibilities that can be applied to other delivery routes.

D.4. Virus particles-based delivery of siRNAs and shRNAs

The use of virus particles in RNAi therapeutics has also been evaluated, and the use of adenoviral vector have been shown to be quite successful, at least *in vitro*, in inhibiting the replication of dengue virus in cells ([44]). The use of viral vectors was motivated by the possibility to insert coding sequences with a size up to 1.9 kb in the virus genome, enabling the use of small-hairpin RNAs (shRNA) ([45]). These shRNAs are 50 to 60 bases-long oligonucleotides which are able to form double stranded stem-loop structures after having been transcribed. Since these molecules are similar to pre-miRNAs, they can be processed into active siRNAs by the action of Dicer ([46]), and are therefore able to trigger RISC-driven knock-down. The potential pitfall of this delivery method is however the possibility for the patients to elicit strong immune response, since the majority of the human population is able to recognize adenoviral antigens ([47]).

D.5. Exosomes as siRNA delivery vehicles

Ways to circumvent this hurdle could be found in the use of naturally occurring microvesicles secreted by most cells, called exosomes, in combination with tissue-specific viral targeting peptides ([48]). These vehicles are 80 to 100 nm large lipidic vesicles and are known to be involved in intercellular miRNA trafficking ([49],[50]), designating them as ideal candidates for siRNA transport. Displaying a tissue-targeting viral peptide on exosomal transmembrane proteins might be a way of selecting the tropism of these vehicles and to purposely direct exosomes towards a given tissue or subset of cells presenting the adequate receptor. A mouse *in vivo* study based on this principle has been performed in the Wood group, and was based on the use of a rabies viral glycoprotein (RVG) fused to the exosomal Lysosome associated membrane protein 2b (Lamp2b), in order to direct the exosomes to the brain via systemic delivery ([51]). According to this study, it would be possible to use engineered exosomal vehicles for tissue-specific delivery of siRNAs and to observe gene silencing specifically in the brain. In a broader context, however, the use of such a delivery route could be used to deliver oligonucleotides in a highly specific tissue-specific manner.

IV. Development of Whole-Body Scanning PCR (WBS-PCR), a highly sensitive method to study the biodistribution of mRNAs, noncoding RNAs and therapeutic oligonucleotides

A. Introduction

The successful development of therapeutic oligonucleotides relies on major advances on the delivery, format, and analytical fronts. As discussed previously, several options have been evaluated for the *in vivo* delivery of therapeutic oligonucleotides. However, not only should delivery means be developed for the successful application of therapeutic oligonucleotides, but also reliable analytical methods for their quantification. Over the years, many techniques have been developed and optimized to provide highly sensitive and specific detection of siRNAs in biological samples. Since siRNAs are morphologically very close to miRNAs, it is quite logically that methods based on northern blot, in situ hybridization but also qPCR were assessed first for the quantification of siRNAs ([52],[53]). The use of northern blot for the quantification of siRNAs might however be largely limited by its throughput and the fact that this method is rather time-consuming. In situ Hybridization (ISH) offers the interesting feature of showing high resolution biodistribution data, almost down to subcellular level. Unfortunately, this method is very time-consuming as well, and a given sample can only undergo one round of In situ Hybridization analysis. Many efforts were also invested in using mass spectrometry in order to quantify siRNAs ([54],[55]), however this method still suffers from serious sensitivity problems ([56]). Compared to these methods, RT-qPCR appears to be one of the best methods for the quantification of siRNAs, mainly on account of its high specificity and sensitivity ([57]). However, classical sample preparation methods for *in vivo* tracking of siRNAs require long handling times, both for organs sampling, but also for RNA extraction and purification. There were therefore efforts made in order to track siRNAs *in vivo* by using fluorescently labeled siRNAs ([58]). However, fluorescent labeling of the oligonucleotides to perform *in vivo* biodistribution studies may alter its physic-chemical properties with the danger of modifying its biodistribution properties as well as biological efficacy ([59]). We therefore oriented ourselves towards methods able to detect oligonucleotides in their native form such as RT-qPCR not only on RNA extracted from sampled organs, but in whole body sections, such as the ones generated for Quantitative Whole Body Autoradiography (QWBA) ([60]). Such a method would indeed allow to fairly quickly establish the *in vivo* biodistribution pattern of a therapeutic oligonucleotide combined to various delivery vehicles and to therefore allow a direct comparison of different delivery methods. This is why we developed a method called Whole-Body Scanning PCR (WBS-PCR) allowing the quantification of various RNA and DNA based molecules by qPCR-based techniques ([61]). To achieve this, we first had to demonstrate whether it was possible to generate *in vivo* biodistribution patterns of known tissue-specific mRNAs. This is indeed a crucial step to evaluate the highest resolution achievable by this method and to confirm its specificity. We subsequently had to develop a RT-qPCR method capable of detecting short oligonucleotides such as miRNAs and siRNAs, with high specificity and high sensitivity.

An additional challenge resides in the increasing amount of chemical modifications such as 2'-fluoro, 2'-O-methyl, 2'-O-methyl-etoxyethyl (2'-MOE) (**Fig. 2**) that are developed and incorporated in therapeutic oligonucleotides ([62]) to increase their pharmacokinetic properties as well as their resistance towards nucleases ([40],[63]). These modifications have the disadvantage of making oligonucleotides incompatible with enzyme-based detection methods, such as PCR for example ([61]). Consequently, we aimed at developing a qPCR-

based method for the detection of heavily chemically modified oligonucleotides such as antagomirs, small oligonucleotide capable of binding specifically to a miRNA and to sequester it away from its biological targets.
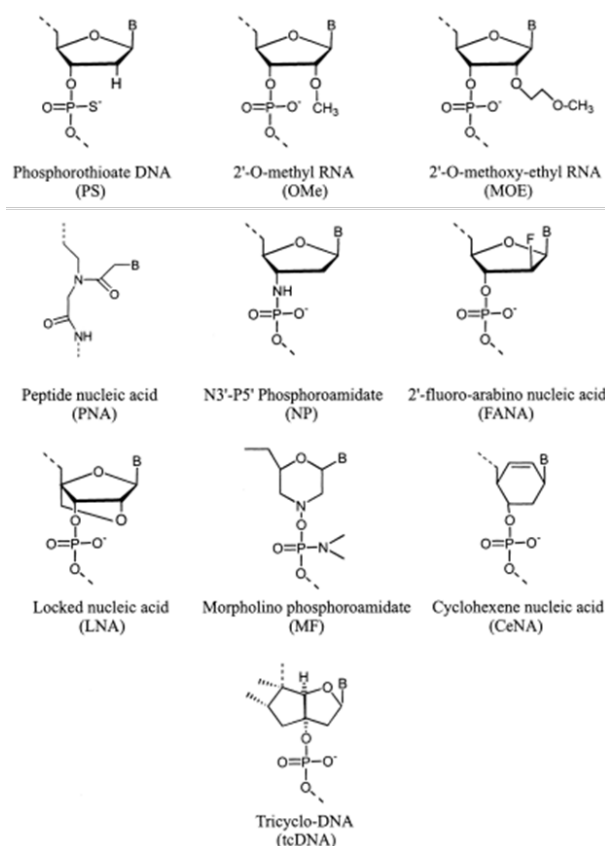
Figure 2: Chemical modifications applied to oligonucleotides and nucleotides analog used for research or therapeutic applications

In this chapter, we will discuss the development of the Whole Body Scanning PCR method, and investigate the applicability of this method for the detection of various coding, noncoding, and heavily chemically modified oligonucleotides.

B.   Validation of the Whole Body Scanning PCR on messenger RNAs

The efficient purification of various nucleic acids such as mRNAs, miRNAs, siRNAs, antagomirs, but also genomic DNA can be quite challenging because of the physic-chemical properties of these molecules. Many kits are commercially available to efficiently purify a specific subset of nucleic acids, taking advantage of their properties such as size or hydrophilicity. In the case of Whole Body Scanning PCR however, we had the need for an extraction method allowing efficient extraction of all these different nucleic acids, from short miRNAs to genomic DNA. This is a crucial feature especially in the case of sagittal whole body sections (**Fig. 3**), since not only must the lysis buffer be able to isolate any nucleic acid material, but it also has to be able to extract material evenly across various tissues. We therefore investigated the possibility to use a lysis buffer without the need of any additional purification step which could have led to a bias in the nucleic acid population extracted from cells. Various methods have been developed for RNA extraction, however the RNA population obtained can vary depending on the method used, some favoring miRNAs, whereas other favor large RNAs (64).
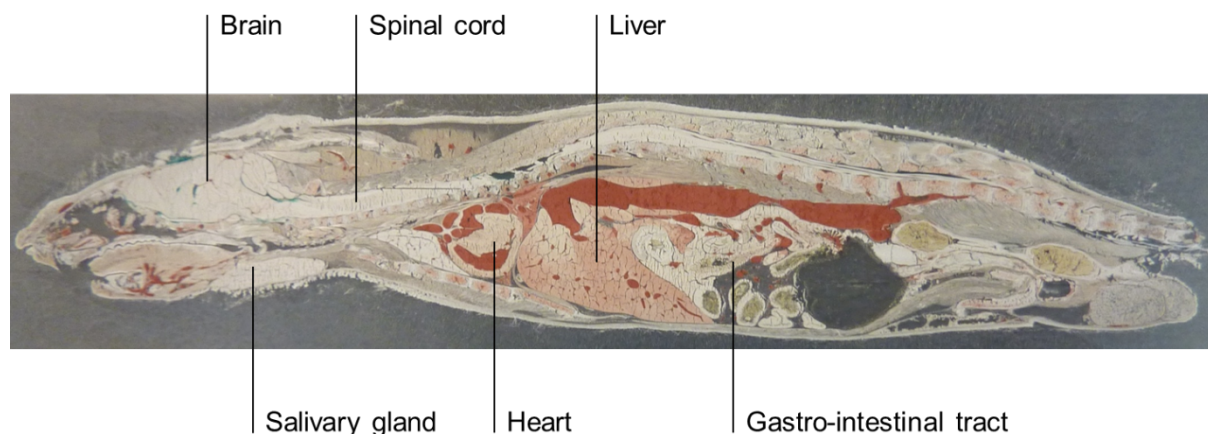
Figure 3: Whole body section typically used in QWBA and Whole Body Scanning PCR experiments

The first advantage of such a method is to allow a very quick sample preparation since once the tissues are lysed, they do not require to undergo additional extraction or purification steps, and an additional advantage of such an approach is the capability to detect genomic signals allowing "per-cell" signal normalization since there are only two genomic copies of each gene per cell (**see section IV.B.2.b**). We can therefore establish a direct link between genomic signals and cell count, thus enabling to correct for the different extraction efficiencies and cell density variations encountered on a whole mouse cross-section ([65](#)). It therefore also enables to compare relative expression signals of an RNA target between different mouse sections. These lysis buffers, on the other hand, might interfere with enzymatic reactions on account of their high salt concentrations and of the protein denaturants and chelating agents they contain. The sensitivity offered by RT-qPCR can nevertheless be used to overcome this disadvantage, since a single dilution step may be sufficient to dilute out the inhibitory components of the lysis buffers. In order to identify the lysis best suited to our needs, we quantified the same RNA target in samples prepared using three different lysis buffers and comparing the signal intensities obtained, as well as the dilution factor that had to be applied to the lysates to allow compatibility with RT-qPCR. From the various lysis buffers tested, the OTX Lysis Buffer supplemented with TCEP, a buffer originally designed for the extraction of oligonucleotides from biological samples for LC-MS analysis, was in our hands the most compatible with RT-qPCR. The reason why this buffer was supplemented with TCEP was because of its ability to reduce disulfide bonds, therefore inactivating the nucleases present in the samples, an important feature for the samples conservation. Since this compound is able to inhibit nucleases, it is also capable of inhibiting the enzymes required for RT-qPCR amplification, hence the need to first validate the use of this buffer on mouse tissues prior to testing it on whole body sections.

B.1. Validation of the sample preparation procedure on tissues

To assess the efficiency of our sample preparation method, we subjected various tissues to total RNA extraction using the classical Trizol method and prepared as well tissues lysates using the OTX Lysis Buffer supplemented with TCEP. A small panel of tissues was selected, including soft tissues such as brain and liver, but also more fibrous tissues like heart and skeletal muscles.
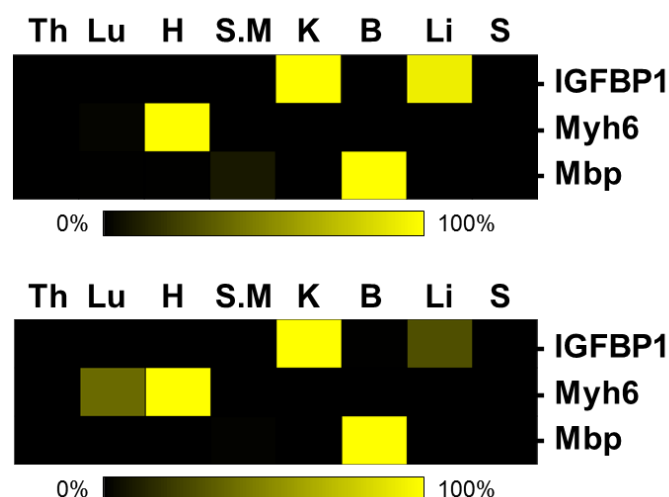
Figure 4: *Detection of tissue-specific mRNAs in total RNA purified with Trizol (**a**) and in tissue lysates prepared with OTX Lysis Buffer (**b**). The expression of Insulin-Like Growth Factor Binding Protein 1 (IGFBP1), Myosin Heavy Chain 6 (Myh6) and Myelin Basic Protein (Mbp) was investigated in Thymus (**Th**), Lung (**Lu**), Heart (**H**), Skeletal Muscle (**S.M.**), Kidney (**K**), Brain (**B**), Liver (**Li**), Spleen (**S**) and Spinal cord (**S.c.**)*

We compared both sample preparation methods by investigating the relative expression signals obtained for three well-characterized tissue-enriched mRNAs, namely Insulin-Like Growth Factor Binding Protein 1 (IGFBP1), Myosin Heavy Chain 6 (Myh6) and Myelin Basic Protein (Mbp). All signals are shown as % relative expressions where 100% corresponds to the highest signal detected for each gene. Relative expression signals obtained from RNA samples were normalized against 18S rRNA, whereas signals obtained in tissue lysates were normalized against genomic 18S. Although data were normalized using different methods, both the RNA samples (**Fig. 4a**) and tissue lysates (**Fig. 4b**) displayed similar results confirming the expression of IGFBP1 in liver and kidney (66), the heart-specific expression of Myh6 (67) and the detection of Mbp in the brain (68). Surprisingly, we could observe a small difference in IGFBP1 levels in liver. Although the IGFBP1 relative expression in liver total RNA is highly similar to the IGFBP1 relative expression obtained in kidney, there is a non-negligible difference in IGFBP1 levels between kidney and liver tissue lysates. This difference can be due to the fact that the samples used for RT-qPCRs performed on total RNAs are all set to the same RNA concentration and normalized using 18S rRNA relative expression, whereas in the case of tissue lysates, the data only undergoes the normalization using 18S rRNA relative expression.

Taken together, this result confirmed the possibility to detect endogenous mRNAs in samples prepared with OTX Lysis Buffer.

B.2. Detection of messenger RNAs in mouse whole body sections

The concept of the whole-body-scanning PCR is to be able, in one single PCR run, to establish the *in vivo* biodistribution pattern of a target RNA molecule, or any therapeutic oligonucleotide available. Such a concept was already established to monitor the biodistribution of radioactively labeled compounds in a method called Quantitative Whole-Body Autoradiography (23). However in the case of WBS-PCR, it would be possible to monitor the biodistribution of any oligonucleotide detectable by PCR-based techniques.

Briefly, the whole-body-scanning PCR makes use of 40 µm mouse sagittal cross-sections, typically used in QWBA studies, overlaid on a 1536-well plate filled with OTX Lysis Buffer

supplemented with TCEP, since it was previously demonstrated that OTX Lysis buffer was suited for the analysis of mRNAs biodistribution patterns. The plate was subsequently sealed and inverted a few times, allowing a very local lysis. The plate was then centrifuged in order to collect the lysates at the bottom of the plate. Transfer of the lysates to a 384-well plate and their dilution in RNase-free water made the lysates ready for downstream PCR analyses. The resolution offered by WBS-PCR is therefore dictated by the size of the lysis plate, which is in our case a 1536-well plate. In order to determine whether this resolution is sufficient to observe tissue-specific expression patterns, we performed WBS-PCRs showing the biodistribution of the same set of tissue-specific mRNAs tested previously on tissue lysates and total RNA.

B.2.a) Conversion of qPCR signals to overlaid heat maps
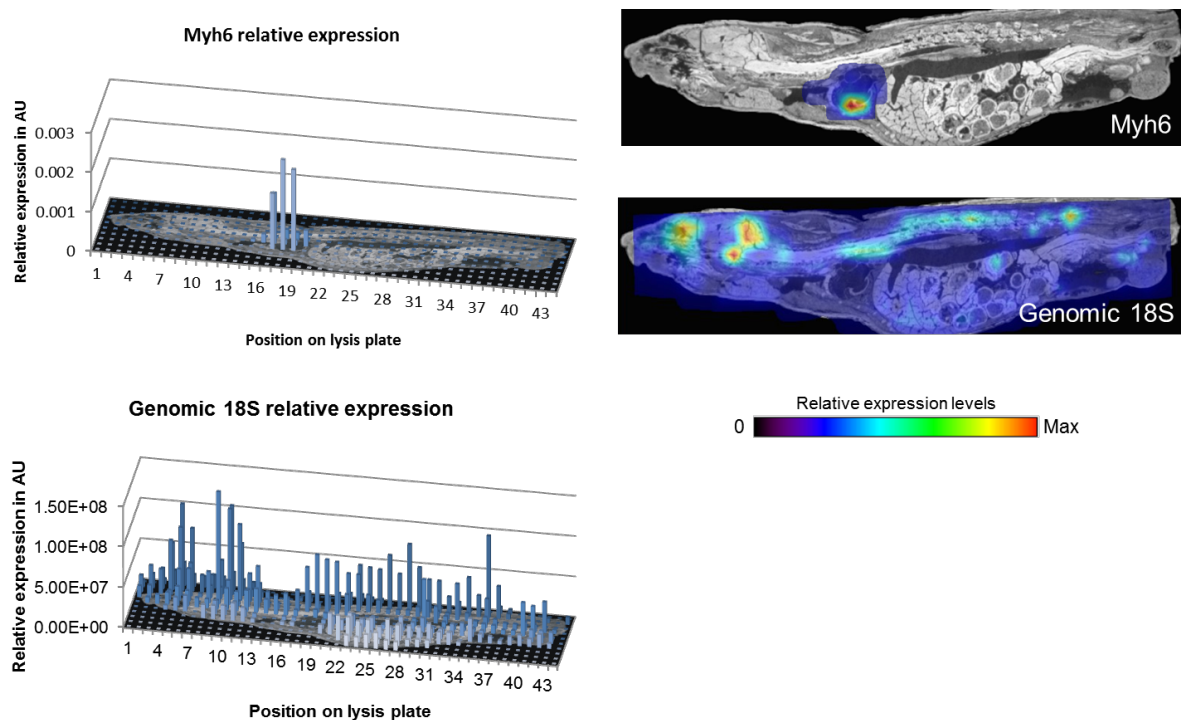
*Figure 5: Comparison of two visualization strategies for WBS-PCR results. Relative expression data obtained using WBS-PCR were depicted using either a 3-D bar graph representation (**a**) or using the TissueView™ imaging software (**b**)*

Visualization of the results obtained by WBS-PCR was an important step in the development of the WBS-PCR method. It was crucial to identify a visualization method allowing to clearly visualize the biodistribution of an oligonucleotide in a mouse section. We therefore tested two imaging methods using the relative expression of Myh6 and genomic 18S. The first method makes use of a 3-D bar graph overlaid on a picture of the analyzed mouse section (**Fig. 5a**). In the case of a localized expression pattern such as the one obtained for the heart-specific Myh6 (**Fig. 5a, upper panel**) the 3-D bar graph representation allows a clear visualization of the relative expression data. However, for a broader expression pattern, such as the one obtained for genomic 18S for example (**Fig. 5a, lower panel**) the 3-D bar graph representation makes it difficult to appreciate and thoroughly analyze the obtained data. We therefore tested a second method using an MS-data imaging software known as TissueView™ (69,70) to display relative expression signals obtained by WBS-PCR (**Fig. 4b**). In order to generate these images, data analyzed in a spreadsheet software was converted into a heat map, in a format compatible with the TissueView™ software. This heat map was subsequently overlaid on a picture of the

20

analyzed mouse section using the coregistration function of the imaging software allowing a precise alignment of the heat map on the section picture. The resulting images show a much clearer expression pattern, especially because of the conversion of the data into heat maps. It is indeed difficult to appreciate variations in signal intensity on a 3-D bar graph since high values in a 3-D bar graph can hide lower data points. The Myh6 expression pattern shows in the case of an image generated by TissueView™ a strong colocalization with the heart region (**Fig. 5b, upper panel**) which could not be fully appreciated on the 3-D bar graph depiction. For the same reasons it is also easier to appreciate the variations of signal intensity in the uniform biodistribution pattern obtained for genomic 18S (**Fig. 5b, middle panel**).

We therefore decided to depict every biodistribution pattern obtained by WBS-PCR by using the TissueView™ software.

B.2.b) Genomic 18S versus 18S ribosomal RNA correction

Since a mouse whole body section displays different cell densities and tissue organization between various organs, we had to identify a normalization method able to account for these variations across the section. A common method used to normalize RT-qPCR data is by using 18S rRNA as a normalizer, since the 18S rRNA levels reflect the RNA amounts present in a sample ([71](71)). Although this method is widely accepted among the scientific community, some authors contest the validity of using 18S rRNA alone as a normalizer, since the level of ribosomal RNA may vary between various tissues ([72](72)). It is therefore recommended to use a dozen housekeeping genes for accurate normalization ([73](73),[74](74)). The quantification of a dozen of housekeeping genes would be impractical since that would interfere with the desired utility of the WBS-PCR to provide quickly biodistribution data. We therefore adopted another method for RT-qPCR normalization. Interestingly, it was also reported that normalization using genomic sequences can be used to absolutely quantify transcripts, and in our case therapeutic oligonucleotides as well ([75](75)). We therefore conducted a study comparing two normalization methods, one based on 18S rRNA and one making use of the 18S genomic DNA copies available in the lysates (**Fig. 6**).

We quantified two target RNAs by WBS-PCR, namely Myh6 and miR-16-5p (**see section IV.C.1.a**), and normalized the obtained expression data using either 18S rRNA or genomic 18S. The expression patterns obtained for both 18S rRNA and genomic 18S show a broad coverage of the mouse section (**Fig. 6a**). Interestingly, areas such as brain, olfactory bulb, spinal cord and liver showing high amounts of 18S rRNA display high levels of genomic 18S as well. This can be explained by the fact that tissues with high cell density display high DNA and RNA levels. Despite these similarities, the 18S rRNA data seems to be not as uniform across the section as the 18S genomic data, since the region corresponding to the gastro-intestinal tract show surprisingly low signals compared to surrounding areas. In order to identify the best normalizer, we measured miR-16-5p (**Fig. 6b**) and Myh6 (**Fig. 6c**) levels in the section. The miR-16-5p biodistribution pattern was highly affected by the normalizer used. Indeed, the uncorrected miR-16-5p data (**Fig. 6b, upper panel**) shows high miR-16-5p amounts in the brain, heart, spinal cord, and blood vessel. The 18S rRNA corrected data on the contrary, showed no miR-16-5p in the brain, and overall low signals across the section. Moreover, a high signal peak could be observed in the gastro-intestinal tract, therefore leading to a completely distorted biodistribution pattern compared to the non-normalized data (**Fig. 6b, middle panel**). This distortion is mainly due to the fact that the 18S rRNA expression levels show high variations across the section, therefore exacerbating the signal variations during normalization. The genomic 18S corrected data

on the other hand, showed a uniform expression pattern across the section with slightly elevated levels in the brain, spinal cord, heart and gastro-intestinal tract (**Fig. 6b, lower panel**). This corrected dataset reflects best the miR-16-5p biodistribution pattern than the 18S rRNA biodistribution pattern. The normalizer used to correct the Myh6 mRNA data, on the other hand, did not result in similar data distortions as could be observed for the miR-16-5p data. The highly heart-localized expression data showed indeed similar results, independent of the normalizer used (**Fig. 6c**).
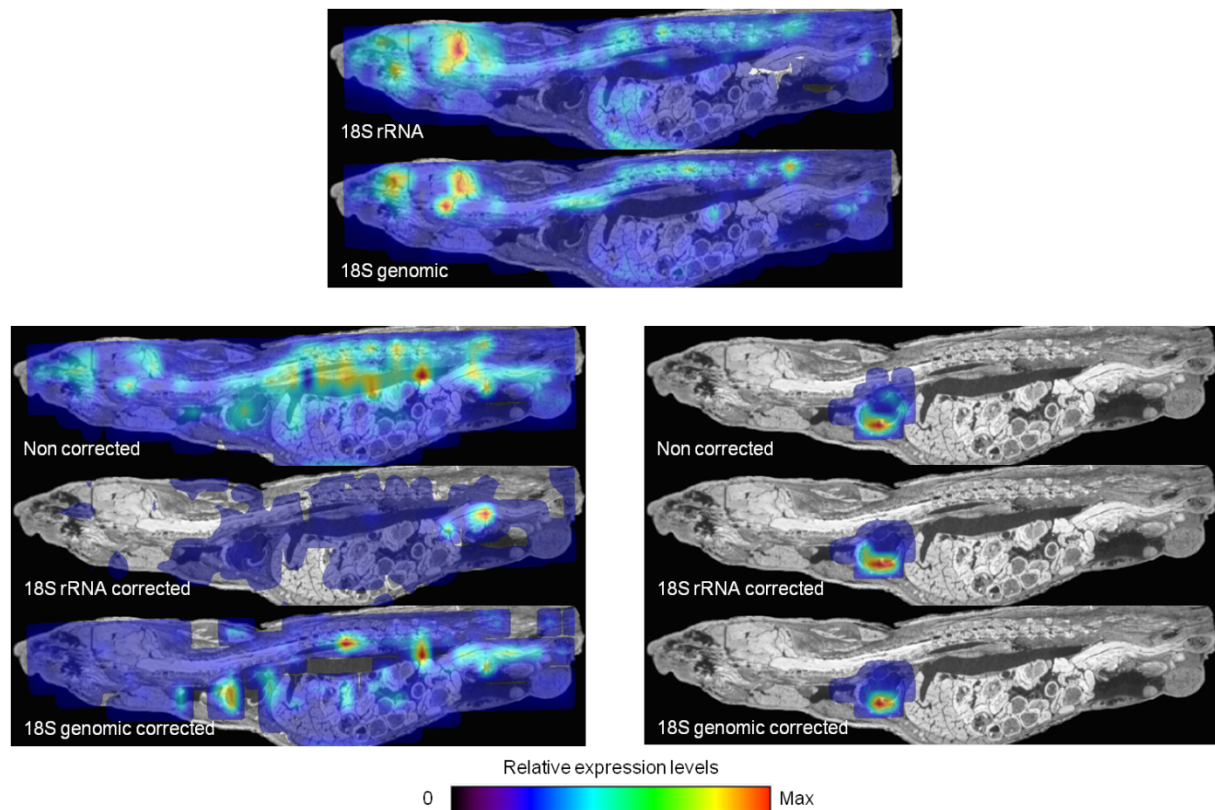
Figure 6: Impact of the normalization method on biodistribution data. Biodistribution pattern of genomic and RNA 18S (a) used for the normalization of miR-16-5p (b) or Myh6 (c) expression data

This study shows that the choice of the normalizer is crucial for efficient data correction. However, it could also be observed that genes showing a broad expression pattern are more prone to distortions compared to genes displaying a highly localized expression pattern when using a non-optimal normalizer such as 18S rRNA for example. This is especially important for the biodistribution pattern of a therapeutic oligonucleotide, which might not display a uniform biodistribution. In such cases, a non-uniformly expressed normalizer can distort the biodistribution, such as showing "artificially" highly elevated signals in regions where the normalizer is only dimly expressed. We therefore decided to use genomic 18S as a normalizer in the rest of these studies.

B.2.c) Detection of endogenous tissue-specific mRNAs

The first step of the validation of the WBS-PCR method consisted in confirming the tissue-specific expression pattern of tissue-specific mRNAs previously tested on a panel of tissues.

Genomic 18S relative expression was measured and was used to assess the extraction efficiency of the lysis of the section (**Fig. 7a, lower panel**). An overall homogeneous biodistribution pattern was observed across the section with elevated genomic 18S levels

in brain and along the spinal cord. These higher signals could either indicate regions with higher cell densities, or regions displaying better extraction efficiencies. In order to take these variations in account during gene expression analysis, relative expression signals obtained for each mRNA were normalized against genomic 18S signals. mRNAs biodistribution patterns (**Fig. 7a, upper panels**), in contrast to genomic 18S signals, did not result in a homogenous expression across the section, but to tissue-specific expression patterns corroborating the expression patterns obtained in tissue lysates (**Fig. 4b**). We could indeed observe that IGFBP1 mRNA expression pattern co-localized with liver, while the Myh6 mRNA signals co-localized with the region of the heart. Unfortunately, there were no kidney tissues on this section, that is why we could detect IGFBP1 only in liver. Interestingly we could detect Mbp mRNA not only in brain, but also in regions along the spinal cord, as could already be seen on total RNA purified from tissues (**Fig. 7b**).
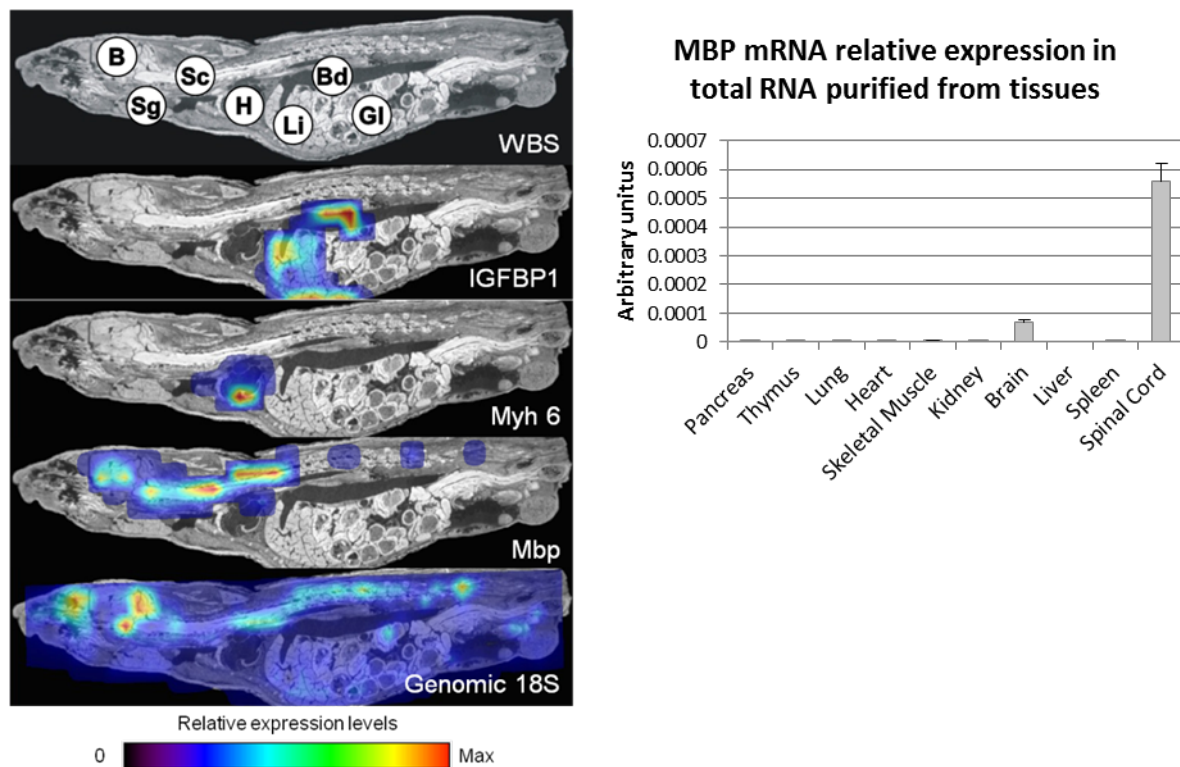
Figure 7: Biodistribution of tissue-specific endogenous coding mRNAs determined by WBS-PCR. (a) Relative expression data obtained by WBS-PCR for IGFBP1, Myh6, and Mbp mRNAs. Major organs and tissues were indicated such as brain (B), spinal cord (Sc), salivary gland (Sg), heart (H), liver (Li), blood vessel (Bd) and gastro-intestinal tract (GI). (b) Relative expression of the MBP mRNA in total RNA purified from tissues. Values are averages of quadruplicate measurements. Error bars, STDEV (n=4)

Taken together, these data suggest that the sample preparation based on the use of OTX Lysis buffer supplemented with TCEP is compatible with WBS-PCR. Furthermore, the resolution offered by the 1536-well lysis plate was sufficient to visualize the biodistribution pattern of a small panel of tissue-specific mRNAs.

B.2.d) Detection of ectopic human mRNAs

In order to further characterize the resolution level that can be achieved using WSB-PCR for the biodistribution of RNAs, we visualized the human-specific mRNAs expressed by a human colorectal carcinoma HCT-116 tumor grown subcutaneously in a mouse model. We

therefore performed WBS-PCR against human ELAVL1 mRNA (embryonic lethal, abnormal vision, Drosophila-like 1), human Actb (Beta-actin) and GAPDH mRNA (Glyceraldehyde-3-Phosphate Dehydrogenase) (**Fig. 8**).

The genomic 18S biodistribution pattern (**Fig. 8, lower panel**) displayed a homogeneous expression across the mouse whole-body section. Interestingly, the 18S genomic signals in the tumor region were significantly higher compared to the rest of the section. This signal increase can be explained by the fact that the 18S qPCR reagents were not designed to discriminate between human and murine 18S genomic sequences. This results in qPCR signals which are the sum of both murine and human genomic 18S signals in the tumor region which does not only contain tissues originating from the tumor but also murine endothelial tissues. This is why the elevated 18S signals might simply be due to a very high cell density in the tumor region, combining cells from human and murine origin.
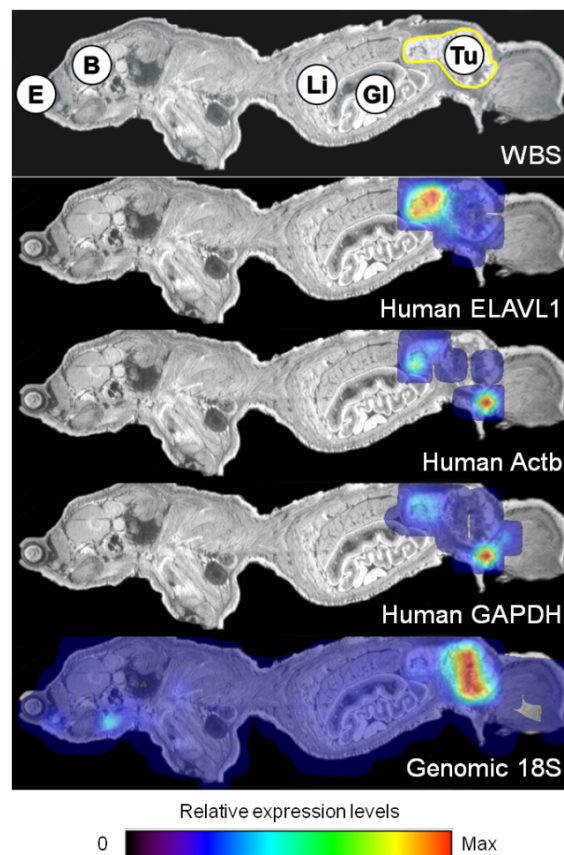
Figure 8: Detection of a human tumor in a mouse whole-body section using RT-qPCR primers against human mRNAs. The eye (E), brain (B), liver (Li) and gastro-intestinal tract (GI) are indicated in the top panel where the tumor (Tu) is highlighted

The signals obtained for the human mRNAs on the other hand, showed a strong co-localization with the tumor region, corresponding to our expectancies. The diffuse signal observed in the close vicinity of the tumor does not represent signal leakage, but is rather an artifact generated by the imaging software (**Fig. 9**).
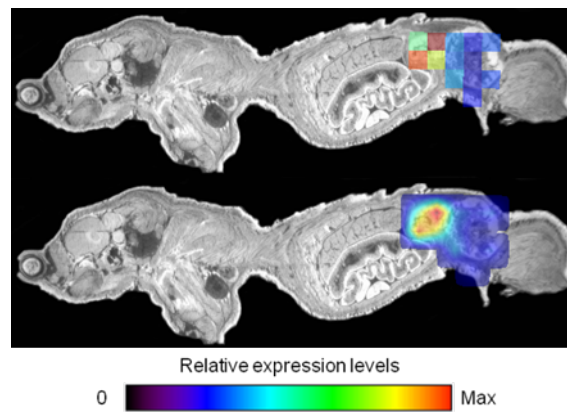
Figure 9: Impact of the signal smoothing on the human ELAVL1 mRNA biodistribution pattern

The imaging software is converting every data point from the spreadsheet software in a pixel. At the same time, the software generates a color gradient based on the maximum and minimum relative expression signals measured by WBS-PCR. This color scale is then used to attribute a color to every pixel (**Fig. 9, upper panel**). In order to generate the heat maps shown previously, the TissueView™ software is then smoothing out the signals obtained for each pixel, therefore generating these "leaking" patterns (**Fig. 9, middle panel**). Although this representation might not be perfect because of these "leaks", it remains the best way to represent this type of data, and in the case of severe doubts on the presence of signal in a given area, it is always possible to go back to the pixel visualization, allowing a closer examination of the data.

In summary, we successfully identified a sample preparation method compatible with WBS-PCR with the use of OTX Lysis Buffer. This allows not only the detection of coding mRNAs, but also of genomic signals enabling "per-cell" normalization of the RT-qPCR signals, rather than using 18S rRNA as a normalizer, which can induce biases depending on the translational activity of a given organs or groups of cells. We also identified a visualization method enabling to appreciate the biodistribution of any oligonucleotide detected by WBS-PCR.

C.   Whole body Scanning PCR for the localization of miRNAs and siRNAs

As a next step, we sought out to investigate the *in vivo* biodistribution patterns of siRNAs by WBS-PCR. In contrast to mRNAs assays, for which Taqman-based RT-qPCR assays were commercially available, there were no commercially available assays for the detection of siRNAs. We therefore developed an assay in-house, which we first validated on miRNAs. Indeed, since miRNAs and siRNAs are highly similar, displaying sizes varying from 19 to 23 nucleotides, their detection by RT-qPCR faces similar challenges.

C.1.   Development of a RT-qPCR method for the detection of miRNAs and siRNAs

C.1.a) Molecular mechanism of the assay

The RT-qPCR assays used for the detection of mRNAs in previous experiments were based on the combination of two primers and the hydrolysis of a Taqman probe. This system can be applied to the detection of miRNAs and siRNAs only if the assay allows the extension of the cDNA to generate enough room for the probe to bind to the amplicon,

since the target sequences are only around 20 nucleotides long. We nevertheless adopted another strategy and designed an assay combining the use of primers displaying short target recognition sequences (TRS) ([76](#)) with the use of a fluorescently labeled primer in association with a quencher-labeled anti-primer ([77](#)).
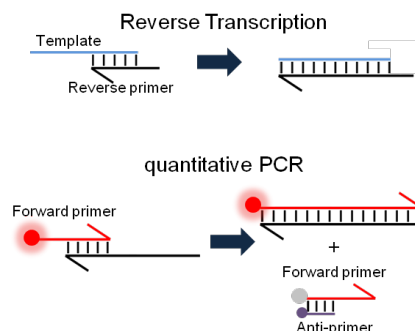
Figure 10: Molecular mechanism of the miRNA RT-qPCR method

As for a RT-qPCR on mRNAs, the first step of the reaction consists in converting the RNA template to a cDNA with the help of the Reverse Transcription (RT) primer (**Fig. 10a**). After having been heated to inactivate the reverse transcriptase, the RT-mix is supplemented with a qPCR-mix containing amongst other reagents a 5'-end fluorescently labeled forward primer, as well as a 3'-end quencher labeled anti-primer, and a reverse primer, identical to the Reverse Transcription primer. While non-incorporated forward primers will be quenched by hybridizing to the anti-primers, the fluorescence signal emitted by forward primers involved in the amplification of the cDNA is monitored during the extension cycle of the qPCR. An exponential increase of the fluorescence signals indicates the successful amplification of the target (**Fig. 10b**).

C.1.b) Importance of the TRS length for optimal amplification

Unlike conventional mRNAs Taqman assays in which the full length of a primer encodes for the TRS, the small size of a miRNA reduces dramatically the TRS size that can be incorporated to a primer. In order to define the optimal TRS length that could be employed for the detection of a synthetic miR-16-5p, we performed a small study in which we tested a panel of RT/Reverse primers displaying various TRS lengths, and did the same with a panel of forward primers displaying various TRS lengths (**Fig. 11**). Since temperature and primer length are critical parameters for successful amplification ([78](#)), we should be able to identify an optimal TRS length range for both the RT/Reverse and forward primers. We not only tested the optimal TRS length of the RT/Reverse primer (**Fig. 11a**) but we also determined the optimal TRS length of the forward primer (**Fig. 11b**). The length of the TRS of the RT/Reverse primer has a big impact on the efficient detection of synthetic miR-16-5p, and the amplification efficiency was assessed by comparing the sensitivity and linearity achieved by using any of the primers tested.

Indeed, although there is an optimal TRS length of 7 nucleotides, a longer TRS does not necessarily increase the quality of the amplification. However, the maximum impact on amplification is observed when shortening the TRS, since TRS shortening decreases the sensitivity of the assay, but also hinders the linearity of the assay. The same study was performed on the TRS of the forward primer, and the results obtained for the forward primer were different in that the TRS length does not have such a strong impact on amplification efficacy as the TRS length of the RT/Reverse primer. Apart from the 9- and 10-mer TRS primers, all forward primers displayed similar amplification efficiency, therefore allowing more liberty in the design of the forward primer.
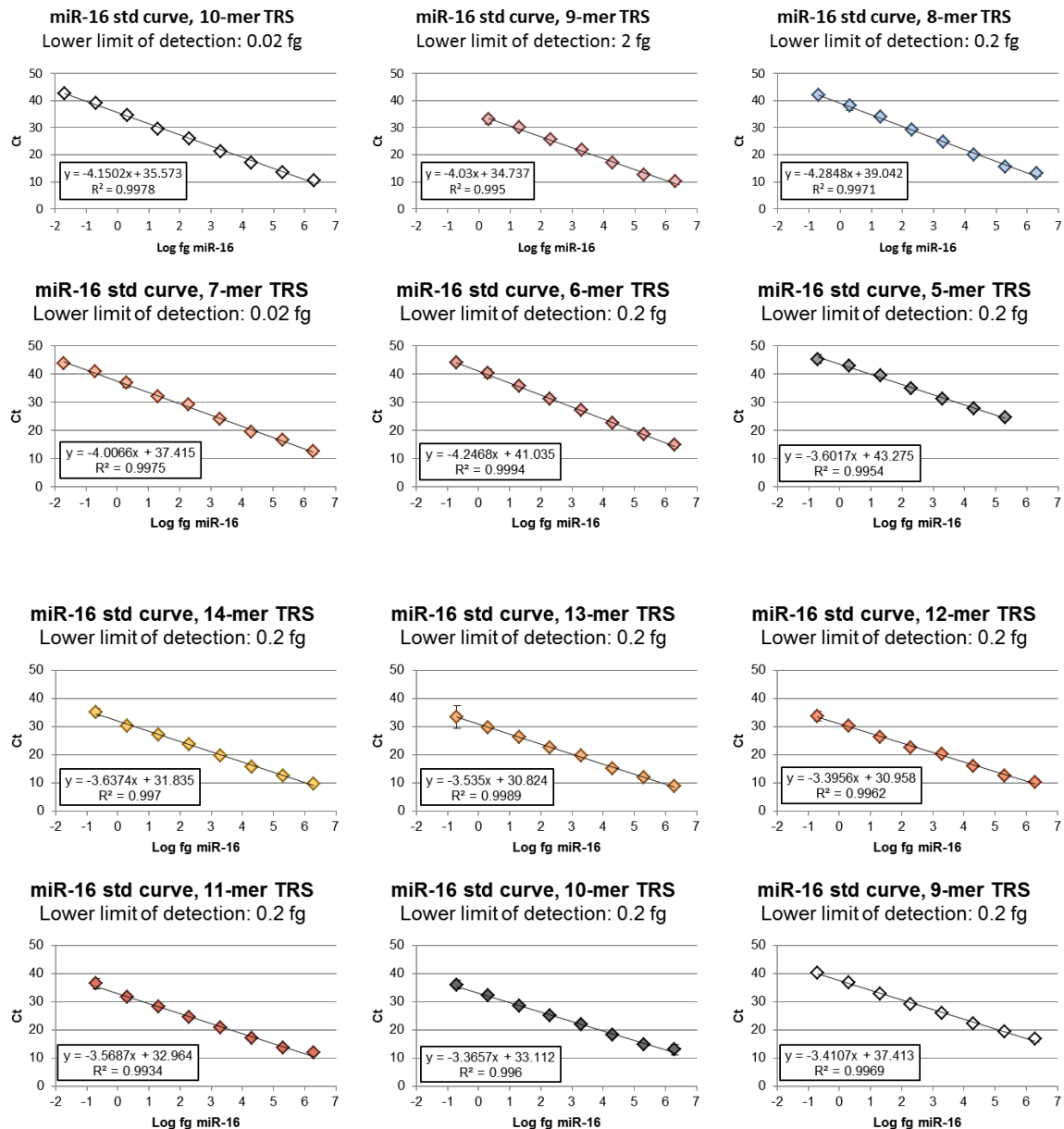
Figure 11: *Impact of the TRS length of the RT/Reverse (a) and forward primer (b) on the amplification efficiency of miR-16-5p. Values are averages of four measurements, error bars, STDEV (n=4)*

This study demonstrated that the design of the primers is absolutely crucial for efficient amplification of a miRNA, the most critical part being the design of the reverse primers. This can however be of a great advantage for the specificity of the assay. An optimal amplification can be observed for a given TRS length and amplification temperature. Thus, in the case of a mismatch between two homologous sequences, when using the same primers, the sequence containing the mismatch will have an artificially shortened TRS. This can have a dramatic impact on the amplification efficacy, allowing to generate reagents able to discriminate between highly homologous sequences, and therefore design highly specific primers. This can be particularly interesting in the case of the Let-7 family of miRNAs for example, in which all miRNAs show highly homologous sequences.

C.1.c) Characterization of the RT-qPCR assay on the Let-7 family of miRNAs

mmu-let-7a	UGAGGUAGUAGGUUGUAUAGUU
mmu-let-7c	UGAGGUAGUAGGUUGUAU**G**GUU
mmu-let-7f	UGAGGUAGUAG**A**UUGUAUAGUU
mmu-let-7e	UGAGGUAG**G**AGGUUGUAUAGUU
mmu-let-7b	UGAGGUAGUAGGUUGU**GUG**GUU
mmu-let-7d	**A**GAGGUAGUAGGUUG**C**AUAGUU
mmu-let-7g	UGAGGUAGUAG**U**UUGUA**C**AGUU
mmu-let-7i	UGAGGUAGUAG**U**UUGU**GCU**GUU

Figure 12: *Members of the Let-7 family of miRNAs, sorted by sequence homology to Let-7a. Sequence variations are indicated in red*

The sensitivity and specificity of this RT-qPCR method was tested using miRNAs of the highly homologous Let-7 family. The members of this family of miRNAs display highly homologous sequences, in some cases varying by only one nucleotide (**Fig. 12**) making it therefore an ideal case study for our RT-qPCR method.
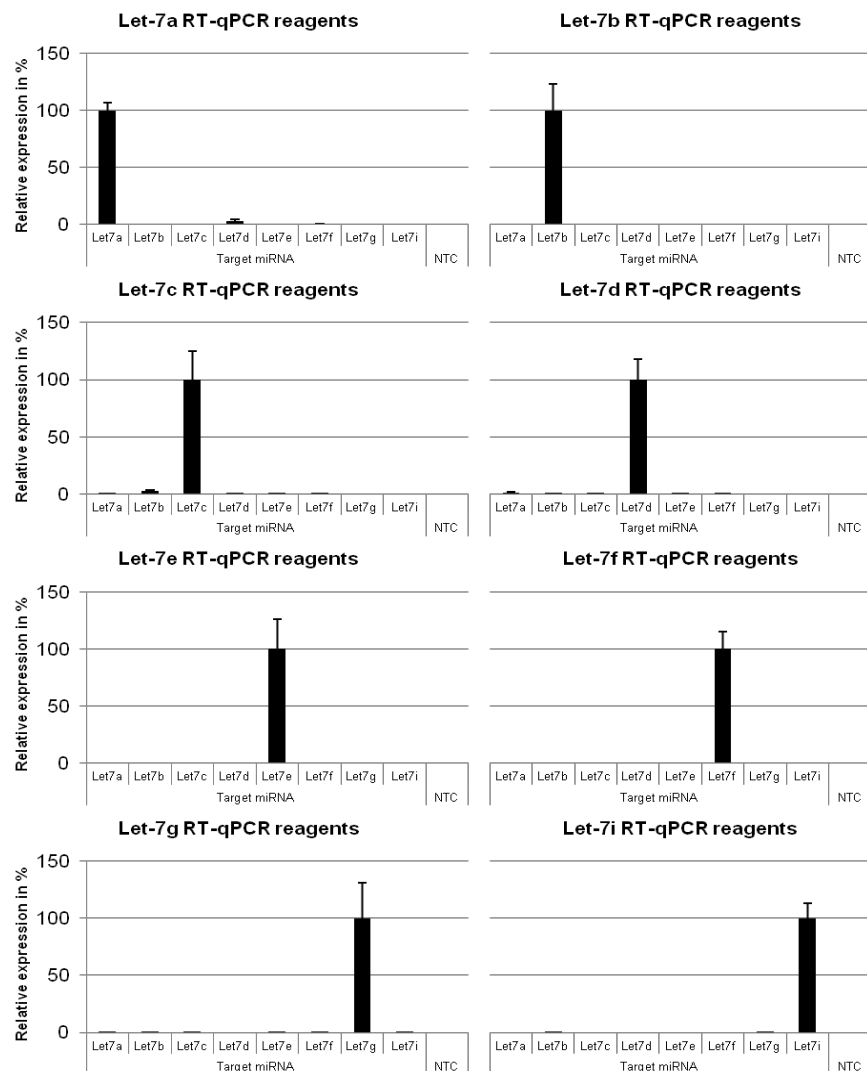
Figure 13: *Verification of the specificity of the RT-qPCR method on members of the Let-7 family of miRNAs. Error bars, STDEV (n=4)*

First we addressed the cross-reactivity of the various primer pairs by performing RT-qPCRs on samples spiked with 2 pg of each miRNA target (**Fig. 13**). The results are

28

shown as % relative expression, where the perfect matches between targets and reagents have been set to 100%. All of the reagents display 100% specificity towards their targets whereas the background levels identified by NTC (No Template Control) did not show any reactivity. However in the case of Let-7a and Let-7c, a cross-reactivity of 3% could be observed towards Let-7d and Let-7b, respectively. This level of cross-reactivity can be explained by the fact that these targets differ only by one nucleotide, and this single mutation is located at the 3'-end of the Reverse primer TRS, therefore suggesting that the primers were able to bind to these targets, although with a significantly reduced affinity than towards their perfect match. These results confirm the ability of our method to perfectly discriminate highly homologous miRNAs which show at least 2 mismatches with each other, and to significantly discriminate sequences differing by only one nucleotide.

Step 1: First-strand synthesis (RT)

Mature microRNA
A) ——————AAAAAAAAAAAAAAAAAAAA
B) ——————AAAAAAAAAAAAAAAAAAAA
        ←——TTTTTTTTTTTTTT
3' degenerate anchor   5' universal tag

Step 2: Real-time PCR amplification

miR-specific forward primer
A) ————→TTTTTTTTTTTTTT
        ←—— miR-specific reverse primer
B) ====

RT-qPCR reagents (panel b)

	Let-7 family templates							
	Let-7a	Let-7b	Let-7c	Let-7d	Let-7e	Let-7f	Let-7g	Let-7i
Let-7a	100	0	5.2	0	0	0.1	5.1	0
Let-7b	0	100	0.5	0	0	0	0	0
Let-7c	1.2	0	100	0	0	0	0.1	0
Let-7d	0	0	0	100	0	0	0	0
Let-7e	0.4	0	0.1	0.3	100	0	0	0
Let-7f	0	0	0	0	0	100	0	0
Let-7g	0	0	0	0	0	0	100	0
Let-7i	0	0	0	0	0	0	0	100

RT-qPCR reagents (panel c)

	Let-7 family templates								NTC
	Let-7a	Let-7b	Let-7c	Let-7d	Let-7e	Let-7f	Let-7g	Let-7i	
Let-7a	100	0	0	3	0	0	0	0	0
Let-7b	0	100	0	0	0	0	0	0	0
Let-7c	0	3	100	0	0	0	0	0	0
Let-7d	1	0	0	100	0	0	0	0	0
Let-7e	0	0	0	0	100	0	0	0	0
Let-7f	1	0	0	0	0	100	0	0	0
Let-7g	0	0	0	0	0	0	100	0	0
Let-7i	0	1	0	0	0	0	0	100	0

Figure 14: Comparison of primers specificity achieved by the miRCURY LNA RT-qPCR method and our in-house developed RT-qPCR assay. a: Molecular mechanism of the miRCURY LNA RT-qPCR. Primers specificity obtained by using the miRCURY LNA RT-qPCR assay (b) or by our own RT-qPCR method (c)

Interestingly our results are very similar to identical experiments published by Exiqon showing results obtained with the miRCURY LNA-based miRNA RT-qPCR method (**Fig. 14**). This assay is based on the use of short PCR primers using Locked Nucleic Acids (LNA) building blocks (**Fig. 2**) since the higher Tm of LNA-DNA duplexes allows the use of shorter primers for the detection of miRNAs (**Fig. 14a**). Briefly, the target miRNA is first poly-adenylated, and is converted to a cDNA. This cDNA is subsequently amplified by short LNA PCR primers and detected by using SYBR Green.

The results obtained in panel **b** and **c** of figure **14** indicate that our miRNA RT-qPCR assay displays a specificity level similar to the one achieved by this commercially available assay ([79](#)).
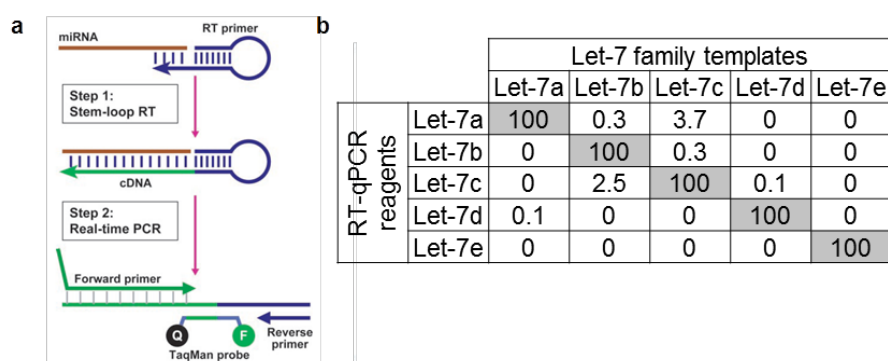
Figure 15: *Characterization of the Taqman miRNA Stem-Loop RT-qPCR method. (**a**) Molecular mechanism of the Taqman-based stem-loop RT-qPCR. (**b**) Specificity of the Stem-Loop RT-qPCR tested on the Let-7 family of miRNAs*

Another company, called Applied Biosystems, offers commercially available miRNAs quantification kits based on stem-loop RT-qPCR and using Taqman probes (**Fig. 15a**). According to the characterization of this miRNA Taqman assay (**Fig. 15b**), the performance of our assay is highly similar to results obtained by using these stem-loop RT-qPCR-based assays ([52]).

Figure 16: *Standard curves prepared with members of the Let-7 family of miRNAs. Values are averages of 4 measurements. Error bars, STDEV (n=4)*

We subsequently set out to determine the sensitivity levels achievable by our assay, by performing RT-qPCR assays on standard curves prepared with members of the Let-7 family of miRNAs. The assays displayed linear standard curves over 8 to 9 logs with a R^2-linearity coefficient higher than 0.99 in all cases (**Fig. 16**). Furthermore, in most cases our RT-qPCR method allowed us to detect as little as 0.02 fg template. However, in some cases sensitivity was as low as 0.002 fg of Let-7a and Let-7e, corresponding to approximately 1640 and 164 target molecules, respectively.

Taken together, these data suggest that we developed an efficient assay to detect miRNAs by RT-qPCR, which is very specific and highly sensitive.

C.1.d) Validation of the miRNA RT-qPCR method on tissue-enriched non-coding miRNAs

To further validate the RT-qPCR method we performed a small study and investigated the relative expression levels of a small panel of well characterized tissue-enriched miRNAs in tissue homogenates described previously (**Fig. 17a**).
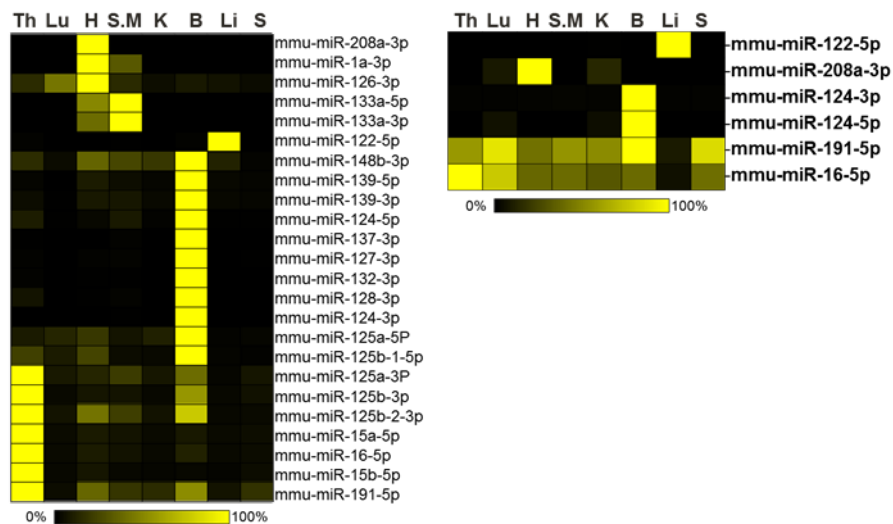
Figure 17: *Screening of a small panel of miRNAs in tissue lysates (**a**) and confirmation of the biodistribution of a sub-fraction of the same panel of miRNAs in total RNA purified from tissues (**b**)*

Not surprisingly we could clearly detect the extensively studied heart- and skeletal muscle-specific miRNAs, miR-208a, miR-1a and miR-133a. Interestingly we could not only detect miR-133a-3p but also its complementary sequence, namely miR-133a-5p in heart and skeletal muscle. The well characterized liver-specific miR-122 could be detected in liver, whereas a panel of brain-enriched miRNAs could be found in brain, such as miR-124, miR-127, miR-128, miR-132, miR-137 as well as miR-139 ([80-82](#)). The results obtained in tissue lysates could be confirmed on total RNA purified from tissues using a smaller panel of miRNAs including miR-122, miR-208a, miR-124-3p, miR-124-5p, miR-16 and miR-191 (**Fig. 17b**). The expression patterns obtained for both the tissue lysates and total RNAs are similar for all miRNAs, except for miR-16 and miR-191. Although these miRNAs show a similar trend indicating a broad expression pattern, small differences in signal intensities could be observed. This can be explained by the same reason which led to signal differences in mRNA detection (**See section IV.B.1**), namely that the relative expression signals obtained from total RNA extracts were normalized using 18S rRNA and the input concentration were all set to 10 ng/uL prior to RT-qPCR, whereas the relative expression signals obtained from tissues lysates were normalized only by using the 18S rRNA expression signals. The possibility to detect tissue-specific miRNAs in the appropriate samples confirms the compatibility of our miRNA RT-qPCR method with the OTX Lysis Buffer, and its possible application in WBS-PCR.

C.2. Validation of the WBS-PCR by unraveling the *in vivo* biodistribution of small RNAs

C.2.a) Tissue-enriched non-coding miRNAs

(C.2.a.1) Endogenous non coding miRNAs

We validated the possibility to combine WBS-PCR with our in-house developed miRNA RT-qPCR assay by determining the biodistribution pattern of a small panel of miRNAs (**Fig. 17b**) in mouse whole body sections (**Fig. 18**).
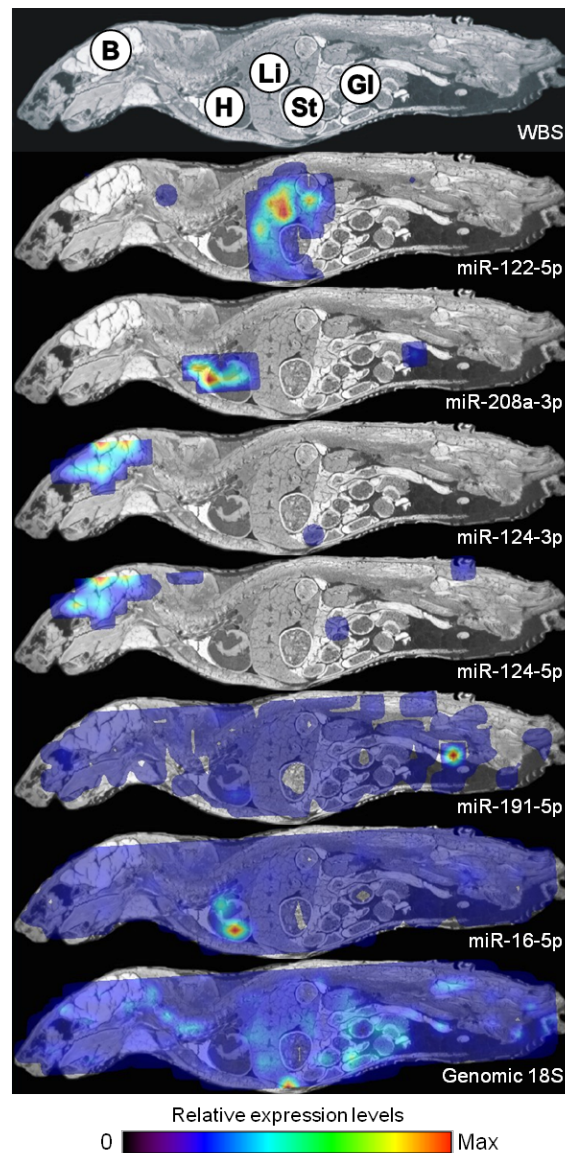
Figure 18: *Biodistribution studies of miRNAs in mouse whole body sections by WBS-PCR. Organs indicated are brain (**B**), liver (**Li**), heart (**H**), stomach (**St**) and gastro-intestinal tract (**GI**)*

First, the efficiency of the extraction procedure was confirmed by determining the biodistribution of genomic 18S (**Fig. 18, lower panel**) which displayed a homogeneous pattern and was used to normalize the miRNAs relative expression data.

The biodistribution study performed on miR-122-5p, miR-208a-3p, miR-124-3p, miR-124-5p, miR-191-5p and miR-16-5p resulted in the same biodistribution pattern as the one observed in tissue homogenates, namely that miR-122-5p co-localized with liver, miR-208-3p with the region of the heart, whereas miR-124-3p and miR-124-5p, both generated from the same pre-miRNA, co-localized with brain. miR-16-5p and miR-191-5p on the other hand showed quite a homogeneous biodistribution pattern, as expected from data shown previously.

In summary, this data clearly indicates that our miRNA RT-qPCR is compatible with the tissue-specific detection of miRNA in tissue homogenates prepared for WBS-PCR. Moreover, similar data could be generated by applying the miRNA RT-qPCR method to WBS-PCR, suggesting that it is indeed possible to detect miRNAs in mouse whole body sections by combining both assays.

(C.2.a.2)   Ectopic non-coding miRNAs
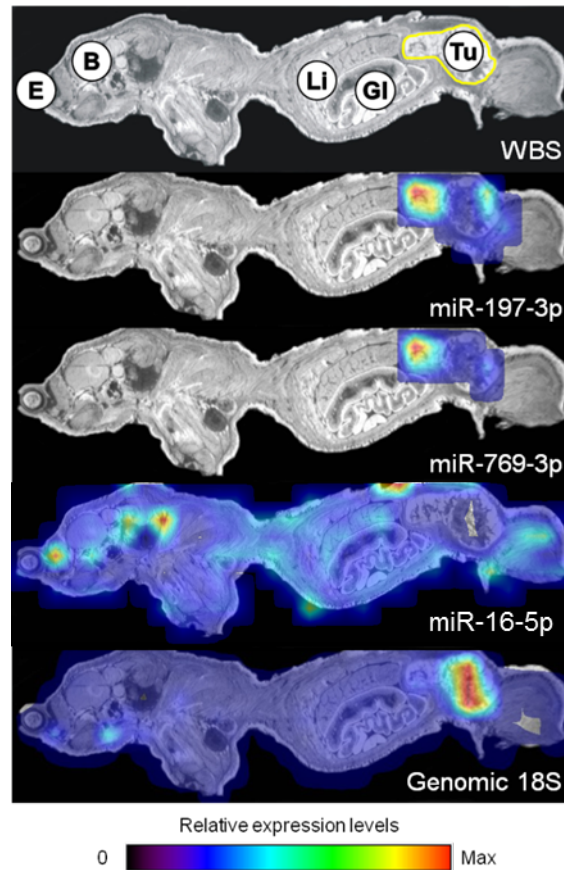
Figure 19: Detection of a human tumor in a mouse whole-body section using RT-qPCR primers against human non coding miRNAs. The eye (*E*), brain (*B*), liver (*Li*) and gastro-intestinal tract (*GI*) are indicated in the top panel where the tumor (*Tu*) is highlighted

Following the successful detection of tissue-enriched endogenous miRNAs, we investigated the possibility to detect ectopic miRNAs in a mouse tumor model, namely the HCT-116 tumor. We therefore developed and characterized reagents against human-specific miRNAs which should only be expressed in human cells, and be absent from the surrounding mouse tissues, namely miR-197-3p and miR-769-3p (83-85) (**Fig. 19**).
The genomic 18S relative expression in the mouse whole body section is quite homogenous across the section (**Fig. 19, lower panel**), although showing elevated signal intensities in the region of the tumor. Both miRNAs, namely miR-197-3p and miR-769-3p, show a highly localized biodistribution pattern in the tumor region, as expected for the detection of a human-specific miRNA. The biodistribution obtained for miR-16-5p on the other hand, showed a uniform pattern across the section, since this miRNA is identical in human and murine cells.

This dataset once more confirms the resolution that can be achieved by using WBS-PCR as well as the specificity level of our miRNA RT-qPCR method.

C.2.b) Validation of the WBS-PCR for the detection of a locally injected siRNA
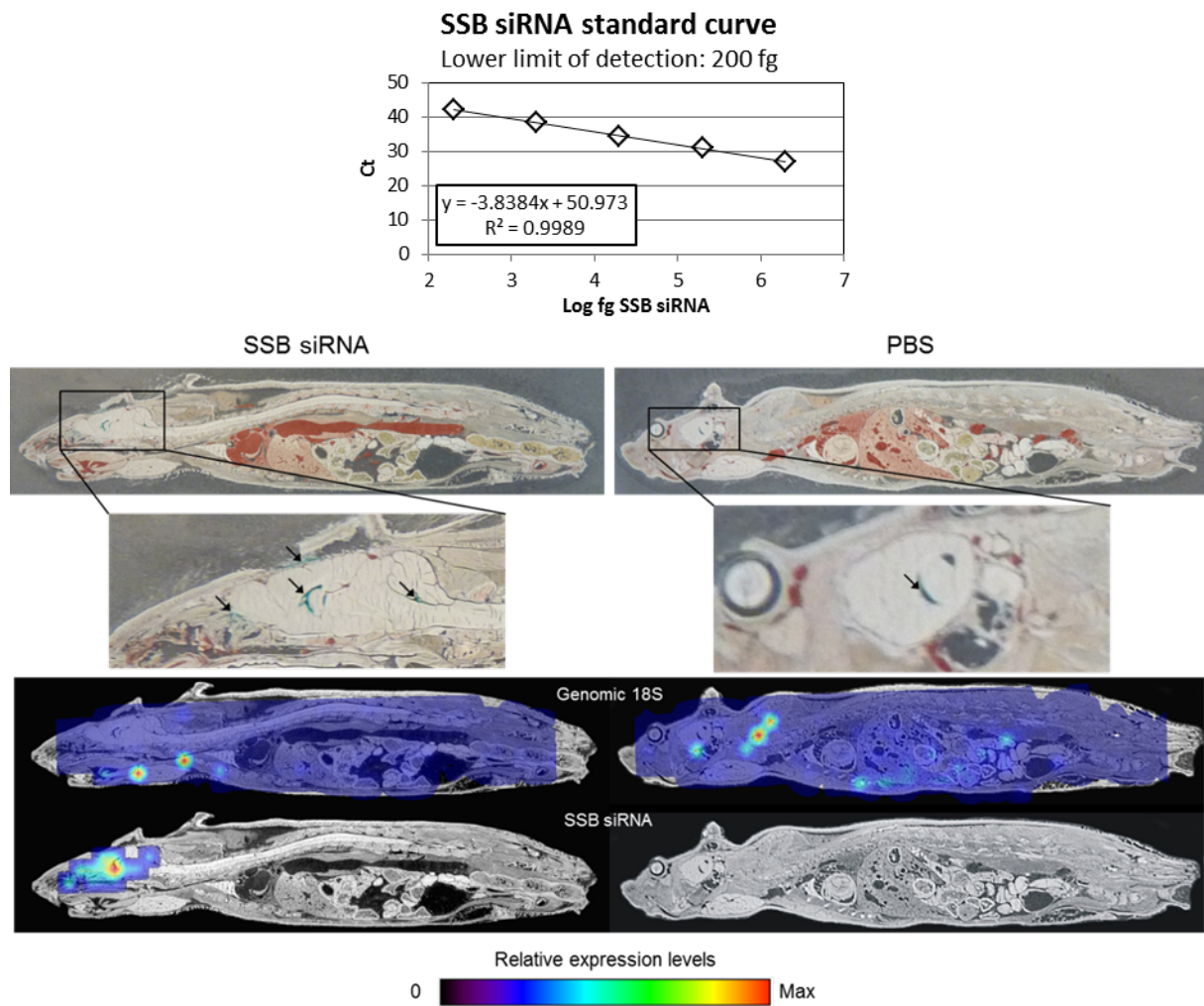
Figure 20: *Biodistribution study of a locally injected siRNA.* **Upper panel:** *Color pictures of the either siRNA- or PBS-injected mice. The injection sites are highlighted by the presence of Light Green in the injected solutions (black arrows).* **Lower panel:** *WBS-PCR results obtained for genomic 18S or SSB siRNA in the siRNA-injected mouse (**left panel**) or in the PBS-injected mouse (**right panel**)*

To validate the WBS-PCR for siRNA detection, we performed a biodistribution study on a locally injected siRNA and its subsequent detection by WBS-PCR. We therefore sacrificed two mice, and injected either an SSB siRNA or a PBS solution into the brain of the animals, and subjected both animals to deep-freezing right after the injection to minimize the diffusion of the solutions into surrounding tissues. In order to locate the injection sites during mouse sectioning, Light Green Dye was added to both the siRNA and PBS solutions (**Fig. 19b**). The quantification of the siRNA in the sections was made possible by subjecting a standard curve prepared with siRNA to RT-qPCR, allowing to determine the amount of siRNA present in a well based on the Ct-value obtained in this well (**Fig. 20a**).

After sectioning, pictures of the mice were taken to locate precisely the injection sites by monitoring the intensity of the green dye present in the injected solution (**Fig. 20b, upper panels, black arrows**). As expected, Light Green Dye was visible in the brain, and in a lesser extend in the cerebrospinal fluid, located between the brain and the skull in the siRNA-injected animal (**Fig. 20b, upper left panel**). WBS-PCR results obtained for this section confirmed the presence of the siRNA in the brain (**Fig. 20b, lower left panel**).

34

Subjecting a section of the PBS-injected animal to similar analytics resulted in slightly different results. Although Light Green Dye could also be seen in the brain of the PBS-injected animal, in a small cavity located in the center of the brain (**Fig. 20b, upper right panel**), no signal was generated by WBS-PCR, confirming the absence of siRNA in this section (**Fig. 20b, lower right panel**).

According to the results obtained for this study, we can conclude that WBS-PCR can successfully be used for the detection of siRNAs in mouse whole body sections, when injected locally.

C.2.c) In vivo biodistribution study of an intravenously injected unformulated siRNA

(C.2.c.1)   Detection of a siRNA in a mouse whole body section by WBS-PCR and QWBA

To further validate our WBS-PCR for siRNA detection, we performed a biodistribution study on a tritium labeled siRNA targeting the rat Multi-drug Resistance Protein 4 (Mrp4) intravenously injected in mouse monitored by either the conventional QWBA method ([60]), or by our WBS-PCR method.

Although we could already show that the RT-qPCR assay that we validated on miRNAs was also applicable to the detection of siRNAs (**Fig. 20**), we had to make sure that the Mrp4 siRNA could be detected with a similar efficacy, that is why we performed a RT-qPCR on a standard curve prepared with the aforementioned Mrp4 siRNA (**Fig. 21a**). The assay displayed a standard curve linear over 6 logs, with a R^2-value higher than 0.99, and allowing the detection of as little as 2 fg siRNA.

The Mrp4 siRNA used in this study was tritium-labeled by Christensen et al ([86]), favoring a tritiated Uridine located in the middle of the oligonucleotide. This particular labeling was selected because of the lower isotope exchange rate of an oligonucleotide tritiated at a single position compared to a fully radiolabeled backbone, using a fully ^{32}P-labeled backbone for example. Furthermore, the central location of this isotope was motivated by the fact that a radiolabeled nucleotide located near the 5'- or 3'-end of the oligonucleotide would be cleaved off by endonucleases much faster than a nucleotide located in the middle of the sequence. The mouse was sacrificed 10 minutes post-injection, deep frozen and subsequently sectioned. While one section was analyzed by QWBA, a neighboring section was analyzed by WBS-PCR.
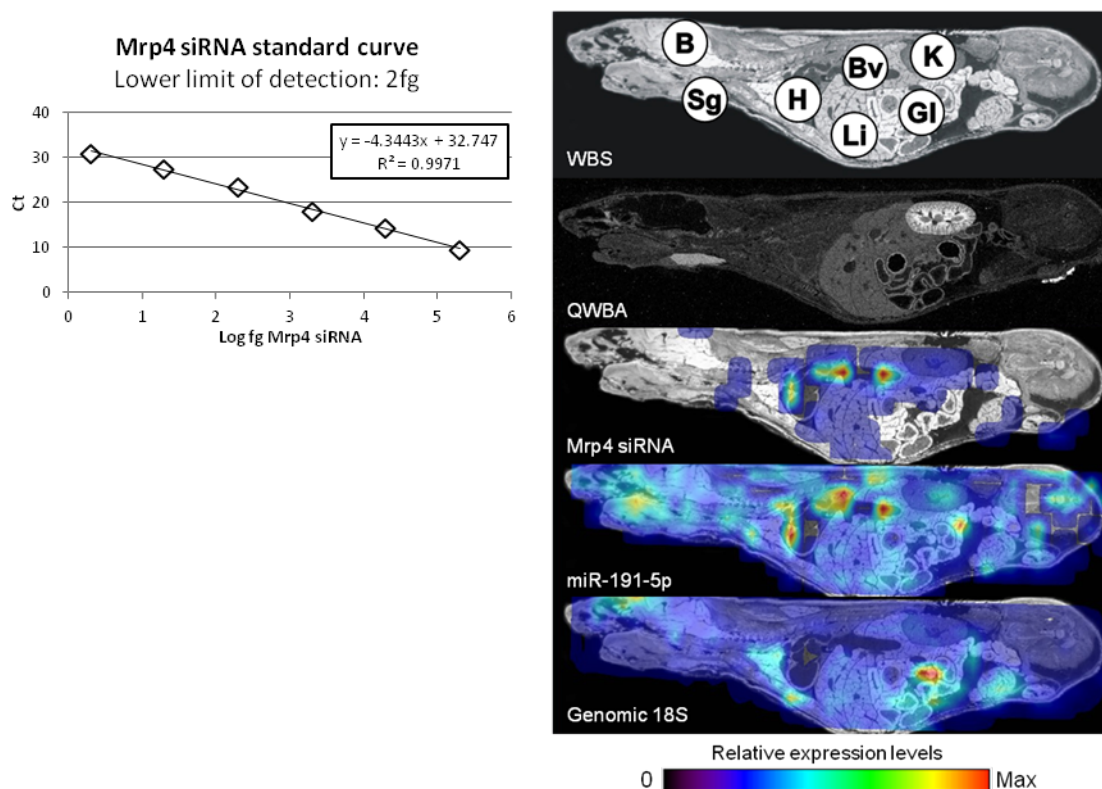
Figure 21: Detection of the Mrp4 siRNA by combining siRNA RT-qPCR and WBS-PCR. Mrp4 standard curve (a) and in vivo biodistribution of the unformulated Mrp4 siRNA (b) analyzed by Quantitative Whole Body Autoradiography (QWBA) and WBS-PCR (Mrp4 siRNA). Tissues indicated are brain (B), salivary gland (Sg), heart (H), liver (Li), blood vessel (Bv), kidney (K) and gastro-intestinal tract (GI)

The profile obtained for the siRNA biodistribution 10 minutes post-injection by QWBA (**Fig. 21b, QWBA**) indicates high levels of radioactivity in white in the kidney and in the salivary gland as well as in liver albeit in lower levels. The WBS-PCR results obtained for the biodistribution of the Mrp4 siRNA (**Fig. 21b, Mrp4 siRNA**) showed elevated siRNA levels in the kidney, liver and blood vessel. The presence of siRNAs in blood vessel could be explained by the fact that the animal was sacrificed only 10 minutes post-injection, thereby limiting its metabolization, while the presence of the siRNA in liver and kidney corroborated data generated by QWBA. Very surprisingly, we could not detect any siRNA in the salivary gland by WBS-PCR, although data generated by QWBA clearly indicates the presence of radioactive material. The fact that we failed to detect any siRNA in this organ could not be explained by poor extraction efficiency, since genomic 18S and miR-191-5p were clearly present in the salivary gland according to WBS-PCR (**Fig. 21b, lower panels**).

(C.2.c.2)   Detection of siRNA metabolites by RT-qPCR and LC-MS

Given the short half-life of unformulated siRNAs in mouse plasma, we hypothesized that the radioactive signals observed in the salivary gland by QWBA were the result of the accumulation of by-products of the metabolization of the siRNA in the salivary gland. To confirm this assumption we performed RT-qPCRs on standard curves prepared with 5'-end, 3'-end or both ends truncated siRNA, in order to mimic the *in vivo* metabolization of the siRNA (**Fig. 22**).

Lower limit of detection in ag

1.E+00 1.E+01 1.E+02 1.E+03 1.E+04 1.E+05 1.E+06 1.E+07 1.E+08

ACAGCUCCUGACACCUCUCdTdT
ACAGCUCCUGACACCUCUCdT*
ACAGCUCCUGACACCUCUC**
ACAGCUCCUGACACCUCU***
ACAGCUCCUGACACCUC****
ACAGCUCCUGACACCU*****

*CAGCUCCUGACACCUCUCdTdT
**AGCUCCUGACACCUCUCdTdT
***GCUCCUGACACCUCUCdTdT
****CUCCUGACACCUCUCdTdT
*****UCCUGACACCUCUCdTdT

CAGCUCCUGACACCUCUCdT
AGCUCCUGACACCUCUC
GCUCCUGACACCUCU
****CUCCUGACACCUC****

Figure 22: Lower limits of detection obtained for truncated versions of the Mrp4 siRNA by RT-qPCR. Values are averages of 3 measurements. Error bars, STDEV (n=3)

In order to compare the amplification efficiency obtained for each truncated template, we performed RT-qPCRs on standard curves prepared with every truncated siRNA, and determined the lower limit of detection achievable for each of these truncated templates. The lower limit of detection obtained for the full-length Mrp4 siRNA was close to 2 ag, and we used this value as a reference for all truncated siRNA versions. The 3'-end truncations (**Fig. 22, upper panel**) seemed to be tolerated by our assay up to 3 nucleotides, at which point the lower limit of detection was increased up to 10,000-fold, indicating a far less efficient amplification. The 5'-end truncations on the other hand (**Fig. 22, middle panel**), displayed a much more gradual effect on RT-qPCR sensitivity, since the truncation of 3 nucleotides at the 5'-end of the siRNA resulted in a 10-fold increase of the lower limit of detection. The loss of 4 and 5 nucleotides resulted however in a 1,000- and 10,000-fold decrease in sensitivity, respectively, indicating a severe drop of sensitivity. The concomitant truncation of both ends of the siRNA however, displayed much more severe impacts on the lower limit of detection of the RT-qPCR assay (**Fig. 22, lower panel**). The truncation of only one base at both sides of the siRNA resulted in a 100-fold higher lower limit of detection, and the lower limit of detection increased dramatically the more the siRNA was truncated. This therefore leads to a shift of the lower limit of detection of truncated siRNAs, indicating that the more an siRNA will be truncated, the less efficient its detection by RT-qPCR will be, and will ultimately be undetectable by RT-qPCR if the truncation is too advanced. When considering the siRNA detection in the mouse whole body section (**Fig. 21b**), where the average siRNA amount is 10 fg siRNA, only a limited panel of truncated siRNAs can be detected, displaying a maximum of 2 nucleotides truncations at the 3'-end, 3 nucleotides at the 5'-end, or 1 nucleotide at each end of the siRNA, and of course the full length siRNA. With WBS-PCR we therefore have the possibility to detect only full-length or slightly metabolized siRNAs. Over time, and if metabolization of the siRNA is going on, the siRNA will be undetectable by RT-qPCR, a phenomenon which we observed in this study, since we were unable to detect any siRNA in a section of a mouse sacrificed 1 hour post-injection, whereas QWBA clearly showed presence of the Mrp4 siRNA.

To further identify the source of the radioactivity detected in the salivary gland by QWBA, we subjected pieces of salivary gland cut out of QWBA sections to LC-MS analysis (**Fig. 23**).
The radioactivity level of the sample was monitored during the LC-MS run and allowed to identify a few radioactive moieties. Unfortunately, only one of the peaks contained an identifiable moiety, namely the peak annotated M1 (**Fig. 23, red square**), corresponding to radio-labeled mono-uridine. Although the other peaks (annotated Px.x, where x.x indicates

their retention time) also showed a certain level of radioactivity, their exact structure could not be identified by MS, since their mass did not correspond to the mass of expected metabolization products.
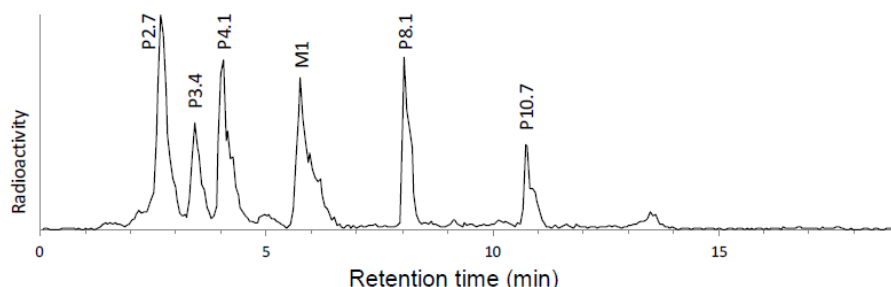
Figure 23: *LC-MS analysis of the radioactively-labeled content of the salivary gland of a mouse sacrificed 10 minutes post-injection*

Neither full-length, nor truncated oligonucleotides could be identified in this experiment, indicating the high level of metabolization of the Mrp4 siRNA in the salivary gland.

In summary, we showed that the miRNA RT-qPCR assay that we developed in house could successfully be used for the quantification of siRNAs. Moreover, similar conclusions could be drawn by using either WBS-PCR or QWBA, known as a standard method used for siRNAs *in vivo* biodistribution studies.

D.   Whole Body Scanning qPCR for the *in vivo* localization of heavily chemically modified oligonucleotides

Therapeutic siRNAs are used for their ability to regulate the expression of coding mRNAs, and their mechanism of action which is similar to the one of cellular miRNAs. In some diseases such as cancer for example, a battery of miRNAs called oncogenic miRNAs can be expressed at elevated levels compared to healthy patients. That is why another class of therapeutic oligonucleotides has been developed to target these miRNAs, called antagomirs or Anti-miRNA-oligonucleotides (AMO). It has already been shown that these antagomirs are biologically active towards their targets and open up new treatment possibilities ([87]). The AMO-miR-221 for example has been shown to significantly increase tumor doubling time, and to increase the life span of tumor mouse models ([88]). Such an AMO has however to be chemically modified to display higher resistance towards nucleases, as well as higher binding efficiencies towards RNA molecules, to increase its cellular uptake and to display better pharmacokinetic and pharmacodynamics properties ([62],[63]).

D.1.   Development of Chemical Ligation qPCR (CL-qPCR), a method for the detection of heavily chemically modified oligonucleotides

D.1.a) The need for a detection method for heavily chemically modified oligonucleotides

The growing interest in using antagomirs as therapeutic oligonucleotides ([24]) and their heavy chemical modifications prompted us to test the possibility to study the biodistribution pattern of such entities *in vivo* using WBS-PCR. We therefore used our in-house developed miRNA/siRNA RT-qPCR method to detect an antagomir targeting miR-16-5p (AMO-miR-16) available in three different chemical formats, namely RNA, 2'O-methyl (2'Ome) and the 2'-O-methoxy-etoxyethyl (MOE) (**Fig. 24**).

38

By using our in-house developed miRNA/siRNA RT-qPCR method we could, as expected, detect the RNA-synthesized AMO-miR-16 (**Fig. 24a**). Surprisingly, we could also detect the 2'-OMe-modified AMO-miR-16 (**Fig. 24b**), though the sensitivity was reduced by 10-fold compared to the RNA-synthesized AMO-miR-16. The MOE-modified AMO-miR-16 on the contrary, could not be detected at all by using this RT-qPCR method (**Fig. 24c**).
We therefore had to develop an assay able to detect oligonucleotides independent from their chemical format.

D.1.b) Molecular mechanism of the CL-qPCR

As could be seen in figure **2**, the 2'-OMe and 2'-MOE chemical modifications only affect the oligonucleotide backbone, leaving the nitrogen bases unaffected. Although these modifications interfere with enzymes such as Reverse Transcriptase and Taq Polymerase, the antagomir is still perfectly able to hybridize to any other oligonucleotides.
The crucial step in this assay is to convert the antagomir in a DNA molecule amplifiable by Taq Polymerase. Since Reverse Transcriptase is not able to generate a cDNA from such a template, we developed a qPCR assay based on a templated chemical ligation described by Kool et al ([89](#),[90](#)).
The assay we ought to develop uses the same qPCR strategy as the assay to detect miRNAs and siRNAs, but we replaced the enzymatic Reverse Transcription step by a chemical ligation step (**Fig. 25a**). The chemical ligation step is an alternative to cDNA synthesis by reverse transcription, where two small ligators have the ability to hybridize to the target, and the close proximity induced by hybridization subsequently allows the formation of a phosphorothioate bond between both ligators. The resulting ligated product can subsequently be amplified and detected by qPCR.
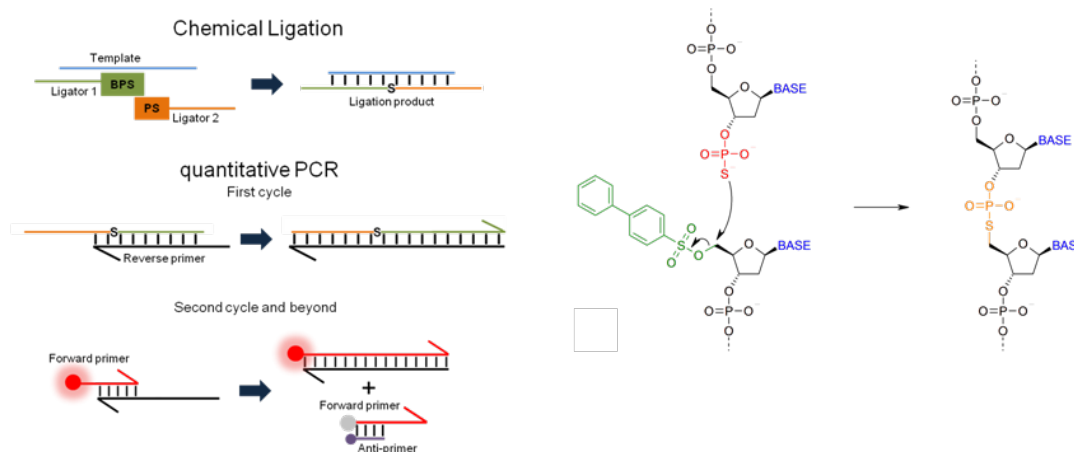
Figure 25: Principle of the Chemical Ligation qPCR (CL-qPCR). Molecular mechanism of the CL-qPCR mediated detection of a highly chemically modified template (**a**) and reaction between a PS-group and a BPS-leaving group, generating a phosphorothioate linkage between both ligators (**b**)

Although Kool et al described a method based on an iodine-leaving group ([91](#)), we observed by quality check that this leaving group was lost when coupled with G- and C-

bases. Although the iodine-group could be efficiently coupled to a T-, or an A-base, coupling to a G- or C-base resulted in the iodine reacting with the bases themselves, therefore rendering these ligators non-usable for ligation. This high reactivity and the low lipophilicity of iodine-coupled ligators did not enable them to be purified by using standard cassette oligonucleotides purification methods. We later identified the BisPhenylSulfonyl (BPS) moiety as an efficient alternative to the use of iodine. This BPS-leaving group works in a similar fashion as a dabsyl-leaving group (92), which allows the formation of a Phosphorothioate bond between both ligators in the case of an nucleophilic attack by a Phosphorothioate group on the leaving group (**Fig. 25b**). Furthermore, the lipophilicity of the BPS-leaving group allows efficient purification of the ligator using standard cassette purification methods, allowing a better quality control of the generated reagents.

D.1.c) Optimization of the synthesis conditions

The generation of highly pure reagents is crucial to develop an efficient assay. It can indeed be very harmful to the assay if a fraction of the reagents does not display the appropriate 3'-PS or 5'-leaving group, since these reagents would be able to bind to their targets, but unable to react and to generate an amplifiable ligated product. That is why we subjected our ligators to LC-MS analysis to check for reagents purity and integrity (**Fig. 26**). The LC-profile obtained for the PS-ligator (**Fig. 26a, left panel**) showed a single peak at 3.11 seconds. The mass calculated for the PS-ligator was of 6133.192 Da (**Fig. 26a, right panel**), and the mass obtained for the molecule present in the LC-peak was of 6132.95 Da, allowing us to conclude that this peak indeed corresponded to the PS-ligator.
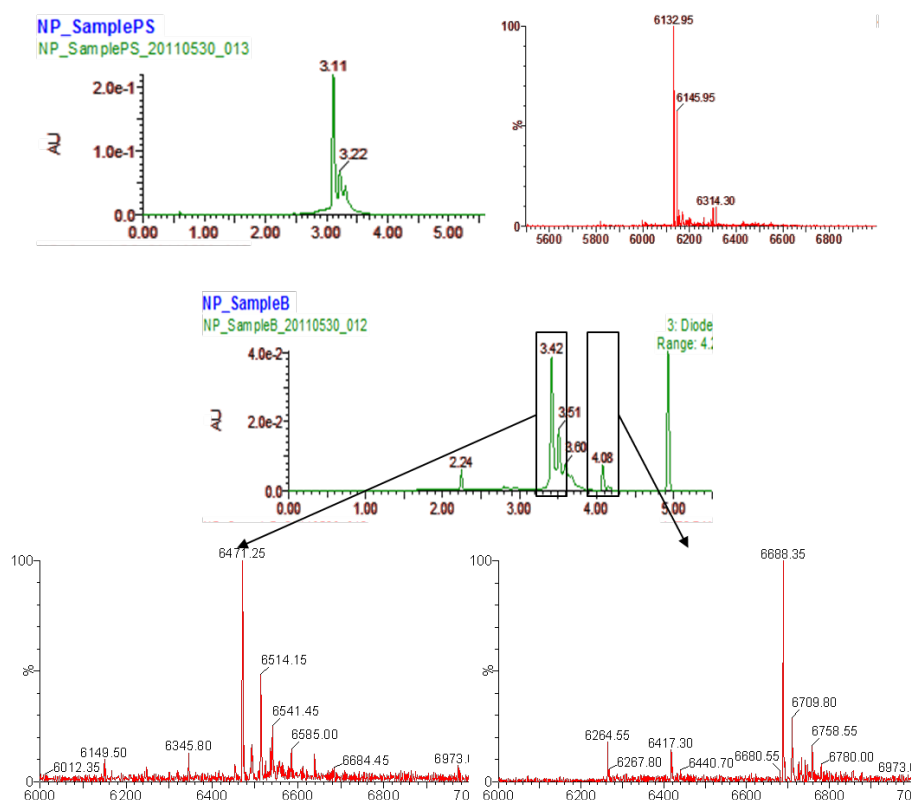
*Figure 26: LC-MS analyses performed on the AMO-miR-16 PS-ligator (**a**) and BPS-ligator (**b**)*

The LC profile obtained for the BPS-ligator on the other hand showed two peaks at 3.42 and 4.06 seconds (**Fig. 26b, upper panel**). The 3.42 peak was analyzed by MS and showed the presence of a 6471.25 Da (**Fig. 26b, lower left panel**) whereas the mass

40

calculated for the BPS-ligator was of 6688.398 Da. Very surprisingly, the major LC-peak did not contain the intact BPS-ligator. We therefore analyzed the secondary peak located at 4.06 seconds, and could identify a molecule displaying a mass of 6688.35 Da (**Fig. 26b, lower right panel**), therefore corresponding to the intact BPS-ligator. We subsequently investigated the nature of the molecule eluted at 3.42 seconds, and after having calculated the mass of the BPS-leaving group, we could conclude that the difference between the calculated and obtained mass in this peak corresponded to 217 Da, the mass of the BPS-leaving group. This led us to the conclusion that the BPS-ligator solution did not consist of only intact BPS-ligator, but contained only 10% intact BPS-ligator, whereas the other 90% corresponded to BPS-free BPS-ligator.

We identified the deprotection reagents and conditions as the initiators of the BPS-group cleavage from the BPS-ligator. The use of soft deprotection reagents (Ultramild CE phosphoramidites) as well as soft deprotection conditions by shortening the incubation time from an overnight to a 4 hours incubation time, as well as performing this reaction at room temperature rather than at 50°C led to the synthesis of a second generation of ligators which were subjected to LC-MS studies as well (**Fig. 27**).
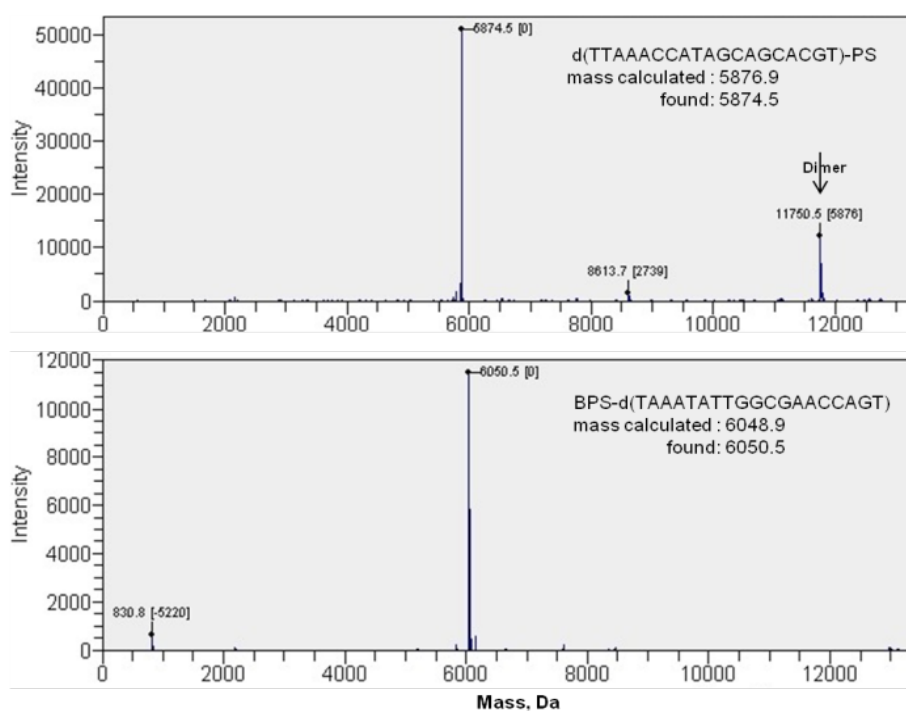
*Figure 27: LC-MS analyses of the AMO-miR-16 PS-ligator (**a**) and BPS-ligator (**b**) generated under optimal synthesis conditions*

The LC-MS analysis provided us this time results confirming the presence of intact PS-ligators (**Fig. 27a**) and BPS-ligators (**Fig. 27b**) since the expected and obtained masses were similar in both cases.

D.1.d) Validation of the CL-qPCR assay

The performance of this assay was assessed by detecting AMO-miR-16 in three different chemical formats (**Fig. 28**). Not surprisingly, similar results were obtained on the three chemical formats tested, since we could detect down to 20 fg AMO-miR-16 when present in RNA (**Fig. 28a**) and 2'-Ome formats (**Fig. 28b**), and as little as 2 fg when present in 2'-MOE (**Fig. 28c**).

Showing that we could actually detect a 2'-MOE modified oligonucleotide was a big step forward in the validation process of our CL-qPCR method. As a next step however, we wanted to show that the BPS-leaving group could be coupled to any base. CL-qPCR was therefore performed with ligators containing either a 5'-BPS-T, -G, -C, or –A, for the detection of synthetically generated variants of the AMO-miR-16 sequence (**Fig. 29**).
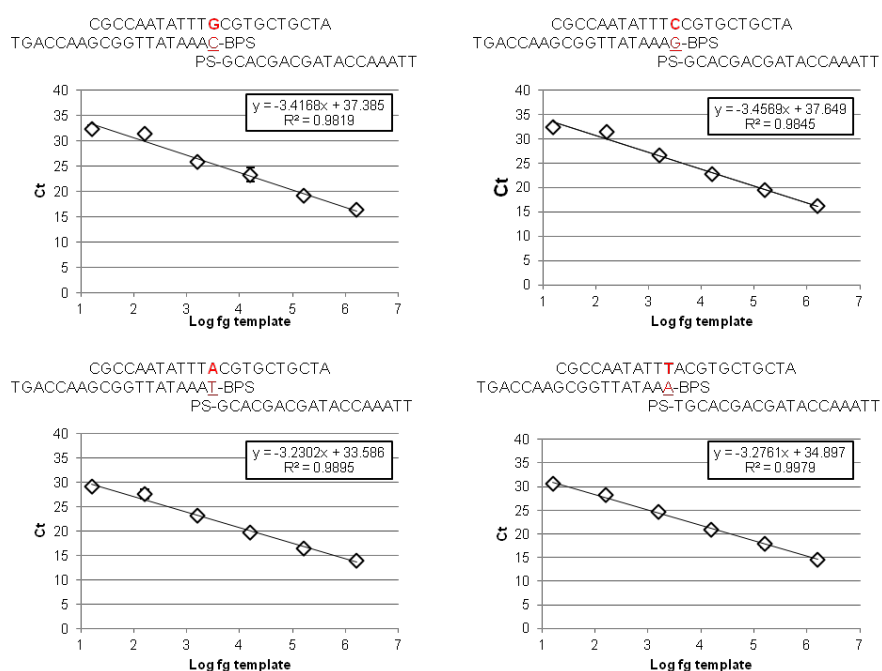
Figure 29: CL-qPCR on mutated versions of the AMO-miR-16 antagomir. Values are averages of 4 measurements. Error bars, STDEV (n=4)

In each graph the sequences of the AMO-miR-16 variants and both ligators are indicated. The template sequence is shown on top, and the mutation is indicated in red. The ligators are also indicated, and the base coupled to the BPS-leaving group is indicated in red, underlined. The assay displayed similar results in all cases, with standard curves linear across 6 logs and allowing the detection of as little as 20 fg template.
This result indicates that the assay performs with similar efficiency independent from which base the BPS-leaving group was coupled to.

D.2.   *In vivo* biodistribution study of AMO-miR-16, an MOE-modified anti-miRNA-oligonucleotide targeting miR-16-5p

D.2.a) Validation of the compatibility of CL-qPCR with WBS-PCR for the detection of a locally injected AMO-miR-16 antagomir

To assess whether CL-qPCR could be used in combination with WBS-PCR, we performed a biodistribution study on a locally injected AMO-miR-16 and its subsequent detection by

WBS-PCR. We therefore sacrificed two mice, and injected either AMO-miR-16 or a PBS solution into the brain of the animals, and subjected both animals to deep-freezing right after the injection to minimize the diffusion of the solutions into surrounding tissues. In order to locate the injection sites during mouse sectioning, we supplemented both the AMO-miR-16 and PBS solutions with Light Green Dye, and we checked by WBS-PCR whether AMO-miR-16 could be detected in the appropriate regions.
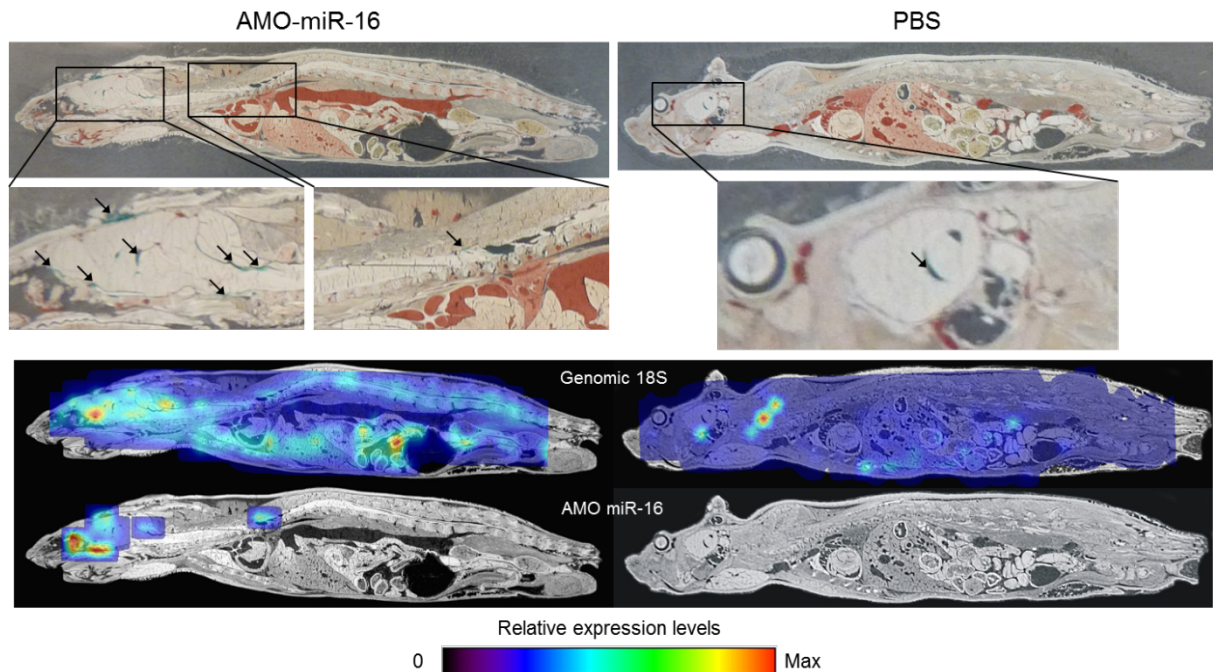
*Figure 30: Biodistribution study of a locally injected antagomir. **Upper panel:** Color pictures of the either AMO-miR-16- or PBS-injected mice. The injection sites are highlighted by the presence of Light Green in the injected solutions (black arrows). **Lower panel:** WBS-PCR results obtained for genomic 18S or AMO-miR-16 in the AMO-miR-16-injected mouse (**left panel**) or in the PBS-injected mouse (**right panel**)*

The injection sites in the sections of the AMO-miR-16- and PBS-treated animals were located using the Light Green dye present in the injected solutions (**Fig. 30, upper panel, black arrows**). The PBS-treated animal displayed an area containing green dye in a small cavity in the brain whereas the AMO-miR-16 could be detected in various places in the brain of the AMO-miR-16 treated animal, as well as in the cerebrospinal fluid of this animal, not only highlighting the space between the brain and the skull of the animal, but also highlighting a small region along the spinal cord.

We performed subsequently a CL-qPCR on the lysates obtained from the lysis of both mouse sections (**Fig. 30, lower panel**). The biodistribution pattern obtained for the AMO-miR-16-treated animal highlighted the regions containing green dye in the brain and along the spinal cord of the animal, confirming the colocalization of the injected solution and presence of the AMO-miR-16 antagomir. As expected, no AMO-miR-16 could be detected in the brain of the PBS-treated animal.

This study confirms the possibility to use lysates generated for WBS-PCR as samples for CL-qPCR, therefore allowing the detection of highly modified oligonucleotides in whole body sections by combining WBS-PCR and CL-qPCR.

D.2.b) Monitoring AMO-miR-16 levels by CL-qPCR in mouse blood and tissues

In this study we tested how the CL-qPCR performed in an *in vivo* biodistribution study performed by either WBS-PCR or by the classical way of sampling various organs from the animals. We injected 5 mice intravenously with 80 mg/kg AMO-miR-16, and 5 control mice with PBS. Blood samples were taken from each single animal until 24 hours post-injection, at which point the animals were sacrificed. After sacrifice, one mouse of each group was deep-frozen, sectioned and subjected to WBS-PCR, while the other animals were subjected to organ sampling.
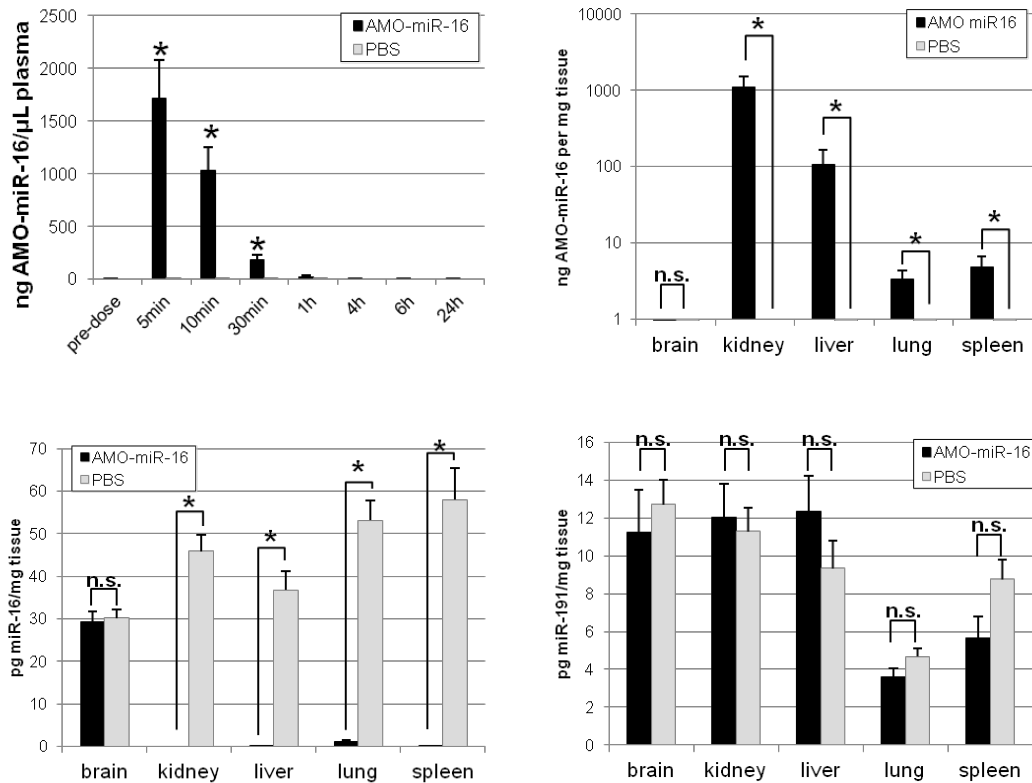
Figure 31: *Quantification of AMO-miR-16 by CL-qPCR in blood samples (**a**) and tissue homogenates (**b**), and RT-qPCR detection of miR-16-5p (**c**) and miR-191-5p (**d**). Values are averages of triplicate measurements from 5 (**a**) or 4 animals (**b-d**). Error bars, s.e.m. (n=15 (**a**), n=12(**b-d**)). *p<0.05 (Mann-Whitney Rank sum test (**a-c**), t-test (**d**), n.s.: not significant)*

No AMO-miR-16 could be detected in mouse plasma after 30 minutes post-injection, suggesting that the AMO-miR-16 was cleared from circulating blood (**Fig. 31a**).
We sampled a few representative organs such as brain, kidney, liver, lung and spleen from 4 mice treated with PBS and 4 mice treated with AMO-miR-16. We subsequently quantified AMO-miR-16, miR-16-5p as well as miR-191-5p as control in tissue homogenates prepared from these organs and signals were normalized against tissue weight (**Fig. 31b-d**).
AMO-miR-16 could be detected in kidney and liver in relatively high levels, whereas lung and spleen displayed levels 500 times lower than the ones found in kidney (**Fig. 31b**). Very interestingly, no AMO-miR-16 could be detected in brain, neither in the PBS-treated animals, nor in the AMO-miR-16 treated animals, suggesting that AMO-miR-16 does not penetrate the blood-brain barrier. The quantification of miR-16-5p in the same tissue homogenates (**Fig. 31c**) resulted in far more elevated miR-16-5p levels in the PBS-treated

animals than in the AMO-miR-16 treated animals. This was however not the case in the brain in which no reduction of miR-16-5p levels could be observed. We subsequently measured miR-191-5p levels to make sure that the lower levels of miR-16-5p in the tissues containing AMO-miR-16 were indeed due to sequestration of miR-16 by AMO-miR-16 (**Fig. 31d**). As expected, no significant differences could be detected in miR-191-5p relative expression levels between tissues isolated from PBS- and AMO-miR-16-treated animals.

Taken together, these data strongly suggest that our CL-qPCR is well suited for the efficient quantification of heavily chemically modified oligonucleotides in *in vivo* studies performed on sampled organs. As a next step, we evaluated the possibility to use WBS-PCR for the detection of AMO-miR-16 injected intravenously and whether results obtained using the classical way of organ sampling could be reproduced by WBS-PCR.

D.2.c) Biodistribution pattern of AMO-miR-16 using WBS-PCR in combination with CL-qPCR

We quantified AMO-miR-16 levels by CL-qPCR and miR-16-5p by RT-qPCR in mouse whole body sections. Both datasets were normalized against genomic 18S (**Fig. 32**).
In order to allow direct comparisons between both mouse sections, signal intensities obtained for each gene were displayed using the same scale. First of all, we noticed that the genomic 18S relative expression levels displayed similar signal intensities in both mice (**Fig. 32, lower panel**), indicating similar extraction efficiencies in both sections. As expected, we could only detect AMO-miR-16 in the AMO-miR-16 treated animal (**Fig. 32, left-hand side**), whereas no signal could be detected by CL-qPCR in the PBS-treated animal (**Fig. 32, right-hand side**). The AMO-miR-16 biodistribution pattern indicated the presence of mild levels of AMO-miR-16 in most organs of the treated mouse, and high amounts of AMO-miR-16 in the kidney, and in a lesser extent in liver. Interestingly, we could not detect any AMO-miR-16 in the brain region, an observation that was already made on tissue lysates. Furthermore, these observations are in accordance with published data using LC-MS measurements in organs sampled from a rat injected with a PO-MOE modified oligonucleotide targeting the human intercellular adhesion molecule-1 mRNA ([93](#)).
We also investigated whether we could see a difference in miR-16-5p levels between both animals, and very much to our surprise, we could observe strikingly lower miR-16-5p relative expression signals across the section of the AMO-miR-16 treated animal, compared to the PBS treated animal. In addition to this, there were still a few organs showing quite elevated miR-16-5p levels in the AMO-miR-16 treated animal, such as lung, a blood vessel close to the salivary gland, liver, heart, and brain. In the case of the brain, this could of course be explained by the absence of AMO-miR-16 in the brain as could already be previously seen in sampled organs. The presence of miR-16 in the other tissues could also be seen in the previous experiment, and although the bar graphs used gave the impression of a complete knock-down of miR-16-5p, there was only a reduction of the expression levels of this miRNA of approximately 50-fold, which explains why miR-16-5p could be visualized in some tissues of the AMO-miR-16-treated mouse section.
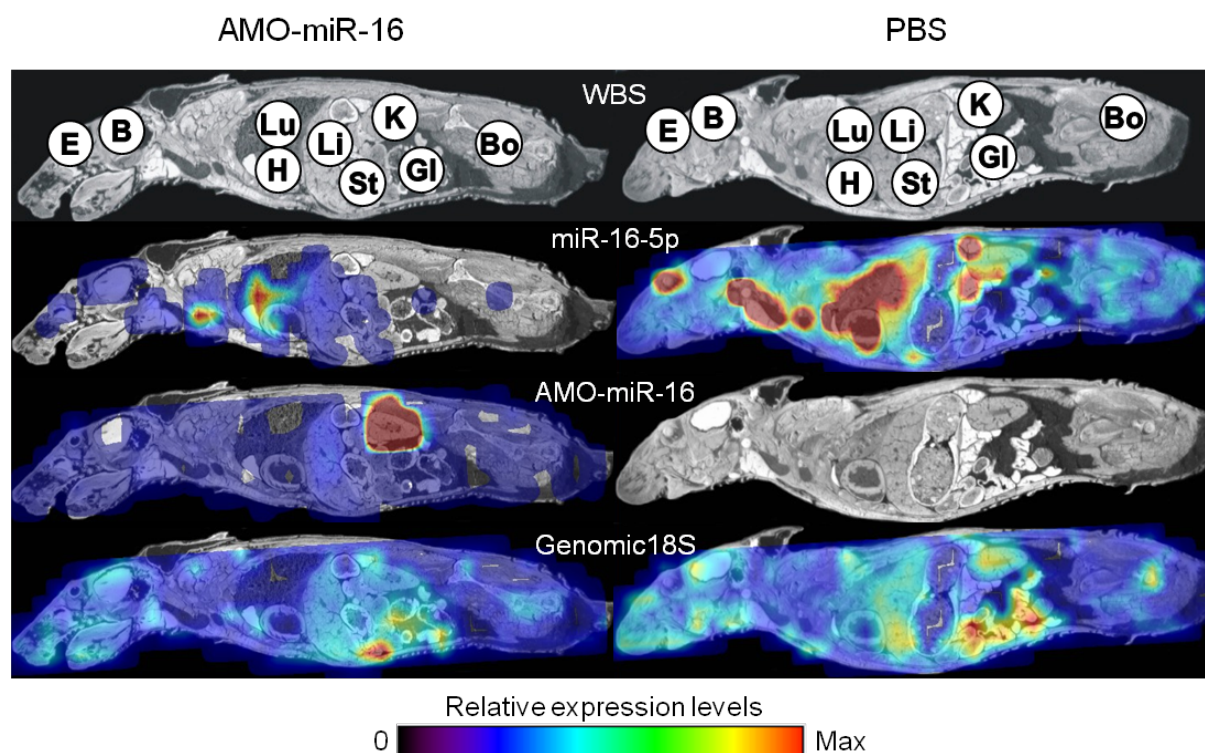
Figure 32: *AMO-miR-16* in vivo *biodistribution monitored by CL-qPCR. The eye (**E**), brain (**B**), heart (**H**), lung (**Lu**), liver (**Li**), stomach (**St**), kidney (**K**), gastro-intestinal tract (**GI**) and bone (**Bo**) are indicated on the Whole Body Section picture (**upper panel**)*

With this study we could show that (*i*) the CL-qPCR can be combined with WBS-PCR in order to monitor the *in vivo* biodistribution of heavily chemically modified oligonucleotides, and (*ii*) that WBS-PCR resulted in the same observations as the classical way of sampling individual organs.

E.   Conclusion/Discussion

First of all, the miRNA RT-qPCR that we developed benefits from many advantages. Indeed, not only does this assay display similar characteristics to commercially available assays in terms of sensitivity and specificity, but it also offers more flexibility to the user. Reagents can easily be designed for any given target, without the need to disclose any sequence of therapeutic interest to the companies offering to generate custom-made reagents. Furthermore, the characterization of the reagents on a synthetic target can be performed in a relatively easy and straight forward manner. The similarities between miRNA and siRNA design makes this assay compatible for the detection of siRNAs. The truncation of the template sequence can nevertheless severely impact the sensitivity of the RT-qPCR, rendering truncated siRNAs barely detectable by RT-qPCR. This can be problematic for the detection of full-length oligonucleotides by WBS-PCR especially when considering the fact that unformulated and non-modified siRNAs are degraded within minutes *in vivo* ([40](#)). In the case of an unformulated or unmodified oligonucleotide, WBS-PCR has to be performed no later than 10 minutes. Being able to detect full-length, and therefore potentially biologically active siRNAs in *in vivo* samples rather than truncated molecules, can on the other hand be considered as an advantage. Despite this advantage, it then becomes quite difficult to monitor the fate of a metabolized siRNA. As it can be seen in this study, radioactive labeling does not allow the discrimination between full-length and metabolized oligonucleotides, but is a very powerful method to provide

information with respect to the location of full-length oligonucleotides and their metabolites. The sum of information provided by both methods can be highly valuable, since it allows the identification tissues where full-length oligonucleotides and their metabolites accumulate (QWBA), and where full-length and therefore functional oligonucleotides might display a biological function (WBS-PCR).

We also developed an assay based on template mediated chemical ligation for the quantification of heavily chemically modified oligonucleotides, which are otherwise undetectable by RT-qPCR. Although the sensitivity of this method seems to be a bit lower than the sensitivity achievable by RT-qPCR, it is an efficient way to detect chemical formats such as 2'-MOE modified oligonucleotides, which are incompatible with conventional or modified PCR enzymes (94). This method allows the quantification of oligonucleotides in a completely independent manner from the chemical format applied to the oligonucleotides since it is based on DNA-RNA hybridization. Moreover, the coupling of chemical ligation with a qPCR readout allows to achieve a greater sensitivity level compared to methods making use of other amplification methods such as rolling circle amplification (95).

Last but not least, the efficiency of WBS-PCR could be successfully demonstrated in biodistribution studies of various RNA species such as mRNAs, miRNAs and siRNAs, as well as heavily chemically modified oligonucleotides. Extraction procedures using tissue sections overlaid on plates filled with lysis buffer have already been investigated by Armani et al and reported as 2D-RT-qPCR (96). However, unlike WBS-PCR, this method only focuses on the sections of a few organs and not on whole body sections, therefore the resolution offered by this method is not as high as the one offered by a 1536-well plate as in the case of WBS-PCR. Furthermore, the extraction method described in this paper, based on poly-T-coupled magnetic beads does not allow the recovery of all kinds of RNA molecules, as well as the recovery of genomic material, thereby limiting the target spectrum.

In order to perform WBS-PCR studies, it was also crucial to determine an efficient normalization method to be able to draw conclusions on relative quantifications of oligonucleotides. Unlike RNA purification with Trizol, the samples generated for WBS-PCR could not be normalized on account of their RNA concentrations. Furthermore, the fact that the samples covered a whole mouse section did not allow the use of house-keeping mRNAs since too many variations could be introduced by the various cell densities, extraction efficiencies and translational status of various tissues.

We could also identify the WBS-PCR as an efficient method to unravel mRNAs expression patterns, since the amount of information that can be obtained from one WBS-PCR run is more considerable than what can be derived from RT-qPCR runs performed on individually isolated organs. A WBS-PCR run covers indeed all the organs that can be found in a mouse section, whereas RT-qPCRs on single organs are often biased by the organs selected in the *in vivo* study.

Furthermore, not only were our WBS-PCR results comparable to results obtained with QWBA, but the observations made by WBS-PCR could also be confirmed in tissue homogenates, showing the high predictability potential of this method. Even if it can be considered as yet another sampling method, one WBS-PCR run provides more information than conventional organ sampling since with 5 whole body sections, it is possible to cover every organ of a mouse body. Furthermore, the preparation procedure is less harmful to the organs since the mice were deep-frozen right after sacrifice, preventing the degradation of RNAs and siRNAs that could have occurred during conventional organs sampling. The number of organs covered by a WBS-PCR run also allows the reduction of

biases induced by arbitrarily choosing organs to be sampled when performing an *in vivo* biodistribution study on a compound with unknown homing characteristics. In that sense, WBS-PCR can be used as a preliminary characterization step to define the homing properties of a therapeutic oligonucleotide, and once the biodistribution of an oligonucleotide has been unraveled, further *in vivo* experiments can be focused on only the organs in which the compound could be detected. The resolution of the WBS-PCR, dictated by the size of the plates used for lysis, in our case 1536-well plate, is not competing yet with other methods such as in situ hybridization. However, such a format can easily be automated using liquid handling robots, thereby increasing the throughput of this method for the screening of novel oligonucleotides delivery methods with unknown homing properties. WBS-PCR can therefore be of great help for the determination of the biodistribution of siRNAs delivered using novel delivery vehicles ([51]).

V. Evaluation of the potential use of exosomes as novel siRNA delivery vehicles

A. Introduction

As discussed previously, efficient and tissue-targeted delivery of siRNAs is still a very challenging feature or RNAi therapeutics ([97]). Although various methods have already been investigated to deliver siRNA *in vivo* ([98]), it is interesting to note that many cells produce vesicles displaying tissue-homing properties ([99]) that could be more than helpful to deliver therapeutic oligonucleotides in a tissue-specific manner. It has already been shown that small vesicles called exosomes are capable or conveying functional miRNAs ([50]). Furthermore, it is possible to modify the tissue-specific homing of these exosomes by adding viral peptides showing a given tissue-specific tropism, allowing the development of a broader spectrum of tissue-specific drug delivery vehicles ([48]).

Exosomes are small lipidic vesicles secreted by many different kinds of cells, and able to withstand the harsh conditions found in blood circulations. They were first observed during sheep reticulocyte differentiation, during which the authors have noticed the transfer of transferrin receptor activity from cells to small vesicles excreted by the cells ([100],[101]). Despite the absence of a clear consensus on the molecular, biochemical and anatomical descriptions of exosomes, some trends emerge from the many studies aiming at unraveling the function of exosomes ([102-109]). According to these studies, exosomes are 60-150 nm large spherical micro-vesicles enriched in various proteins, such as Lamp2b, Alix, CD63, and displaying various miRNAs such as miR-16-5p for example ([110]). Many studies are focused on unraveling the role of exosomes in inter-cellular transfer of nucleic acids, and more precisely miRNAs ([50],[111],[112]). These studies suggest that it might be possible to transfer small RNA molecules, i.e. therapeutic oligonucleotides, in a tissue-specific manner by engineering exosomal membrane proteins. However, prior to achieving this goal, many challenges have to be overcome with respect to exosomes isolation and characterization, especially given the high level of characterization that any *in vivo* injected material must undergo, from both an ethical and from an experimental point of view.

In order to establish protocols for the *in vivo* delivery of exosomes, it is essential to make sure that the entities isolated are indeed exosomes. One part of this work therefore aims at investigating the use of various methods for the characterization of exosomes, including qPCR-based detection of miRNAs, western-blotting against exosomal proteins, as well as size measurement by dynamic light-scattering.

Besides the difficulty to demonstrate the presence of exosomes in an absolute manner in a sample, there is the recurrent concern of determining the best exosomes isolation process.

The second part of this thesis therefore aims at testing a few methods amongst the most popular isolation processes used in the exosomes field, such as precipitation methods, differential ultracentrifugation, as well as particle size separation methods. The ideal exosomes isolation procedure should consist of as few handling steps as possible, while generating highly pure exosomes preparations.

B. Characterization of differential ultracentrifugation, the most common exosome isolation procedure

B.1. Evaluation of the necessity of a linear sucrose gradient for exosomes isolation

Differential ultracentrifugation has been established as a method of choice to isolate pure exosomes ([113]). This method, already used for the fractionation of cellular organelles ([114]), takes advantage of the capability of centrifugation to separate particles according to their weight and size by the mean of centrifugal forces. This isolation procedure consists in sequential centrifugation and ultracentrifugation steps aiming at sorting out vesicles from cell culture supernatant and can be performed with or without sucrose gradient (**Fig. 33**).

First, it is necessary to remove dead cells and cell debris present in the culture supernatant by subjecting it to low speed centrifugations and discarding the pellet. The supernatant is subsequently subjected to an ultracentrifugation step at 100,000g for 1 hour, to allow the pelleting of exosomes. After resuspension in a saline buffer like PBS, the exosomes are ready for characterization or further use. In order to confirm the presence of exosomes, this pelleted material can be run on a linear sucrose gradient allowing a thorough analysis of the exosomal markers ([115]). Most papers found in the literature therefore use the linear sucrose gradient only as a mean to confirm the presence of exosomes in a sample, such as a study performed by Chen et al ([115]). In this work, the author ran the exosome pellet on a linear sucrose gradient and shows presence of exosomes in his sample by showing the presence of various exosome markers such as CD63 or MHC-1 proteins. He then used the previously obtained exosomes pellet for his subsequent work.

However, the author can not be sure that his exosome sample does not contain any other contaminating protein. That is why we performed a small study to evaluate whether the linear sucrose gradient could indeed only be used during exosomes characterization, or whether it would be preferential to integrate this gradient in the exosomes isolation procedure.

*Figure 33: Differential ultracentrifugation protocols for exosomes isolation. Two protocols were tested, one without linear sucrose gradient (**a**) and one with a linear sucrose gradient (**b**)*

We subjected HeLa cell culture supernatant to ultracentrifugation without (**Fig. 33a**) or with a linear sucrose gradient step (**Fig. 33b**). In order to compare both exosomes preparation methods, we selected a parameter easy to monitor, which is particle size, and which appears to be a hallmark of exosomes, namely their size, comprised between 50 and 100 nm ([116]). To monitor the particle size distribution of the exosome preparations we used a technique called Dynamic Light Scattering (DLS). DLS is a physics technique making use of the scattering patterns observed when light meets on reflects on small particles. The integration of these measurements subsequently allows the determination of the size of the particles present in the analyzed solution ([117]).

The samples we analyzed consist of cell culture supernatant prior to ultracentrifugation, resuspended material from a 100,000 g centrifugation step, and the fractions of a linear sucrose gradient performed on the pelleted material obtained after a 100,000 g centrifugation step (**Fig. 34**).

Every sample was measured at least 3 successive times. Non overlapped profiles indicate an unstable solution or a highly non-homogeneous solution most likely presenting

sedimentation or aggregation events, this is why a slight shift can be observed across the measurements towards the detection of particles displaying on average a larger size.

The particle size determination obtained for an unprocessed medium (**Fig. 34a**) sample displayed predominantly particles with a size around 8 to 10 nm, as well as two minor peaks around 60 to 70 nm, and around 200 nm. This shows that an unprocessed cell culture supernatant contains a broad spectrum of particle sizes indicating a highly heterogeneous sample. Subjecting this conditioned medium to a 100,000 g ultracentrifugation step showed a shift of particle sizes towards bigger particles, predominantly around 300 to 500 nm as well as a minor peak around 80 to 100 nm (**Fig. 34b**). These two particle size distribution patterns indicate that a 100,000 g centrifugation step results in an enrichment of two groups of particles one of which displays a size range close to the one expected for exosomes. However, these particles seemed to be in minority compared to the other particles displaying larger sizes. This is why we overlaid this pelleted material on a discontinuous linear sucrose gradient, and determined whether we could enrich the sample in particles displaying the expected size of 80 to 100 nm (**Fig. 34c-j**).
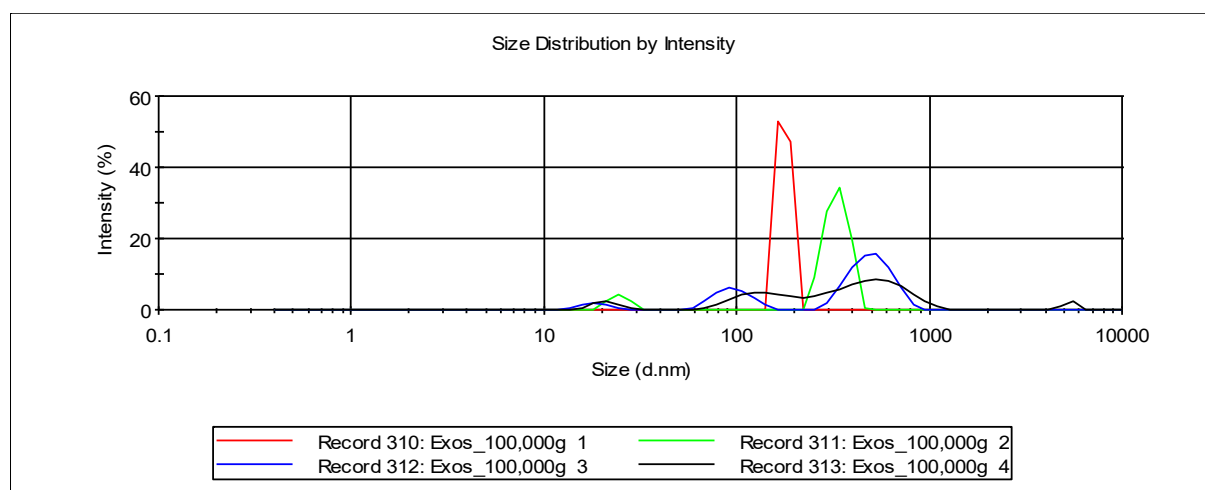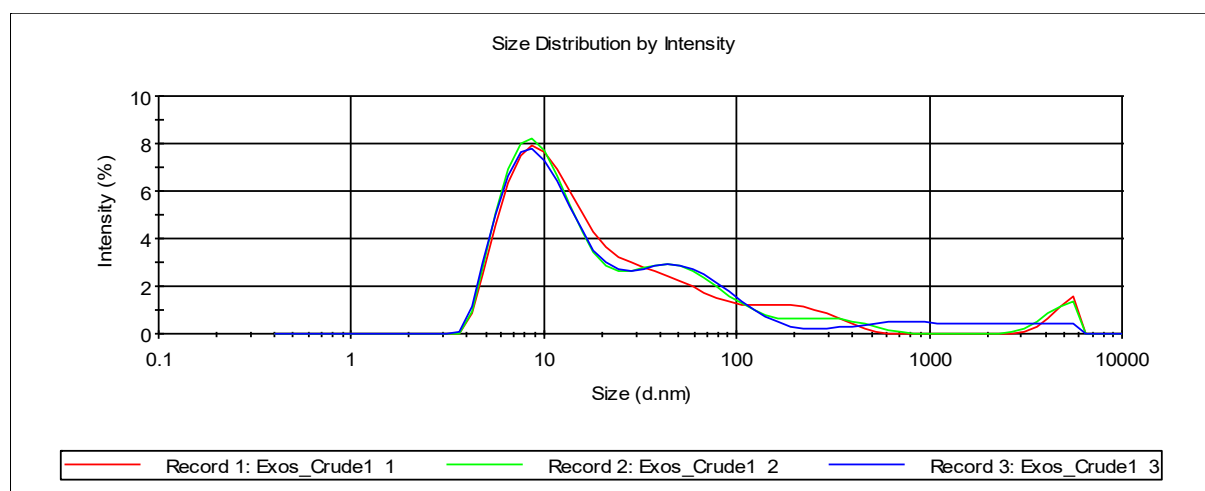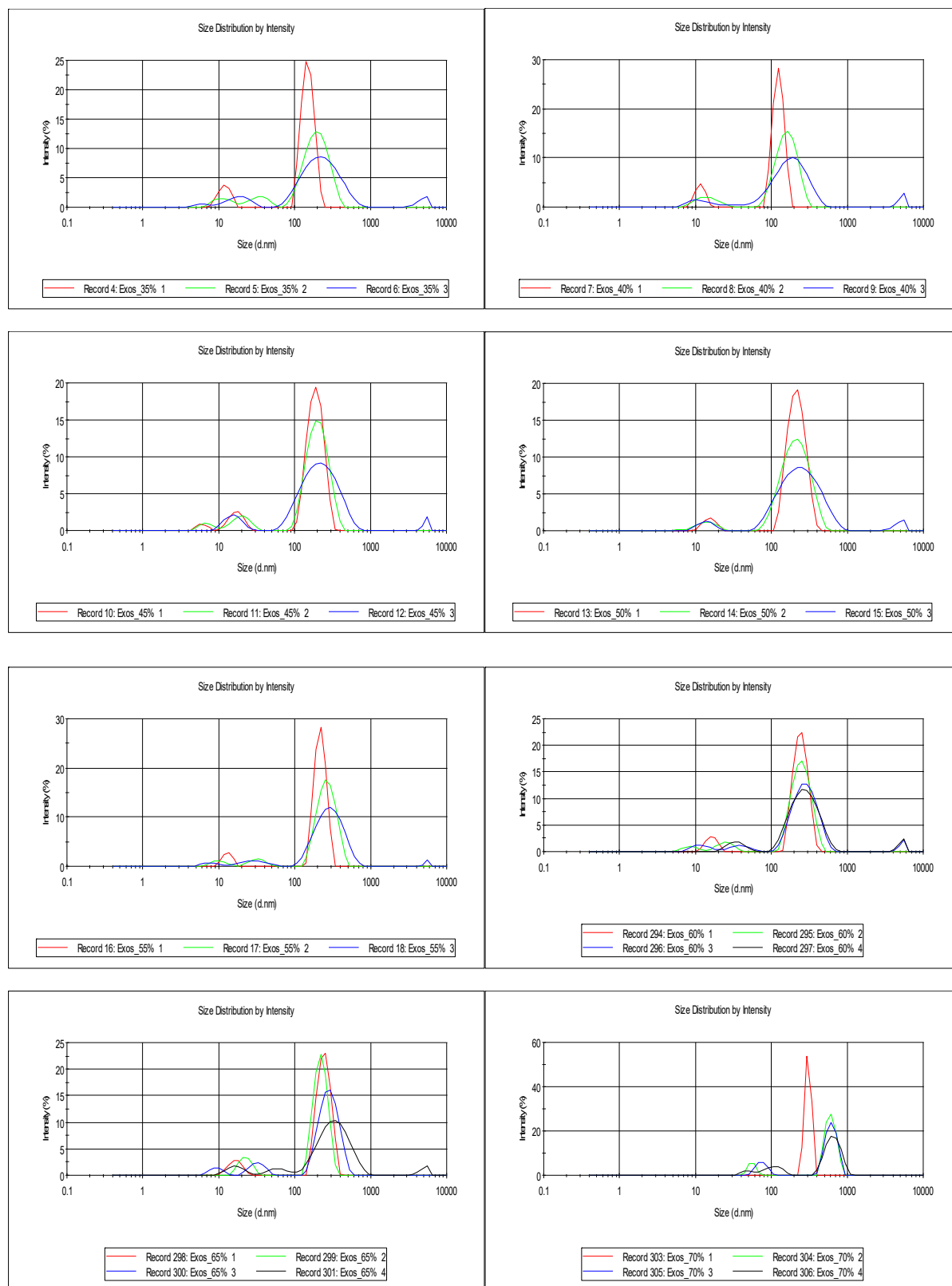
Figure 34: *Particle size distribution of samples prepared by ultracentrifugation. Cell culture supernatant was subjected to DLS measurements prior to any centrifugation (**a**), or after having undergone a centrifugation step at 100,000 g (**b**). Pelleted material was subsequently overlaid on a linear sucrose gradient, and the fractions of the gradient were subjected to DLS measurements (**c-j**). The samples are shown according to the fraction of the sucrose gradient they were in, going from 35% sucrose (**c**) to 70% sucrose (**j**)*

The correct establishment of the gradient could be monitored by the disappearance of the interphases located between each of the overlaid sucrose fractions. The particles present

in the 70% sucrose fraction (**Fig. 34j**) displayed a size around 600 to 700 nm, whereas the particles isolated from other fractions of the linear sucrose gradient displayed a size around 200 nm, independent of the sucrose content (**Fig. 34c-i**). Although exosomes are expected to display a density allowing them to be enriched in fractions containing 40 to 60% sucrose ([118]), there was no correlation between sucrose concentration and particle size in this study. However, the fact that we could see a selective enrichment in particles displaying a size around 200 nm, as well as the fact that the particle size distribution profiles indicated homogeneous samples because of the overlapping profiles, prompted us to conclude that an efficient exosomes isolation process can only benefit from the addition of a linear sucrose gradient. This linear sucrose gradient should however not be used only for exosomes characterization as it can be seen in some studies, but rather as an essential preparative step.

As to the use of dynamic light scattering as an exosomes quality control, the fact that the particle size distribution did not change as a function of sucrose concentration led us to hypothesize that particle size determination was not an ideal characterization method for exosomes and could not be used on its own as an efficient way to assess the presence of exosomes in a given sample.

B.2. Molecular biological characterization of exosomes by triton-dependent detection of miRNAs and siRNAs

A.1.a) Triton-dependent detection of miR-16-5p in exosome samples

The accumulation of evidences showing the presence of various mRNAs and miRNAs in exosomes and the role of exosomes in inter-cellular communication via transfer of RNAs prompted us to develop an assay based on the RT-qPCR detection of exosomal RNAs ([111],[119],[120]).
Since a common method used to investigate the encapsulation of siRNAs in Lipid Nanoparticles (LNP) consists in a Triton-dependent siRNA detection ([121]), we applied our in-house developed miRNA RT-qPCR method to exosome samples subjected or not to Triton-mediated solubilization. The detection of miRNAs in Triton-treated exosomes samples vs. untreated exosomes samples should therefore allow us to assess the presence of exosomal miRNAs in a sample.
According to a study by Gibbings et al ([122]), the major constituent of the exosomal miRNome is miR-16-5p. We therefore designed RT-qPCR primers against miR-16-5p and used Triton-X-100 to release the exosomal content, and thus make it available for RT-qPCR-based detection. Exosomes were prepared by differential ultracentrifugation followed by a linear sucrose gradient step (**Fig. 33b** on page **49**).
In order to benchmark the Triton-X-100 dependent detection of miR-16-5p, we diluted fractions from the sucrose gradient 1:2 in either TCEP Lysis Buffer containing Triton-X-100 or PBS as a negative control, since PBS should not be able to release the exosomal content. The samples were subsequently diluted 1:5 or 1:10 in DEPC-treated water to avoid buffer-mediated inhibition of the RT-qPCR reaction (**Fig. 35**).

Figure 35: Triton-X-100 dependent miR-16-5p quantification by RT-qPCR. Bar graph showing the miR-16-5p quantities detected in each fraction of the sucrose gradient, treated either with PBS (grey) or with Triton and diluted 1:5 (dark blue) or 1:10 (light blue) in DEPC water

Only the samples treated with TCEP Lysis Buffer supplemented with Triton-X-100 displayed detectable amounts of miR-16, whereas signals obtained for the PBS-treated samples were non-detectable.

An average 2-fold difference in miR-16 levels observed between the 1:5 and 1:10 diluted lysed exosomes indicated that the PCR amplification did not suffer from the inhibitory elements present in the lysis buffer. In all following experiments the lysates were diluted 1:10 in DEPC water prior to RT-qPCR measurements.

Unfortunately this profile was not completely satisfactory, since exosomes are supposed to be contained in the fractions containing 40 to 60% sucrose (118). Although a slight increase in miR-16 signals could be observed in the fractions containing 40 to 70% sucrose, this observation did not appear to be significant, since the levels were barely higher in these fractions than the ones detected in the 10 to 35% sucrose fractions.

As a next step, we also tested the possibility to detect a less abundant exosomal miRNA, namely miR-191-5p, in a Triton-dependent manner (122). Unfortunately, we were unable to detect miR-191-5p in any of these samples. This can be explained by the fact that the amount of exosomes recovered by differential ultracentrifugation was too low to allow the detection of a low abundant miRNA. The low amounts of exosomes in the samples could also be confirmed by the fact that the highly abundant exosomal miRNA miR-16-5p could only by detected in limited amounts.

To confirm this hypothesis we repeated this experiment by increasing the amount of starting material, in our case HeLa cell culture supernatant, subjected to differential ultracentrifugation (**Fig. 36**).

Figure 36: Triton-dependent detection of miR-16-5p in fractions of a sucrose gradient used for exosomes preparation

The profile obtained for the quantification of miR-16-5p in figure **36** shows an increase in signals in fractions containing 40 to 60% sucrose, precisely the fractions reported to contain exosomes (118). Moreover the signals measured in these fractions are Triton-X-100 sensitive, since the same fractions treated with PBS did not display any signal. An interesting fraction though is the fraction containing 70% sucrose, located at the bottom of the tube during the ultracentrifugation step allowing the establishment of the sucrose gradient. The fact that this fraction displays such a high miR-16 level may be explained by either the presence of smaller vesicles containing miR-16 not floating at the same density as exosomes, or by the existence of a Triton-sensitive protein complex containing miR-16.

Taken together these data suggest that it is possible to isolate Triton X-100-sensitive entities containing miR-16-5p by subjecting cell culture medium to differential ultracentrifugation followed by a linear sucrose gradient. Further characterization was required to confirm the presence of exosomes in the fractions of the sucrose gradient.

A.1.b) Triton-dependent detection of a YFP siRNA encapsulated in exosomes

The capability to detect an endogenous miRNA encapsulated in exosomes in a Triton-sensitive manner prompted us to pursue the detection of exogenous oligonucleotides in exosomes. We therefore tested the capability of cells to pack a siRNA into exosomes by transforming HeLa cells with a plasmid encoding a shRNA targeting YFP. The YFP shRNA

was selected in order to perform exosomes transfer experiments in a YFP-expressing HeLa cell line we had at our disposal.

After their transformation, we subjected HeLa cells conditioned medium to exosomes isolation by differential ultracentrifugation, and quantified both miR-16-5p and the YFP siRNA by Triton-sensitive RT-qPCR (**Fig. 37**).
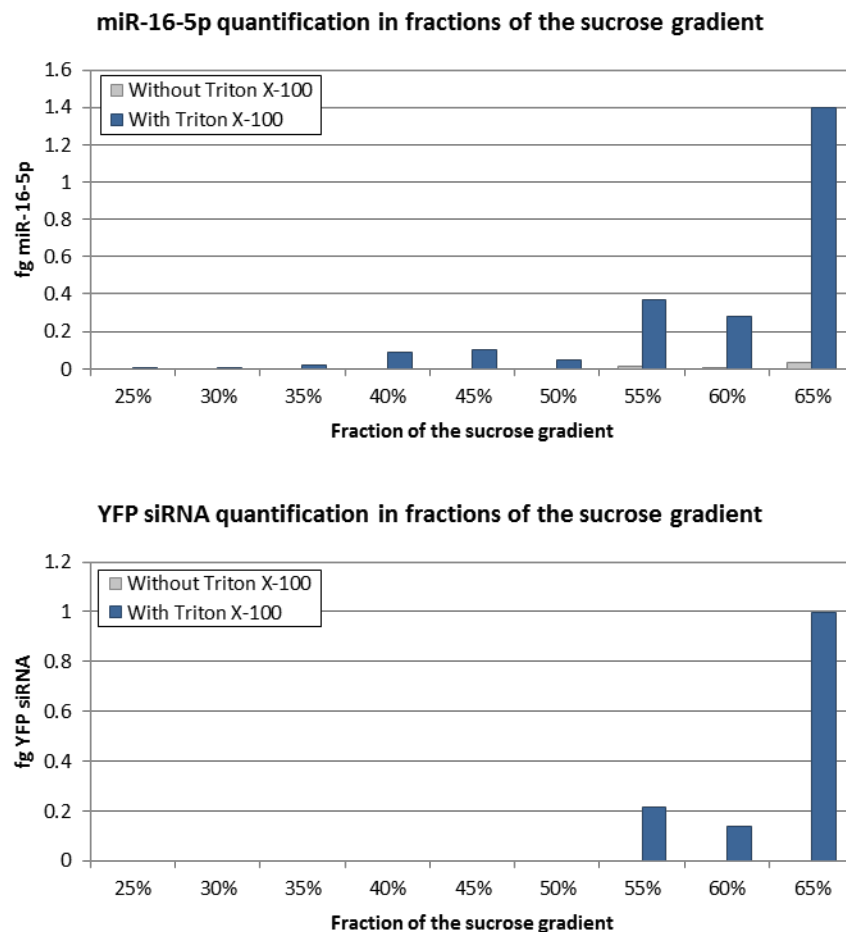
Figure 37: Triton-dependent detection of miR-16-5p and YFP siRNA in fractions of a sucrose gradient used for exosomes preparation

Both miR-16-5p and the YFP siRNA could be detected in a Triton-sensitive manner in fractions from the linear sucrose gradient. Both targets could be detected in higher amounts in the fraction containing 55, 60 and 65%. In the case of the YFP siRNA however, the amounts obtained were lower than the ones obtained for miR-16-5p, but since they vary by only 2-fold, this difference could be due to the error range of the PCR reaction.

Performing this experiment suggested that it was possible to encapsulate a siRNA in exosomes by transforming a cell line with the according shRNA.
Transwell assays aiming at showing the transfer of this YFP siRNA to a recipient YFP-expressing HeLa cell line unfortunately did not show any variations in the expression level of the YFP mRNA in the recipient cell line. This might suggest that even encapsulation of an siRNA in exosomes is possible, delivery of the siRNA via exosomes might be not efficient enough to promote the knock-down of an mRNA, or that the siRNA

amounts present in these exosomes were too low to enable efficient knock-down of the target mRNA.

B.3. Proteomic characterization of exosomes by detection of exosomal proteins

In the previous section we discussed the possibility to use the exosomal miRNome as an indication of the presence of exosomes. Even though we could detect miR-16-5p in a Triton-dependent manner, this only shows that we isolated a detergent-sensitive entity containing miR-16-5p. In order to make sure that we indeed isolated exosomes, we had to show that the fractions displaying high miR-16-5p levels also showed presence of exosomal protein markers. In order to select an exosomal protein marker we used the ExoCarta database, which offers a compilation of every RNAs and proteins reported to be present in exosomes ([110]). Although several surface proteins are described as "exosomes markers", we decided to use a protein located in the exosomes, or a protein known to interact with a protein known to be present in the exosomes. This way, we hoped to decrease the risk of false positives that could occur by using a surface protein which could otherwise be present on a variety of cellular vesicles. During our investigations we identified the Endosomal Sorting Complex Required for Transport (ESCRT) as a key player in the selection of exosomes content ([123],[124]). However this protein complex is located on the membrane of Multivesicular Bodies (MVB), and is most of the time not included in exosomes. Therefore we investigated the use of an ESCRT associated proteins, namely the Programmed Cell Death 6 Interacting Protein (PDCD6IP), also known as Alix, as an exosomal marker ([125-127]). Interestingly this protein is one of the most used exosomal markers in the studies listed in the ExoCarta, further validating our idea to use Alix as exosomal marker.

In order to better correlate our previous observations with respect to miR-16-5p Triton-dependent detection with the presence of exosomes, we subjected cell culture supernatant to differential ultracentrifugation. The fractions of the sucrose gradient were subsequently analyzed by RT-qPCR, as described previously, and by western-blot to check for the presence of Alix. The differential ultracentrifugation protocol was performed on the cell culture medium obtained from two different cell lines, namely HeLa cells and MS1 cells, previously shown to secrete exosomes (unpublished data, Bonenfant et al).

While the HeLa cell culture supernatant was used only to benchmark the exosome characterization methods, the use of MS1 cell culture supernatant was motivated by the possibility to perform mouse *in vivo* studies, requiring the use of exosomes of murine origin to minimize immune responses induced by exosomes ([128]).

A.1.a) Characterization of exosomes isolated from HeLa cell culture medium

We followed the same procedure as the one already described in the previous section, namely that we tested the Triton-dependent quantification of miR-16-5p in each fraction of the sucrose gradient and we subsequently performed a western-blot using an anti-Alix antibody on the same fractions (**Fig. 38**). The miR-16 profile obtained in this experiment is showing increased miR-16 levels in the fractions containing 45 and 60% sucrose compared to the other fractions (**Fig. 38, upper panel**). However, in these two fractions we also observed relatively high miR-16 levels when the sample was treated with PBS. This indicates a high level of non-encapsulated miR-16-5p, suggesting either the existence of a subpopulation of miR-16-5p molecules which are not associated with exosomes, or that sample handling during differential ultracentrifugation procedure mechanically disrupts exosomes, and therefore releases miR-16-5p.

miR-16-5p quantification in exosomes isolated from HeLa cell culture supernatant

Averages +/- STDEV, n=3
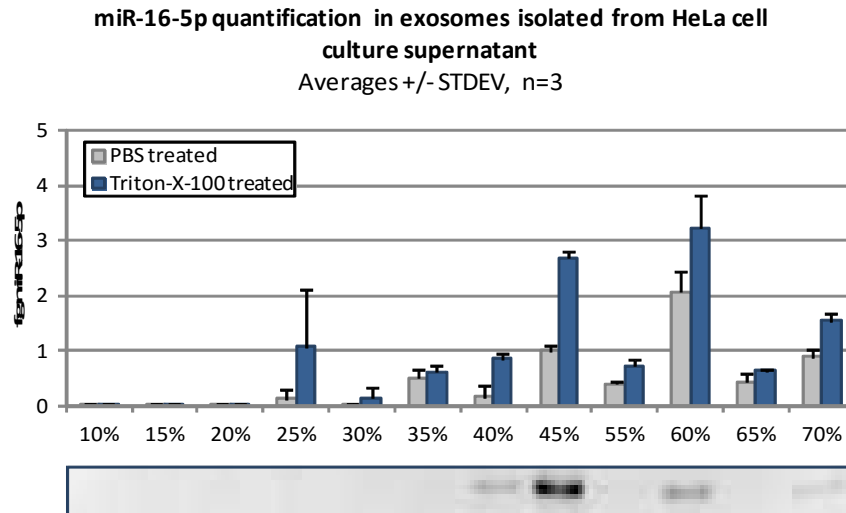
Figure 38: Correlation between miR-16 positive signals and Alix protein detection by Western-blot in HeLa cell culture supernatant. Triton-sensitive quantification of miR-16-5p (upper panel) and western blot with an Anti-Alix antibody (lower panel)

Western blot analysis against Alix (**Fig. 38, lower panel**) correlated with miR-16 positive sucrose gradient fractions, namely in the fractions containing 45 and 60% sucrose, but in a lesser extent in the fractions containing 40 and 70% sucrose. After a closer examination of the miR-16 quantification results, we noticed that high levels of miR-16 are not enough to show the presence of exosomes, but that the signal difference between PBS- and Triton-treated samples is a better indicator of the presence of exosomes in a given sample.

In summary this data seems to indicate presence of exosomes given the observed correlation between triton-dependent miR-16 detection and western blot results obtained for Alix.

A.1.b) Characterization of exosomes isolated from MS1 cell culture medium

The miR-16-5p profile obtained in exosomes samples prepared from MS1 cell culture medium is a perfect example of what is expected from such an experiment, namely that miR-16 levels should display a gauss curve-like distribution centered on 40-50% sucrose, and that signals obtained for PBS-treated samples should remain relatively low (**Fig. 39, upper panel**).

Moreover, as it could be shown in the previous experiment, a western blot performed on these samples targeting Alix showed signals in the fractions which were shown to be miR-16 positive (**Fig. 39, lower panel**), thereby confirming the presence of exosomes in these fractions of the sucrose gradient.
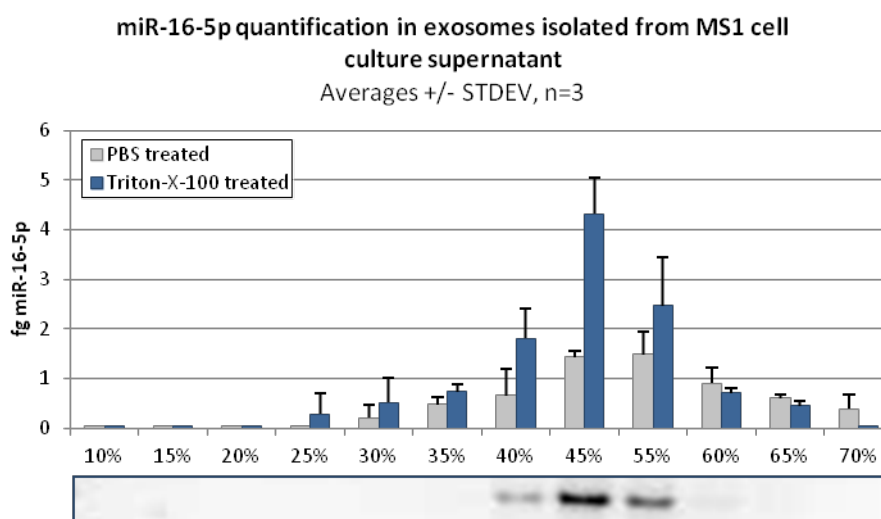
Figure 39: *Triton-sensitive quantification of miR-16 in fractions of a sucrose gradient performed using MS1 cell culture supernatant (upper panel) and western blot using an Anti-Alix antibody (lower panel)*

As a conclusion, we could successfully show the possibility to use Triton-dependent detection of miR-16-5p as an assay to demonstrate presence of exosomes in a given sample, since only the miR-16 positive samples did show detectable and significant amounts of Alix protein. The other advantage of RT-qPCR over western-blot for the characterization of exosomes preparations is the higher speed and less handling steps required for sample analysis. RT-qPCR is however not a perfect tool either, since a high amount of the isolated material is required for this analysis step. Samples characterization using non-invasive methods such as DLS could also not be used on their own, because of the low amount of information they provide. A good compromise could reside in the combination of particle size determination and Triton-dependent detection of miRNAs abundant in exosomes, since this would give us the possibility to monitor two important characteristics of the exosomes.

Although the exosomes analytics has been established, the exosomes isolation procedure based on differential ultracentrifugation is still questionable. Among the various experiments performed with this technique it was almost impossible to obtain twice the same miR-16-5p detection profile, indicating the low reproducibility of this technique. Moreover the detection of miR-16-5p in samples which were not treated with Triton-X-100 tends to suggest that this isolation procedure damages the exosomes to the point of releasing their content because of the intermediate handling steps and high centrifugal forces. Moreover, since the aim of these studies is to generate exosomes for *in vivo* applications, and since this protocol requires a high hands-on level, it would be a challenge to adapt this method to the sterile and highly controlled conditions required for *in vivo* experimentation. Furthermore, this protocol displays a rather elevated batch-to-batch variation level, unsuited to comparative *in vivo* studies. It is therefore crucial to identify a highly reproducible and sterile exosomes isolation method, other than differential ultracentrifugation.

C. Use of particle size-based isolation methods for exosomes isolation

Methods allowing the purification of liposomes in sterile conditions to perform *in vivo* silencing studies using LNP-siRNA complexes offer characteristics that could be

applicable to exosomes isolation. Tangential Flow Filtration (TFF) for instance, frequently used for the purification of LNP-encapsulated siRNAs ([129](#)), could be used for exosomes isolation.

In this section, we therefore tested TFF as well as ultrafiltration, another method based on particle size separation, taking advantage of the characteristic size of exosomes.

C.1. Exosomes isolation by ultrafiltration

In order to test the potential of ultrafiltration we tested two different ultrafiltration devices from Pall, one with a 100 kDa cut-off membrane, and one with a 300 kDa cut-off membrane. Both devices were tested on cell culture supernatant from two different cell lines, HeLa cell line and a human monocyte derived dendritic cell line. The advantage of these devices is the possibility to select and enrich a sample in particles of a given size, but also to use far lower centrifugal forces than the ones required in differential ultracentrifugation procedures. Briefly, these devices are composed of two compartments separated by a membrane characterized by its pore size and the molecular weight of the molecules it will be able to retain. The solution to process is added to the top compartment, onto the membrane, and the device is subsequently submitted to centrifugation at maximum 3,000 g. The liquid will end up in the bottom compartment, containing all particles smaller than the molecular weight cut-off of the membrane and is called the flow-through. All particles bigger than the molecular weight cut-off of the membrane will on the other hand be retained by the membrane, and this solution will be called the retentate. The flow-throughs and retentates were subjected to exosomes analytics by particle size determination and Triton-dependent miR-16-5p detection.

A.1.c) Ultrafiltration of HeLa cell culture medium

The cell culture supernatant was subjected to ultrafiltration according to the manufacturer's recommendations, using two different molecular weight cut-offs. In both cases the retentate as well as the two flow-throughs were analyzed by Dynamic Light Scattering and tested for their miR-16 content (**Fig. 40 and 41**).

All the samples were subjected to Triton-dependent miR-16 detection by RT-qPCR; however despite the good sensitivity obtained, no miR-16 could be detected in any samples.

The DLS profile of the samples isolated on the 100 kDa cut-off membrane (**Fig. 40a**) interestingly indicated 2 major peaks, centered on 8 and 55 nm as well as a minor peak centered on 300 nm. The flow-throughs (**Fig. 40b-c**) displayed major peaks at 0.8, 8 and 300 nm, confirming the retention of particles with a size around 55 nm.

Figure 40: *Dynamic Light Scattering profiles obtained by purifying HeLa cell culture supernatant with a 100 kDa cut-off ultrafiltration device. **a**: particle sizes profile of the retentate. **b-c**: particle sizes profile of the two flow-throughs*

The results obtained for samples isolated on the 300 kDa cut-off membrane were surprisingly similar, although we could notice the presence of only two major peaks in the retentate fraction (**Fig. 41a**) centered on 8 and 60 nm. In this experiment the flow-throughs (**Fig. 41b-c**) showed as well peaks centered on 0.8 and 8 nm confirming again the retention of 55-60 nm large particles on the membrane.

Figure 41: Dynamic Light Scattering profiles obtained by purifying HeLa cell culture supernatant with a 300 kDa cut-off ultrafiltration device. a: particle sizes profile of the retentate. b-c: particle sizes profile of the two flow-throughs

Taken together, these data indicate the possibility to select particles based on their size in quite a robust fashion. However, since we failed to detect miR-16-5p it is difficult to confirm that the isolated particles were indeed exosomes.

In the previous DLS measurements involving particles isolated from HeLa cell culture supernatant by differential ultracentrifugation, the average size of the particles was around 200 nm. By using ultrafiltration, we isolated 4-fold smaller vesicles, so this could suggest that an event of aggregation or vesicles fusion might occur during ultracentrifugation, thus artificially generating bigger vesicles.

Although it is reported that HeLa cells also secrete exosomes ([130](#)), the amount of exosomes secreted by HeLa cells could be insufficient to perform extensive work using exosomes generated using this cell line. We therefore tested cell culture supernatant from human monocyte derived dendritic cells, a cell line which was more extensively investigated in the exosomes field than HeLa cells, and which supposedly secrete higher amounts of exosomes ([131-133](#)).

A.1.d) Ultrafiltration of monocyte derived dendritic cells (MODC) cell culture supernatant

The cell culture supernatant was subject to the same analysis than the HeLa cell culture supernatant and the results obtained are shown in the figures **42** and **43**.

As in the previous experiment, no miR-16-5p could be detected in these samples, although miR-16-5 is expressed in these cells ([134](#)). The fact that we failed to detect miR-16-5p in the processed samples suggests that the exosomes amount might have been too low to allow detection of this miRNA.

The very first observation that can be made is the very low variability observed between the various measurements indicating a very homogenous sample preparation and stable solutions over time (**Fig. 42a** and **43a**). Only two major peaks could be observed at 8 and 90-100 nm (**Fig. 42a**), whereas the flow-through displayed peaks at 8 and 50 nm and a very broad peak indicating the presence of particles with a size comprised between 200 and 5,000 nm (**Fig. 42b**), thereby confirming the retention of 90-100 nm large particles.
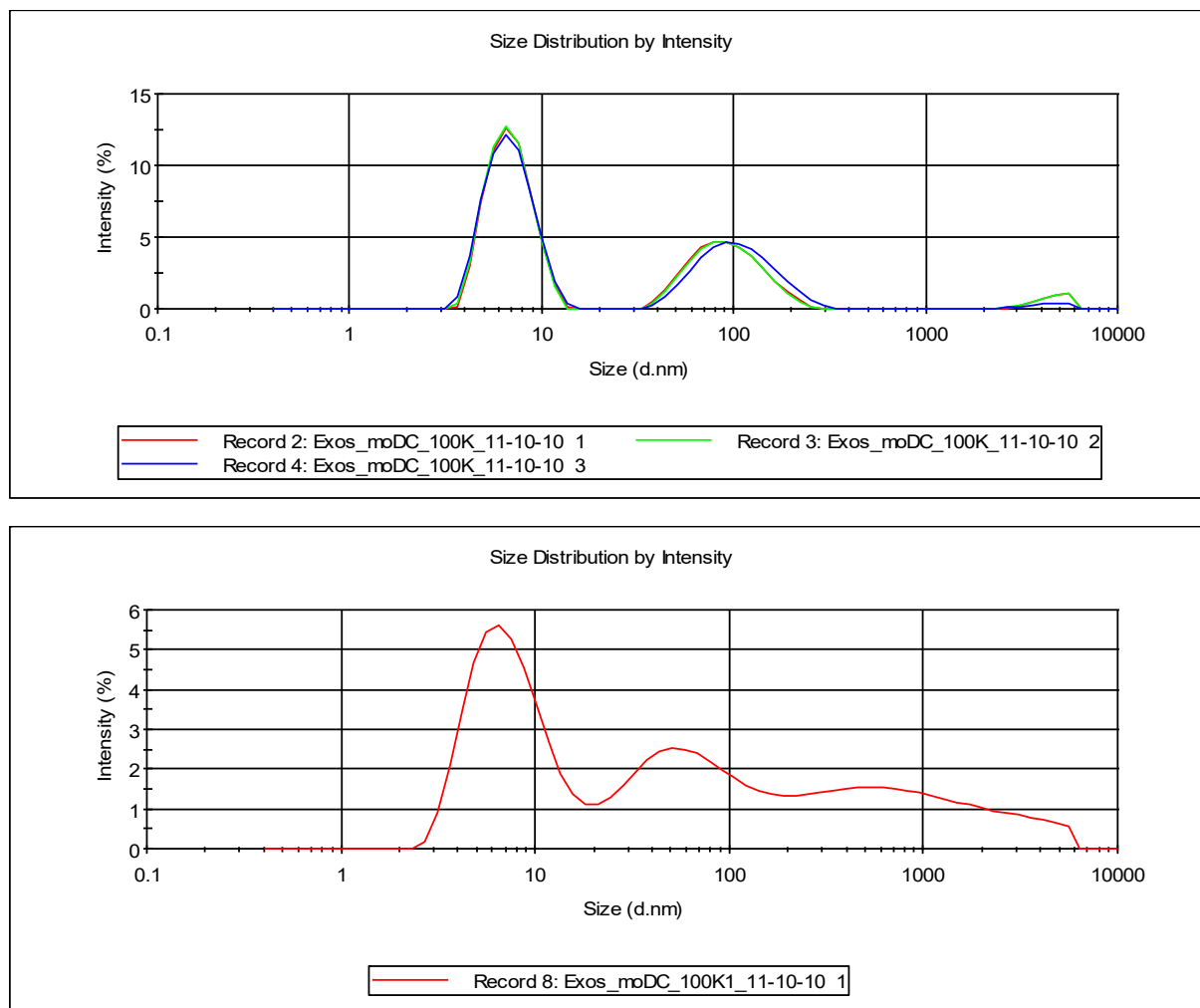
Figure 42*: Dynamic Light Scattering profiles obtained by purifying MODC cell culture supernatant with a 100 kDa cut-off ultrafiltration device. **a**: particle sizes profile of the retentate. **b**: particle sizes profile of the flow-through*

The results obtained with the 300 kDa cut-off membrane were almost identical to the results obtained with the 100 kDa membrane. We indeed observed two major peaks at 8 and 90-100 nm in the retentate (**Fig. 43a**), whereas the flow-through displayed peaks at 0.8, 8 and 200 nm (**Fig. 43b**).

The presence of the 8 nm peak in all the analyzed samples might suggest the presence of protein aggregates or fractionated vesicles both in the retentates and in the flow-throughs. It is highly probable that these 8 nm particles were artificially generated by the centrifugal force applied on the vesicles which forced them to pass through the pores of the various membranes tested thereby fractionating them.

As a conclusion, although the centrifugal forces applied on the exosomes in such devices is significantly lower than the ones applied in differential ultracentrifugation protocols, there is still the danger to artificially generate fusion of particles in the retentate fraction and to damage particles located directly on the membranes.

Furthermore, the fact that we failed to detect miR-16-5p in any of the previously analyzed samples did not prove that the entities isolated were indeed exosomes, therefore invalidating even more the use of such ultrafiltration devices for the preparation of exosomes for *in vivo* applications.
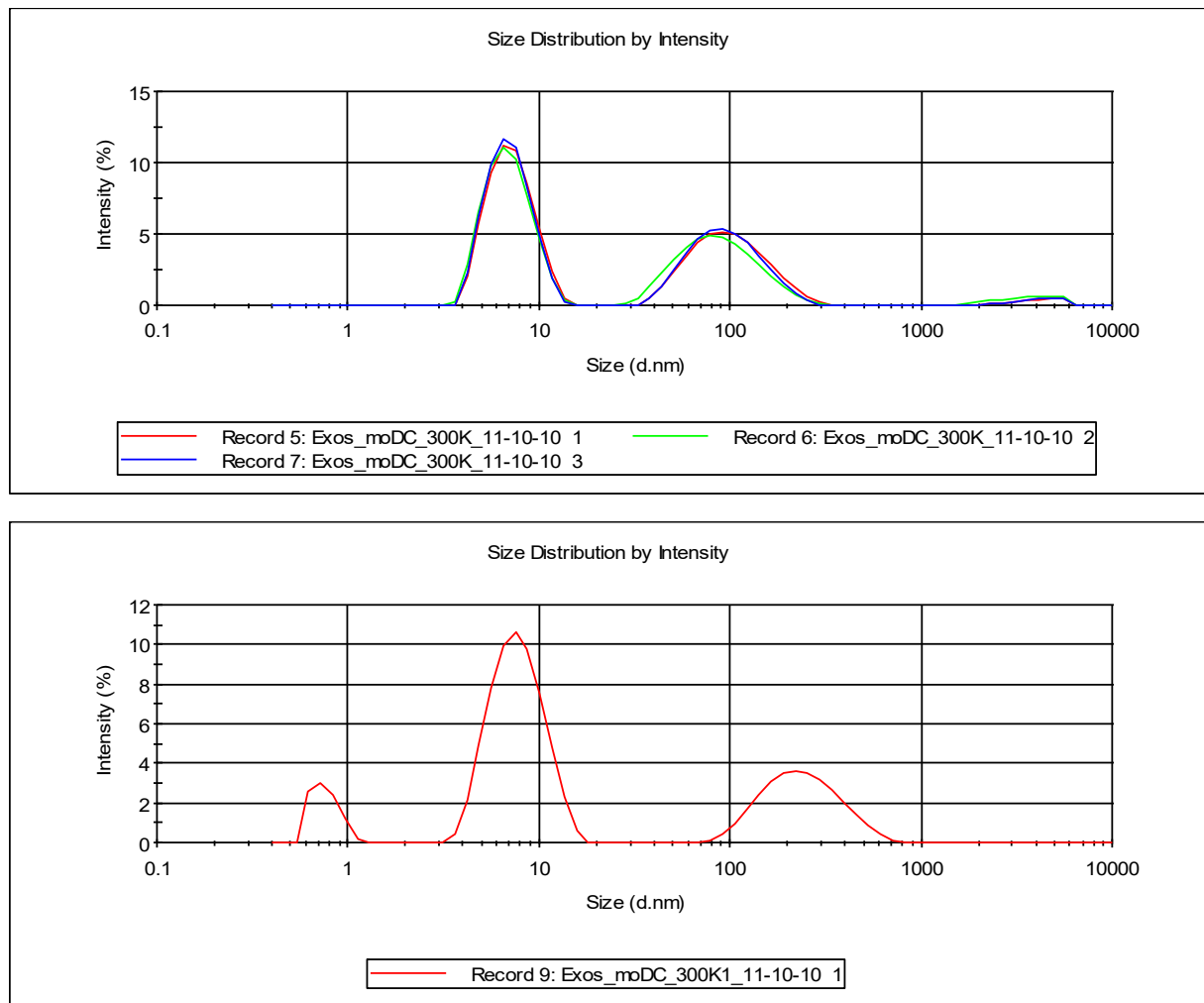
Figure 43: Dynamic Light Scattering profiles obtained by purifying MODC cell culture supernatant with a 300 kDa cut-off ultrafiltration device. a: particle sizes profile of the retentate. b: particle sizes profile of the flow-through

C.2. Exosomes isolation via Tangential Flow Filtration, a method used for Lipidic Nanoparticles purification

The TFF method is based on the continuous circulation of a solution on a filtration cassette allowing the retention of particles of a given size (135). The particle size is defined by the pore size of the filtration cassette, and pressure applied on the cassette allows particle-free liquid to pass through the membrane, resulting in a reduction of circulating fluid (**Fig. 44**).
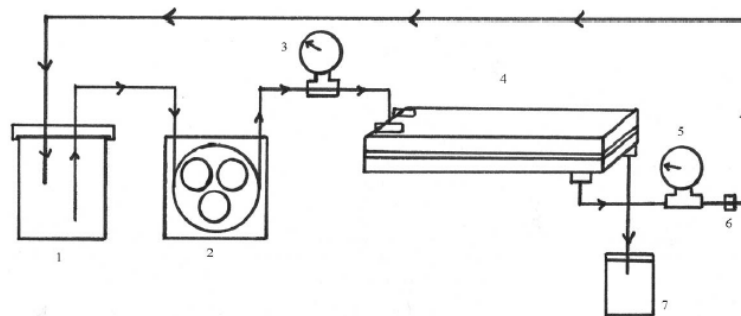
This mechanism is used to concentrate particles and to possibly eliminate non-encapsulated material ([136](#)). The solution still present in the system after processing and which contains the particles of the desired size is called the retentate, while the solution passing through the membrane is called the filtrate. In our case, TFF will be used as a mean to concentrate cell culture supernatant, and to select ideally particles with a size around 60 to 100 nm, namely the size range of exosomes.

We therefore subjected 500 mL HeLa cell culture supernatant to TFF and analyzed the retentate both by Triton-dependent miR-16 detection by RT-qPCR and to particle size measurement by DLS (**Fig. 45**).

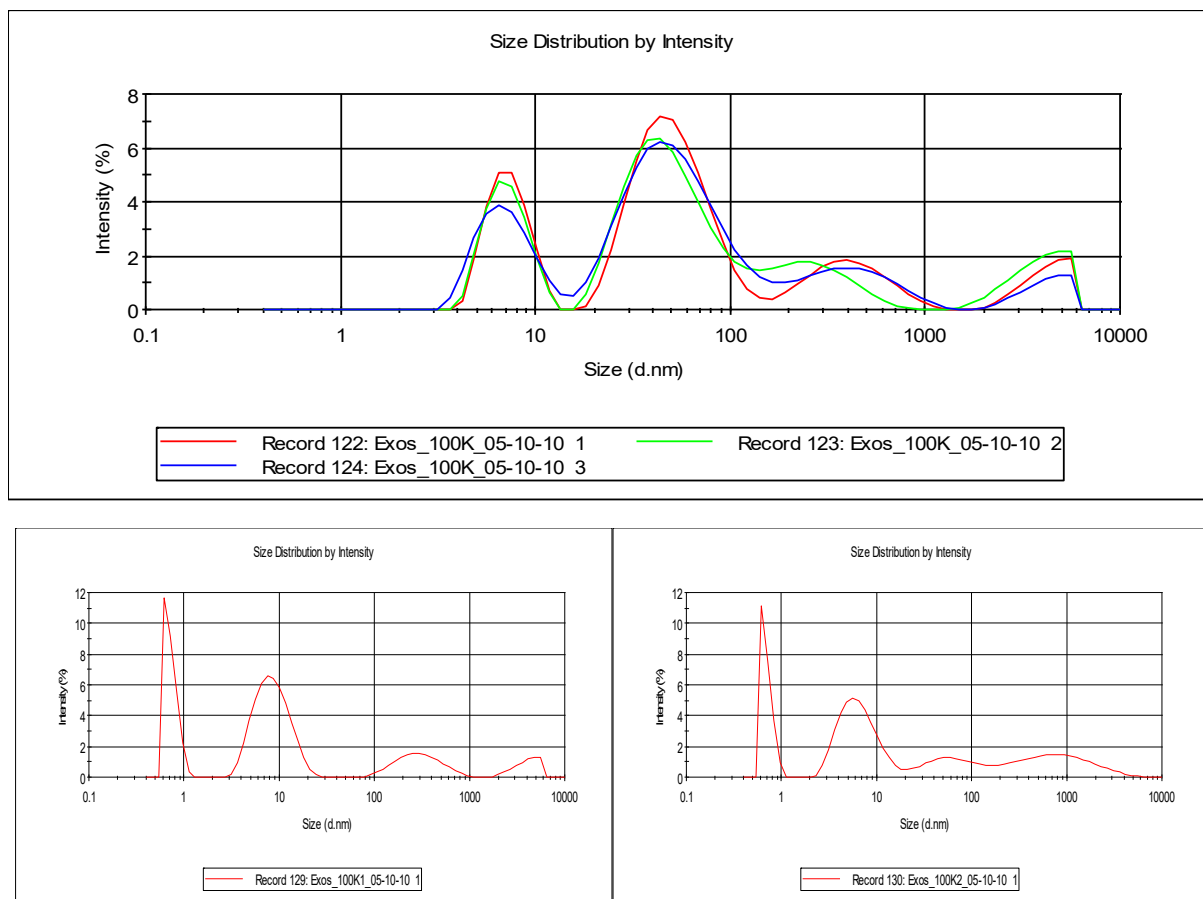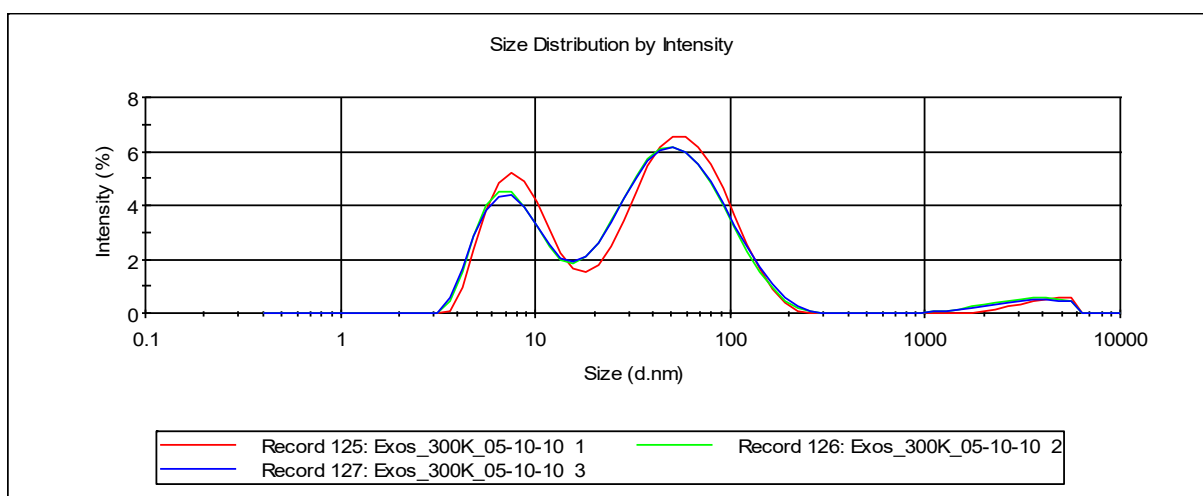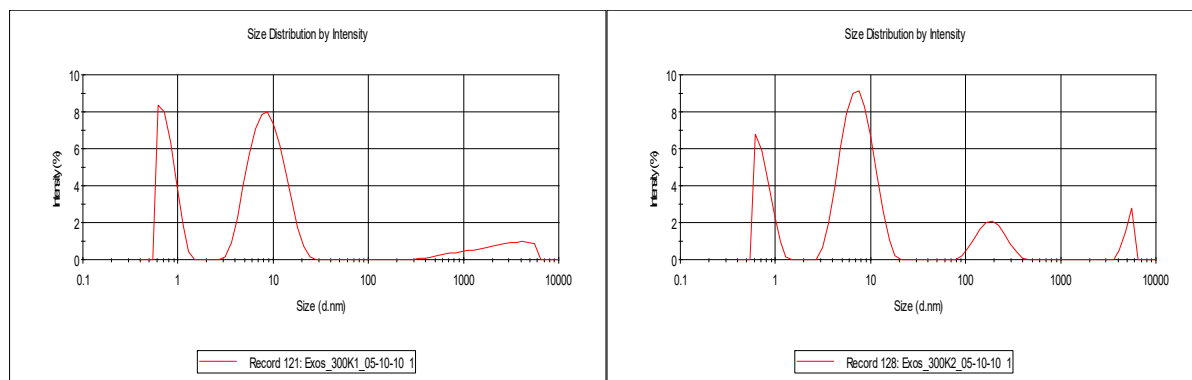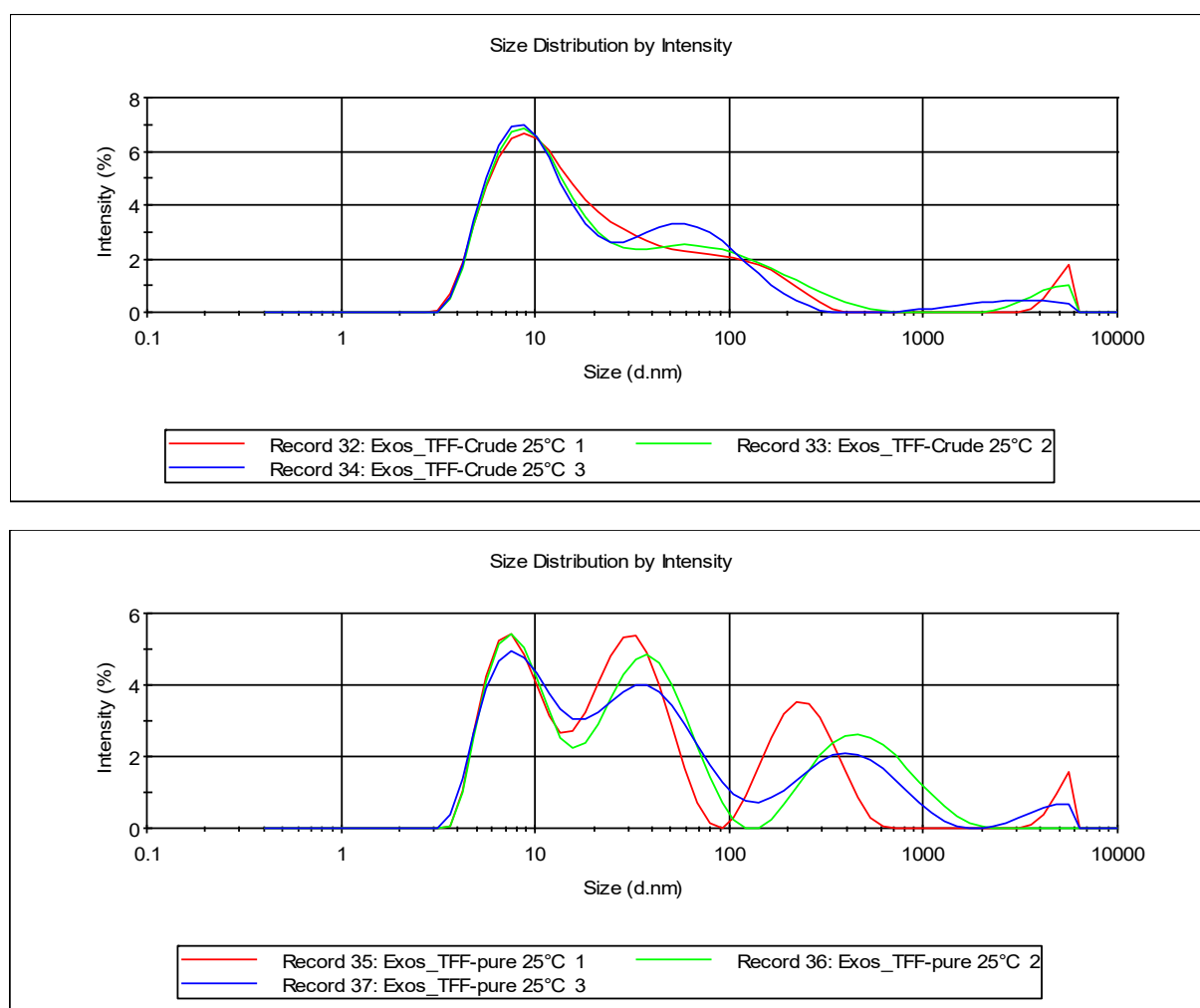*Figure 45: Dynamic Light Scattering profiles obtained by purifying HeLa cell culture supernatant with a 100 kDa cut-off TFF device. a: particle sizes profile of the conditioned medium. b: particle sizes profile of the TFF retentate*

The particle size profile obtained for a sample which did not undergo TFF purification (annotated as crude) show a major peak at 8 nm, as well as minor peaks at 60 nm and 5,000 nm (**Fig. 45a**), whereas the TFF-purified material showed major peaks at 8, 40 and 200-500 nm (**Fig. 45b**). This dataset might therefore suggest an enrichment of particles with a size around 40 nm after TFF purification. Surprisingly, the three consecutive measurements were not perfectly overlaid indicating a highly heterogeneous solution

suggesting that although it is in theory possible to select a minimal particle size, it is very difficult to select a specific size range.

Furthermore, despite an enrichment in particles with a size around 40 nm, no miR-16-5p could be detected in any of the tested samples making it difficult to conclude whether the samples indeed contained exosomes. Another possibility could be the presence of too many PCR inhibitory compounds from serum in the retentate since it was highly concentrated. We therefore decided to run the retentate on a linear sucrose gradient, hoping to reduce the amount of inhibitory compounds in the samples and to therefore allow Triton-dependent miR-16-5p detection by RT-qPCR (**Fig. 46**).

Figure 46: Triton-dependent miR-16-5p quantification in TFF retentate purified on a linear sucrose gradient

The crude sample, which did not undergo TFF purification, as well as the fractions of the sucrose gradient, were subjected to Triton-dependent miR-16-5p detection by RT-qPCR. Although the 60 and 65% sucrose fractions show higher amounts of miR-16-5p compared to other fractions, the fraction containing 70% of sucrose displayed even higher levels of miR-16-5p compared to the 60 and 65 % sucrose fractions, suggesting again loss of miR-16 encapsulation due to damages caused to the exosomes by the handling procedure.
Very much to our surprise, the miR-16-5p levels detected in the crude, unprocessed, sample were close to the amounts detected in the 60 and 65% sucrose fractions, although we were expecting a significant enrichment of the miR-16 amounts since we were able to concentrate 500 mL cell culture supernatant down to 15 mL retentate. This might suggest that a significant amount of miR-16-5p is not encapsulated in exosomes and might rather be involved in a complex or bound to an entity smaller than 100 kDa, allowing it to pass through the membrane pores and to therefore be less abundant than expected in the retentate.

As a summary, the isolation of exosomes based on particle size separation seems to be not as efficient as expected, since we could not detect miR-16-5p in a Triton-X-100 sensitive manner, suggesting that either exosomes were present in too low amounts in the sample, or that there were no exosomes at all in our sample. Moreover, the heterogeneous particle size distributions obtained indicated the possible presence of various unidentified particles or protein complex, making the use of these samples impossible in *in vivo* studies.

D.   Isolation of exosomes by polymers-driven precipitation

D.1.   Evaluation of a commercially available exosomes isolation kit, ExoQuick

A few years ago, the company System Biosciences commercialized an exosome precipitation solution called ExoQuick ([137](#)). ExoQuick is a polymer-based reagent created to enrich a sample, i.e. cell culture supernatant, blood, urine, in exosomes. Moreover the very few steps required in this isolation protocol make it quite eligible for the establishment of a sterile and controlled preparation procedure for *in vivo* studies. This isolation method relies on a single overnight incubation step at 4°C followed by a centrifugation step at 3,000 g, enabling the precipitation of exosomes. The ExoQuick isolation method was tested on cell culture supernatant and the pelleted material was subjected to a Triton-dependent miR-16-5p detection (**Fig. 47**).

The precipitation of 15 mL HeLa cell culture supernatant using ExoQuick allowed us to detect a small amount of Triton X-100 dependent miR-16-5p, but given the size of the error bars obtained, the data did not allow to draw conclusions on the exosomes isolation procedure using ExoQuick. None of the similar experiments performed using ExoQuick-based isolation did result in a better miR-16-5p detection profile, showing the poor efficacy of this isolation kit, at least in our hands. However, when considering that the polymers constituting this kit are unknown, we invalidated its use to prepare exosomes for *in vivo* studies, since it would be unethical to inject an unknown compound *in vivo*. Moreover, the constituents of this solution might interfere with subsequent transfection or transfer experiments involving exosomes, and therefore rendering these experiments non-interpretable.

D.2. Evaluation of a virus particle isolation method, Polybrene/CSC precipitation

Since growing evidence suggests that exosomes and enveloped virus such as HIV are generated by the same secretory mechanisms in the multi-vesicular bodies (MVB) (138-141), we explored the use of virus particle isolation methods for exosomes purification. Taking advantage of the structural similarities between enveloped virus and exosomes, such as negatively charged membranes and the presence of transmembrane proteins on their surface, should allow us to investigate the use of a virus isolation method for exosomes isolation. This precipitation method is based on the complexation of negatively charged particles with the positively charged polymer polybrene, and the negatively charged polysaccharide Chondroitin Sulfate C (CSC) (142). These complexes are subsequently centrifuged at low speeds involving not more than 3,000 g. This method is later referred to as Polybrene/CSC precipitation (**Fig. 48a**).

However, since the fate of the exosomes we isolate is to be injected *in vivo* to trigger targeted delivery of therapeutic siRNAs, it is crucial for our exosomes preparations to not contain any moiety other than exosomes. The presence of the polymers used for precipitation can therefore not be tolerated in the samples. By using a polymer which charges can be modified by pH variations, we could initiate the disassembling of the exosomes-polymers complex and therefore release the exosomes in solution (143). This is possible by using polyethylenimine, which is protonated, and therefore positively charged at low pH, whereas at a pH superior to its pKa, this polymer becomes neutral (144), therefore disrupting the polymers-exosomes complexes (**Fig. 46b**).
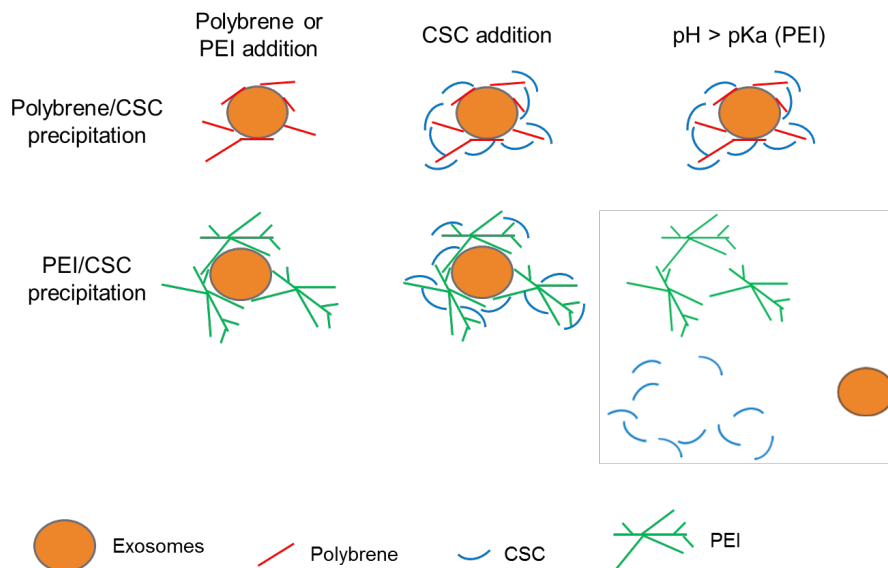
Fig. 48: *Mechanism of Polybrene/CSC (a) and PEI/CSC (b) precipitation methods*

Prior to any work with the pH-labile PEI, we tested the possibility to use the polybrene/CSC precipitation method for the isolation of exosomes out of cell culture supernatant.

A.1.e) Titration of the reagents for optimal polybrene/CSC precipitation for exosomes isolation

This experiment aimed at determining the optimal amounts of both polymers that have to be used for an optimal recovery of exosomes, which presence was assessed by both miR-16-5p quantification by RT-qPCR and western blotting (**Fig. 49**).
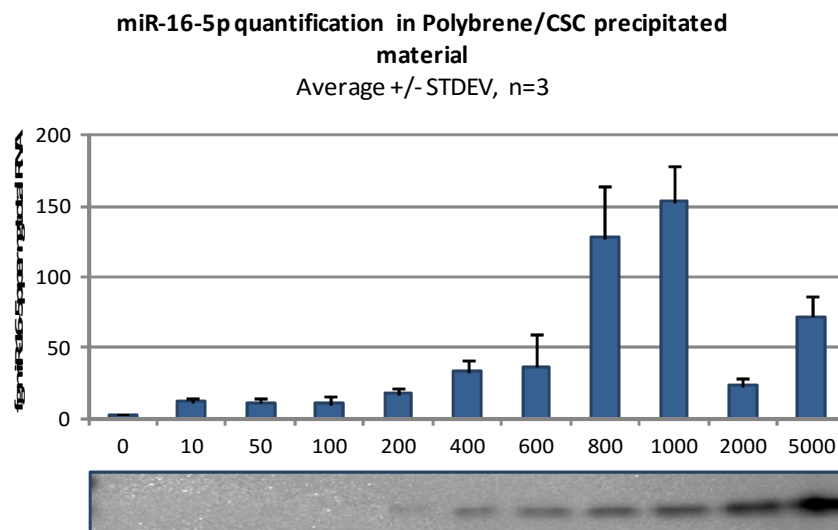
Figure 49: *Characterization of the Polybrene/CSC material by RT-qPCR and Western Blotting. **upper panel:** miR-16-5p levels in Polybrene/CSC precipitated material. The x-axis indicates the concentration of CSC in µg/mL. **lower panel:** western blot analysis using an anti-CD63 antibody*

The first characterization of this precipitation method consisted in determining the optimal ratio between both polymers. To achieve this, we subjected HeLa cell culture supernatant

to Polybrene/CSC precipitation by keeping the Polybrene constant, at 500 µg/mL and by increasing the CSC concentration from 0 to 5,000 µg/mL. Every sample was then split in two fractions, one for western blotting (**Fig. 49, lower panel**) and one for total RNA extraction with Trizol (**Fig. 49, upper panel**). Unfortunately we could not detect any Alix protein by western-blotting, and we therefore selected another exosomal marker, namely the tetraspanin protein CD63 ([110](#)).

The quantification of miR-16-5p, showed an interesting dose response effect (**Fig. 49, upper panel**). There is indeed an increase in miR-16 levels along with the increase in CSC concentration used in the precipitation. Surprisingly, this correlation was only observed up to a CSC concentration of 1,000 µg/mL, although the CD63 western blot (**Fig. 49, lower panel**) displayed increasing signals along with increasing CSC concentration up to 5,000 µg/mL.

We therefore decided to use 1,000 µg/mL CSC in the following experiments, since the correlation between CSC concentration, CD63 and miR-16 signals was only observed up to this specific concentration.

A.1.f) Co-precipitation of miR-16-5p and Ago2 in polybrene/CSC precipitated material

We subsequently intended to prepare samples for more extensive proteomics studies, aiming at confirming the presence of exosomes specific proteins in the samples isolated by Polybrene/CSC precipitation, using Liquid Chromatography Mass Spectrometry (LC-MS). The samples used in this study were assessed for the presence of exosomes markers prior to any further analysis (**Fig. 50**).
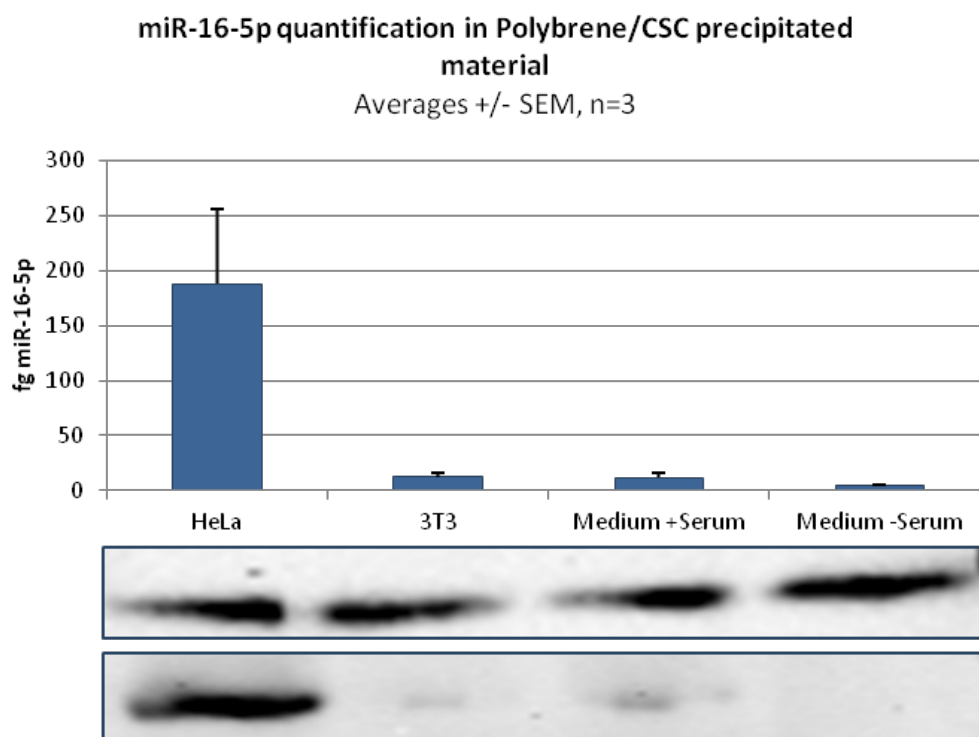
Figure 50: *Characterization of Polybrene/CSC precipitated material by RT-qPCR and western blot. **upper panel:** miR-16-5p levels in Polybrene/CSC precipitated material. The x-axis indicates the sample tested: HeLa or 3T3 cell culture supernatant, DMEM Medium supplemented with 10% FCS, or DMEM Medium without serum. **middle panel:** western blot analysis using an anti-CD63 antibody. **lower panel:** western blot analysis using an anti-Ago2 antibody*

The cell culture supernatant of two different cell lines were analyzed, HeLa cells since all previous work had been performed on this cell line, and 3T3 cells, since cell culture of this cell line had already been subjected to LC-MS by Debora Bonenfant and could therefore be used as a reference. We furthermore complemented the sample set with two negative controls, namely non-conditioned cell culture medium supplemented or not with Fetal Calf Serum (FCS).

The miR-16 amounts detected in the HeLa cells conditioned medium were higher than the miR-16 levels detected in any of the other samples (**Fig. 50, upper panel**), possibly indicating the presence of exosomes in the sample. The 3T3 cell culture supernatant however, did not contain more miR-16-5p than non-conditioned medium. We could therefore not conclude on the presence or the absence of exosomes in this conditioned medium.

The presence of exosomes had therefore to be confirmed by western blotting against an exosomal marker, namely CD63 (**Fig. 50, middle panel)**.

The CD63 antibody surprisingly generated signal in all samples, although we only expected CD63-positive signals in miR-16-positive samples (**Fig. 50, middle panel**).

The fact that non-conditioned medium containing no serum displayed signal suggested that either the CD63 or secondary antibody was non-specifically binding to a reagent used in polybrene/CSC precipitation. A more thorough analysis of the western blots results obtained in the previous experiment (**Fig. 49**) suggested that this non-specific binding increased over titration of the CSC in the precipitation mix, indicating that one of the antibodies might non-specifically bind to CSC, therefore we could see positive signals in non-conditioned medium using the CD63 antibody (**Fig. 50, middle panel**).

The non-specific binding of the CD63 antibody to the polymers however does not explain why we could detect miR-16-5p in the HeLa cells conditioned culture supernatant. Surprisingly, it was reported at the same time that miRNAs circulating in blood, i.e. excreted miRNAs, might not only be encapsulated in exosomes, but could also be found in complex with proteins such as Ago2 for example ([145],[146]). We therefore investigated the presence of Ago2 by western blot in the previously analyzed samples and compared the miR-16-5p and the Ago2 levels (**Fig. 50, lower panel**). Only the miR-16-positive HeLa cell culture supernatant displayed substantial Ago2 signals, indicating co-precipitation of the Ago2 protein along with miR-16-5p.

Intrigued by the co-precipitation of both the Ago2 protein and miR-16-5p, we subjected HeLa cell lysate to Polybrene/CSC precipitation in order to better understand the mechanisms which could have led to this observed co-precipitation.

A.1.g) Identification of RNA- and DNA interacting proteins in Polybrene/CSC precipitated cell lysate

A list of 1042 peptides could be identified in polybrene/CSC precipitated HeLa cell lysate (**see Appendix II**). The analysis of their function resulted in the striking observation that a little less than 60% of these peptides were originating from DNA- or RNA-interacting proteins (**Fig. 51**, **dark orange**).
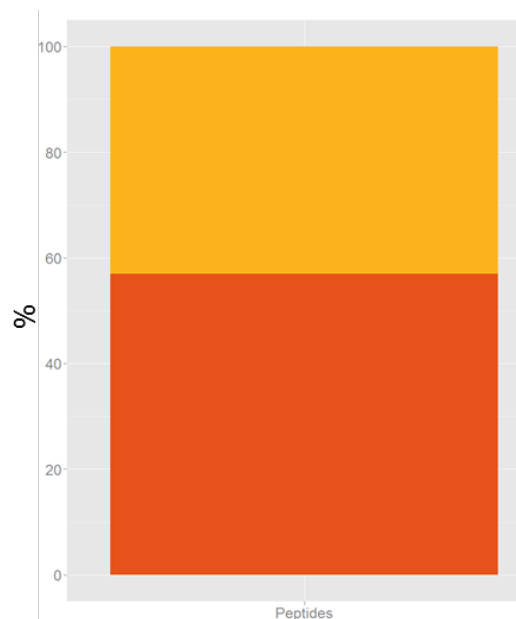
*Figure 51: Classification of the identified peptides as DNA/RNA interacting proteins (**dark orange**) or non-DNA/RNA interacting proteins (**light orange**)*

Although a vast majority of the DNA/RNA-interacting proteins identified in this sample were ribosomal proteins, subunits of the translation initiation factors 2 and 3 could also be found in this sample. The high proportion of these proteins, involved in mRNA translation, in the precipitated material suggests that either the polybrene/CSC precipitation is able to pull down a certain type of proteins, or that the conditions used for polybrene/CSC precipitation allow the complexes formed between mRNA, rRNA and the translational machinery to remain intact. This second hypothesis therefore suggests that the polybrene/CSC precipitation is able to precipitate negatively charged material, such as RNA, and that the proteins in complex with this RNA are being pulled-down along with the precipitated RNA. Further analysis of the precipitated proteins revealed the presence of several types of DNA-interacting proteins, such as histones, transcription factors, nucleolar proteins, RNA Polymerase II interacting proteins, suggesting, as for proteins involved in mRNA translation, that these protein complexes are kept intact throughout precipitation, and that Polybrene and CSC interact with negatively charged polymers such as RNA and DNA.

Interestingly, not only could nuclear and cytoplasmic RNA- and DNA-interacting proteins be identified, but also mitochondrial proteins involved in DNA and RNA interactions, such as mitochondrial ribosomal proteins, mitochondrial translation and transcription factors. This observation suggests that although the lysis conditions used prior to precipitation allowed the release of cytoplasmic, but also nuclear and mitochondrial material in solution, nucleoproteic complexes remained intact, allowing their pull-down via negatively charged nucleic acid molecules.

This observation raised many hopes for potential applications of the Polybrene/CSC precipitation method, such as for example identifying the actors of miRNAs circulation in blood, the proteins allowing their delivery to specific tissues, assuming there would be a cell-to-cell transfer of miRNAs-containing protein complexes.

LC-MS experiments aiming at identifying proteins isolated from mouse plasma with Polybrene/CSC however did not allow the identification of many DNA/RNA interacting

70

proteins, apart from Ago2, and translation factors known to be present in blood. The vast majority of the identified proteins were part of the immune system and of the complement. When trying to perform similar studies in human plasma, we unfortunately failed to detect any miRNAs, leading to the halt of the project.

B. Conclusion/Discussion

The data presented here illustrates the challenges and technical hurdles faced by scientists working in the field of exosomes. It indeed shows how difficult it is to annotate specific molecular markers, i.e. miRNAs and proteins, to exosomes and to develop analytical tools for their identification, and to develop large scale exosomes isolation methods generating highly pure exosomes preparations under sterile conditions for *in vitro* and *in vivo* studies.

The characterization of exosomes is a crucial step when working in this field. It is of the highest importance for further studies to make sure that the entities present in a sample are indeed exosomes, especially if exosomes are meant to be used in *in vivo* studies. When going through the published works on exosomes, a striking observation was made in the sense that there was no clear definition of what an exosome actually is, and which markers can be used to show with the highest confidence that exosomes are indeed present in a sample, although efforts have been made to compile all these markers (110). Surprisingly, one of the major discrepancies is related to the size of the exosomes. Although there is a trend indicating particles with a size around 80 nm, some papers also include particles with a size between 30 and 100 nm (147,148), or even 200 nm (149,150) in their definition of exosomes. It is therefore quite difficult to define exosomes hallmarks, based only on particle size. The morphology of these particles is also often mentioned, stating that exosomes are cup-shaped lipidic vesicles after visualization by Transmission Electron Microscopy (TEM). However this cup-shape could just well be an artifact induced by the various treatments required to visualize samples by TEM (151,152). Apart from size and morphology, various reports also describe exosomes by determining their biochemical and molecular biological content (49,132,153-158). Numerous studies were performed in order to unravel the exosomal RNome and proteome in order to provide further insights into the biological functions in which exosomes could be involved. Along these lines, many studies showed that exosomes could be involved in the immune system, where they could serve as intermediates between various actors of the immune system (159-162), or as active entities able to trigger signal cascades inducing cell death (163,164). This is of course to be taken in consideration when trying to develop drug delivery vehicles based on exosomes, since that would mean that extreme care will have to be taken as to which sub-class of exosomes can be used.

Although the role of exosomes in the immune system is gaining increasing interest, and even if growing evidence is accumulating to demonstrate that exosomes can be involved in the immune system, many studies also describe exosomes as simple intercellular communication means, and some only consider exosomes as a way for the cells to clear out unwanted proteins, enzymatic activities, or nucleic acids (100,101,116). By comparing reports defending these various hypotheses a trend slowly emerged with respect to the most abundant or most representative miRNAs/proteins in exosomes (110,122). These studies allowed us to identify miR-16-5p as one of the most abundant miRNAs in exosomes, as well as CD63 and Alix as being major constituents of the exosomal protein population. In this work I realized that exosomes characterization required the conjunction of several of the markers mentioned previously, such as displaying the right particle size, the right protein markers and showing the detergent-sensitive detection of the exosomes

content. Following this observation, it became clear to me that one has to be careful when trying to demonstrate the implication of exosomes in a given biological process. One of the key features in all exosomes-related works would be to perform an extensive and thorough exosomes characterization study prior to being able to draw any conclusions as to the effect of exosomes, such as showing exosomal hallmarks as well as several exosomal markers.

The fact that none of the methods tested in our study allowed us to detect particles displaying the three exosomes hallmarks which are their size, and several markers such as Alix or miR-16-5p prompted us to not pursue any *in vitro* nor *in vivo* work. It would indeed have been difficult to appreciate any biological activity if we would not have been sure that our samples contained highly pure exosomes. Because of the complexity of the input material (conditioned cell culture supernatant) it was crucial to make sure that no other protein or vesicle could trigger a biological effect which could have led to a "false positive". Although some results were clearly encouraging, such as seeing a direct correlation between miR-16-5p and Alix signals in the same fractions of a linear sucrose gradient, other factors such as exosomes amount and reproducibility issues for example never allowed us to bring the project to the next step which was the *in vitro* characterization of exosomes-mediated siRNA delivery.

To sum up, I find it very interesting that although the first observation of exosomes was made more than 25 years ago, it is only very recently that scientific consortiums emerged, aiming at combining the efforts of the many scientists working on exosomes and affiliated microvesicles. The combination of their knowledge and experience on exosomes could potentially lead to the identification of novel and trustworthy exosomal markers, as well as the development of better exosomes isolation processes. Once these two major milestones are in place, I have no doubt that exosomes could eventually be used as anti-cancer vaccines, as it was already reported from various authors (115,165-169). According to these authors, the MHC complexes carried by the exosomes secreted by cancer cells could elicit an immune response, and would therefore direct the immune response towards cancer cells.

Exosomes could however be useful in other fields of human health. They could indeed be used as efficient disease diagnostic tools since they can be found in many biological fluids, such as blood, urine, breast milk, or saliva. It could therefore be possible, by analyzing the exosomes population secreted by a patient, to detect proteins or nucleic acid moieties indicating a certain type of cancer, inflammation, or disease (170-173). This has already been observed for liver injuries, where in the case of an inflammatory liver disease for example, miR-122 levels can be found in higher amounts in exosomes, compared to exosomes from healthy patients (174).

VI.   Conclusion and outlook

In this study, we investigated the possibility to use exosomes as delivery vehicles for siRNA, and we developed in parallel a PCR-based visualization method to study the *in vivo* biodistribution of oligonucleotides in mouse whole body sections.

We successfully developed the WBS-PCR method to perform oligonucleotides biodistribution studies, including endogenous and ectopic mRNAs and non-coding miRNAs, as well as non-modified siRNAs. The detection of highly chemically modified oligonucleotides, such as antagomirs for example, was possible as well with CL-qPCR, a method we developed which was also shown to be compatible with WBS-PCR. We therefore had a nice tool at our disposal to screen exosomes from various origins, and various tissue-targeting peptides conjugated with exosomes for siRNA delivery. However, our attempts in isolating exosomes were highly disappointing, since none of the methods tested in this study resulted in an efficient isolation of pure exosomes, as could be seen by the difficulty for our samples to meet the established criteria indicating the presence of exosomes. Although two of the methods tested are clearly mentioned as reference methods in the exosomes field, namely differential ultracentrifugation and ExoQuick isolation, it remains unclear whether the samples we prepared by using these methods did contain exosomes. Taken together, these observations indicate that despite an increasing amount of publications on exosomes, work conducted on exosomes has to be extensively controlled to make sure that the effect(s) attributed to exosomes are indeed due to these vesicles. It would however be a huge step forward if we could use the exosomes as non-invasive diagnostic tools, since they could provide, in a single saliva drop, access to the circulating proteome and RNome of patients.

VII. Material and methods

A. Whole-Body Scanning PCR

A.1. Oligonucleotides and RT-qPCR assays

Synthetic RNA sequences and DNA PCR primers for miRNA, siRNA and antagomir detection were ordered from Microsynth AG (Switzerland) (**Supplementary table 1**).

Sequence ID	Sequence	Forward primer	Reverse primer
mmu-miR-1a-3p	UGGAAUGUAAAGAAGUAUGUAU	FAM-CTCCCTCCCTCGATTTTGGAATGTAAAGAA	GCGCTGGATAATACATAC
mmu-miR-122-5p	UGGAGUGUGACAAUGGUGUUUG	FAM-CTCCCTCCCTCGATTTTGGAGTGTGACAAT	GCGCTGGATACAAACACC
mmu-miR-124-3p	UAAGGCACGCGGUGAAUGCC	FAM-CTCCCTCCCTCGATTTTAAGGCACGCGGT	GCGCTGGATAGGCATTC
mmu-miR-124-5p	CGUGUUCACAGCGGACCUUGAU	FAM-CTCCCTCCCTCGATTTCGTGTTCACAGCGG	GCGCTGGATAATCAAGGT
mmu-miR-125a-3P	ACAGGUGAGGUUCUUGGGAGCC	FAM-CTCCCTCCCTCGATTTACAGGTGAGGTTCT	GCGCTGGATAGGCTCCCA
mmu-miR-125a-5P	UCCCUGAGACCCUAACCUUGUGA	FAM-CTCCCTCCCTCGATTTTCCCTGAGACCCTT	GCGCTGGATACACAGGTTA
mmu-miR-125b-2-3p	ACAAGUCAGGUUCUUGGGACCU	FAM-CTCCCTCCCTCGATTTACAAGTCAGGTTCT	GCGCTGGATAAGGTCCCA
mmu-miR-125b-1-3P	ACGGGUUAGGCUCUUGGGAGCU	FAM-CTCCCTCCCTCGATTTACGGGTTAGGCTCT	GCGCTGGATAAGCTCCCA
mmu-miR-125b-5P	UCCCUGAGACCCUAACUUGUGA	FAM-CTCCCTCCCTCGATTTTCCCTGAGACCCTA	GCGCTGGATATCACAAGT
mmu-miR-126-3P	UCGUACCGUGAGUAAUAAUGCG	FAM-CTCCCTCCCTCGATTTTCGTACCGTGAGTA	GCGCTGGATACGCATTAT
mmu-miR-126-5P	CAUUAUUACUUUUGGUACGCG	FAM-CTCCCTCCCTCGATTTCATTATTACTTTTG	GCGCTGGATACGCGTAC
mmu-miR-127-3p	UCGGAUCCGUCUGAGCUUGGCU	FAM-CTCCCTCCCTCGATTTTCGGATCCGTCTGA	GCGCTGGATAAGCCAAGC
mmu-miR-128-3p	UCACAGUGAACCGGUCUCUUU	FAM-CTCCCTCCCTCGATTTTCACAGTAACCGG	GCGCTGGATAAAAGAGA
mmu-miR-132-3p	UAACAGUCUACAGCCAUGGUCG	FAM-CTCCCTCCCTCGATTTTAACAGTCTACAGC	GCGCTGGATACGACCATG
mmu-miR-133a-3p	UUUGGUCCCCUUCAACCAGCUG	FAM-CTCCCTCCCTCGATTTTTTGGTCCCCTTCA	GCGCTGGATACAGCTGGT
mmu-miR-137-3P	UUAUUGCUUAAGAAUACGCGUAG	FAM-CTCCCTCCCTCGATTTTTATTGCTTAAGAA	GCGCTGGATACTACGCGTA
mmu-miR-139-3P	UGGAGACGCGGCCCUGUUGGAG	FAM-CTCCCTCCCTCGATTTTGGAGACGCGGCCC	GCGCTGGATACTCCAACA
mmu-miR-139-5P	UCUACAGUGCACGUGUCUCCAG	FAM-CTCCCTCCCTCGATTTTCTACAGTGCACG	GCGCTGGATACTGGAGAC
mmu-miR-148b-3p	UCAGUGCAUCACAGAACUUUGU	FAM-CTCCCTCCCTCGATTTTCAGTGCATCACAG	GCGCTGGATAACAAAGTT
mmu-miR-15a-5p	UAGCAGCACAUAAUGGUUUGUG	FAM-CTCCCTCCCTCGATTTTAGCAGCACATAAT	GCGCTGGATACACAAACC
mmu-miR-15b-5p	UAGCAGCACAUCAUGGUUUACA	FAM-CTCCCTCCCTCGATTTTAGCAGCACATCAT	GCGCTGGATATGTAAACC
mmu-miR-16-5p	UAGCAGCACGUAAAUAUUGGCG	ROX-CTCCCTCCCTCGATTTCAGCAGCACGTAAA	GATTTGTTCTGGTTCGCCAAT
mmu-miR-191-5p	CAACGGAAUCCCAAAAGCAGCUG	TAMRA-CTCCCTCCCTCGATTTCAACGGAATCCCA	GCGCTGGATAAGCTGCTTT
mmu-miR-208a-3p	AUAAGACGAGCAAAAAGCUUGU	FAM-CTCCCTCCCTCGATTTATAAGACGAGCAAA	CCGAGGTACAAGCTTTTTG
mmu-let-7a-5p	UGAGGUAGUAGGUUGUAUAGUU	FAM-CTCCCTCCCTCGATTTTGAGGTAGTAGGTT	GCGCTAAGGATAAACTAT
mmu-let-7b-5p	UGAGGUAGUAGGUUGUGUGGUU	FAM-CTCCCTCCCTCGATTTTGAGGTAGTAGGTT	GCGCTGGATAAACCACAC
mmu-let-7c-5p	UGAGGUAGUAGGUUGUAUGGUU	FAM-CTCCCTCCCTCGATTTTGAGGTAGTAGGTT	GCGCTAAGGATAAACCAT
mmu-let-7d-5p	AGAGGUAGUAGGUUGCAUAGUU	FAM-CTCCCTCCCTCGATTTAGAGGTAGTAGGTT	GCGCTGGATAAACTATGC
mmu-let-7e-5p	UGAGGUAGGAGGUUGUAUAGUU	FAM-CTCCCTCCCTCGATTTTGAGGTAGGAG	GCGCTGGATAAACTATAC
mmu-let-7f-5p	UGAGGUAGUAGAUUGUAUAGUU	FAM-CTCCCTCCCTCGATTTTGAGGTAGTAGATT	GCGCTGGATAAACTATAC
mmu-let-7g-5p	UGAGGUAGUAGUUUGUACAGUU	FAM-CTCCCTCCCTCGATTTTGAGGTAGTAGTTT	GCGCTGGATAAACTGTAC
mmu-let-7i-5p	UGAGGUAGUAGUUUGUGCUGUU	FAM-CTCCCTCCCTCGATTTTGAGGTAGTAGTTT	GCGCTGGATAAACAGCAC
Mrp4 siRNA	ACAGCUCCUGACACCUCUCdTdT	FAM-ACTCCCTCCCTCGATTTACAGCTCCTGACAC	CAAGCAGAAGACGAAGAGAGG
Chemical Ligation product AMO-miR-16	TTAAACCATAGCAGCACGTAAATAT TGGCGAACCAGT	FAM-CTCCCTCCCTCGATTTAAACCATAGCAGCACG	TCTGGTTCGCCAATATTTACG

Supplementary Table 1: List of the reagents used for miRNA, siRNA and CL-qPCR assays

TaqMan gene expression assays were ordered from Applied Biosystems (USA) (**Supplementary table 2**).

Target	AoD ID
Mouse IGFBP1	Mm008334477_m1 Igfbp1
Mouse Myh6	Mm00440354_m1 Myh6
Mouse Mbp	Mm01266402_m1 Mbp
Human ELAVL1	Hs00171309_m1 ELAVL1
Human Actb	Mm006707939_s1 Actb
Human GAPDH	Mm99999915_g1 Gapdh
Genomic 18S	Hs03003631_g1 18S
18S rRNA	Hs99999901_s1 18S

Supplementary Table 2: List of the ABI Taqman assays

A.2. Design of miRNA and siRNA RT-qPCR primers

The RT-primer, which also serves as reverse primer during the PCR-reaction, contains a generic sequence at the 5'-end and a Target Recognition Sequence (TRS) at the 3'-end. The optimal TRS sequence in most assays consists of 8 nucleotides but can vary in

74

length, ranging from 6 to 12 nucleotides, depending on the sequence of the target molecule. For example, if the 3'-end of the RT-primer ends with a palindromic motif (i.e – ccgg, -aatt, -ggcc, -ttaa, -atat, -tata, -cgcg and -gcgc), the performance of the assay can be considerably improved by either removing or extending the TRS sequence by a single nucleotide so that the palindromic sequence is disrupted. The generic sequence is required to increase the Tm of the oligonucleotide and to modulate the G/C-content since the same primer will function as reverse primer in the subsequent PCR-reaction.

The 5'-fluorophore labeled forward-primer contained a generic sequence at the 5'-end and a gene-specific region spanning at least 12 nucleotides at the 3'-end. The optimal length of the gene-specific region depends on the target sequence and the TRS length of the RT-primer. Excessive overlap (more than 3 nucleotides) with the RT-primer and palindromic sequences at the 3'-end should be avoided. The generic sequence of the forward-primer should be complementary to the quencher-labeled anti-primer sequence (5'-AAATCGAGGGAGGGAG-BHQ$_2$-3').

A.3.   Synthetic miRNA standard curves preparation

Synthetic miRNAs were serially diluted into Poly(A) (10 ng/µL diluted in RNAse-free water/GE Healthcare, #27-411-01) to generate a dilution series ranging from 10 ng/µL down to 1 zg/µL. A sample containing only 10 ng/µL Poly(A) in RNase-free water was included as No Template Control (NTC) and was used to determine the background level of RT-qPCR primers.

A.4.   siRNA duplex standard curve preparation

siRNA was serially diluted into 10 ng/µL total rat liver RNA to generate a dilution series ranging from 10 ng/µL down to 1 zg/µL. A sample containing only 10 ng/µL Poly(A) in RNase-free water was included as NTC and was used to determine the background level of RT-qPCR primers.

A.5.   AMO-miR-16 standard curves preparation

AMO-miR-16 was serially diluted in either Poly(A) (10 ng/µL diluted in RNAse-free water/GE Healthcare, #27-4110-01) or in diluted (1:750 in RNAse-free water) tissue lysates from a PBS treated mouse. The dilution series ranged from 8 ng/µL down to 0.8 zg/µL. A sample containing only 10 ng/µL Poly(A) in RNase-free water was included as NTC and was used to determine the background level of RT-qPCR primers.

A.6.   *In vivo* experiments

All experimental animal procedures were approved by the Animal Care and Use Committees of the Kanton Basel, Switzerland.

A.7.   Whole tissue lysates preparation

Isolated organs were weighed, transferred into Lysing matrix A tubes (MP Biomedicals, #16910050), frozen on dry ice and stored at -80°C until processing. The tissues were lysed by adding 10 volumes/weight Clarity OTX buffer (Phenomenex, #AL0-8498) supplemented with 20 mM TCEP (Sigma-Aldrich, #C4706-2G) followed by shaking for 60 seconds at 4m/s in a FastPrep-24 instrument (MP Biomedicals). Subsequently, tubes were centrifuged at 4°C for 30 seconds at 12.000 rpm. Supernatant was transferred to a fresh tube and stored at -80°C. The concentrated lysates were diluted 1:750 in RNase-free

water prior to RT-qPCR analysis. Diluted lysates should be stored at -80°C and repeated freeze-thawing cycles should be avoided.

A.8. Implantation of HCT116 tumor in mice

The human colorectal carcinoma cell line, HCT-116 (Catalog #CCL-247), was obtained from ATCC (Rockville, Maryland, USA). The cells were maintained and cultured according to established techniques as recommended by the supplier. Briefly, HCT-116 cells were cultivated in McCoy's 5A medium (Amimed/Bioconcept, #1-18F01-I) supplemented with 10% v/v FCS (Amimed/Bioconcept, #2-01F26-I), 2 mM L-Glutamine (Amimed/Bioconcept, #5-10K00-H) and 2.2 g/L sodium pyruvate (Amimed/Bioconcept, #5-60F00-H). Cells were split 1:8 or 1:10 every 3rd or 4th day depending on confluence. Female Hsd:Athymic nude mice (Harlan Laboratories, Nederland) at age of 6-7 weeks were group housed in individually ventilated cages with access to food and water *ad libitum*. Tumors were established by subcutaneous injection of $5×10^6$ cells in 100 µl of HBSS (Invitrogen, #14175-046) per mouse into the left flank of the animals under Isoflurane (Provet, Lyssach, Switzerland) anesthesia. Tumor volume and body weight were monitored twice weekly. The tumor volume was 429 mm^3 at the time of sacrifice (38 days after inoculation).

A.9. Mrp4 siRNA QWBA

Male albino CD-1 mouse (Charles River France, 29-32 g) received intravenous administration of unformulated [^{3}H]-MRP4 siRNA in 0.9% sodium chloride at a dose of 5 mg/kg, under anesthesia (by inhalation of an oxygen/isoflurane mixture) as a bolus injection into the *vena saphena*. The dose volume was 2 mL/kg, and the total amount of radioactivity administered was 21 MBq/kg. The mouse was sacrificed by deep isoflurane inhalation at 10 minutes post *i.v.* dosing. Whole body sections were prepared as described previously and exposed for two weeks to Fuji BAS III imaging plates (Fuji Photo Film Co., Ltd., J-Tokyo) in a lead-shielded box at room temperature, and scanned in a Fuji BAS 5000 phosphor imager (Fuji Photo Film) at a 50 µm scanning step.

A.10. AMO-miR-16 injection

Mice were treated intravenously with 80 mg/kg AMO-miR-16 (dissolved in PBS) via tail vein injection. Blood plasma was collected pre- and 5, 10, 30, 60, 240, 360 and 1440 minutes post dosing. Mice were sacrificed at 1440 minutes post-dosing and prepared for whole body sectioning or tissue sampling as described previously.

A.11. Whole Body sectioning

Right after sacrifice, animals were submerged in -70°C n-hexane (VWR International, #BREN81631-156) / dry ice mixture for about 30 min. The carcasses were stored at -80°C until embedding and all subsequent procedures were performed at temperatures of about -20°C to minimize diffusion of compound. The frozen carcasses were embedded in a mold on a microtome stage by adding an ice-cold aqueous solution of 2% carboxymethylcellulose (low viscosity, Sigma-Aldrich Chemie GmbH, #C5678-1KG) and freezing it by placement in an n-hexane/dry ice bath for about 40 minutes. The frozen block was removed from the mold and stored at -20°C until sectioning. Whole-body sections were performed in the sagittal plane (from cranial to caudal) using CM3600XP cryomacrotome (Leica Microsystems), and the sections collected on an adhesive tape (Scotch Magic Tape 810, 118 mm x 66 m, Voegtli Bürotechnik AG, #1939899). Several sections of 40 µm thickness were taken at varying depths throughout the body. Sections

were mounted on a wooden frame after collection and dehydrated for 72 h at -23°C in the cryomacrotome chamber. The sections were stored at -20°C until further handling.

A.12. WBS-PCR

Firstly, a picture of the section was taken using a ChemiDoc XRS+ System from Bio-Rad. Subsequently, a matrix of 363 wells was outlined on a 1,536-well Polypropylene plate (Greiner Bio-One, #789270) with a permanent pen (Staedtler) and each well was filled with 15 µL Clarity OTX buffer (Phenomenex, #AL0-8498) supplemented with 20 mM TCEP (Sigma-Aldrich, #C4706-2G). The whole body section was placed within the matrix on the plate (tissue facing the well) and firmly sealed with a Microseal `B´ film (Bio-Rad, #MSB1001) with the help of a rubber brayer (Speedball). Another picture of the section was taken at this point and was used in the data analysis process. The plate was subsequently inversed several times, and centrifuged for 3 minutes at 1,450 g in a Sigma 4-15C centrifuge (Qiagen) containing a Nr 09100 rotor (Qiagen). Lysates were transferred to a 384-well Hard-Shell PCR Plate (Bio-Rad, #HSP3901) and stored at -80°C. Samples were diluted 1:75 in RNase-free water prior to RT-qPCR analysis. Diluted lysates should be stored at -80°C and repeated freeze-thawing cycles should be avoided.

A.13. Quantification of rRNA and mRNA

The detection of 18S rRNA and various mRNAs was performed in a one-step reaction. 8 µL RT-qPCR mix containing: 5.35 µL DEPC-water, 0.15 µL 100 mM dNTPs (Applied Biosystems, #362271), 1 µL 10x PCR Buffer I (Applied Biosystems, #4379876), 1 µL 25 mM MgCl$_2$ (Roche, #12032953001), 0.1 µL Rox Reference Dye (Invitrogen, #12223-012), 0.2 µL Assay On Demand (Applied Biosystems), 0.1 µL Multiscribe (50 U/µL) (Applied Biosystems, #4319983), 0.1 µL Hot Start Taq Polymerase (5 U/µL) (Roche, #12032953001) was added to a 384-well Hard-Shell PCR Plate (Bio-Rad, #HSP3901) followed by the addition of 2 µL sample. After sealing (Microseal `B´ film, Bio-Rad, #MSB1001), the plate was mixed and centrifuged for 3 min at 1.450 g. The PCR reaction was performed in a 7900HT Fast Real-Time PCR System (Applied Biosystems) and consisted of 1 cycle: 30 minutes/50°C, 1 cycle: 10 minutes/ 95°C followed by 40 cycles: 3 seconds/95°C; 30 seconds/60°C. The data was acquired and analyzed using the software provided by Applied Biosystems. In accordance with Applied Biosystems guidelines, Ct values bigger as 35 were considered as noise.

A.14. Quantification of 18S genomic DNA

The detection of 18S genomic DNA was performed in a one-step reaction. 8 µL qPCR mix containing: 5.45 µL DEPC-water, 0.15 µL 100 mM dNTPs (Applied Biosystems, #362271), 1 µL 10x PCR Buffer I (Applied Biosystems, #4379876), 1 µL 25 mM MgCl$_2$ (Roche, #12032953001), 0.1 µL Rox Reference Dye (Invitrogen, #12223-012), 0.2 µL Assay On Demand (Applied Biosystems), 0.1 µL Hot Start Taq Polymerase (5 U/µL) (Roche, #12032953001) was added to each well of a 384-well Hard-Shell PCR Plate (Bio-Rad, #HSP3901) followed by the addition of 2 µL sample. After sealing (Microseal `B´ film, Bio-Rad, #MSB1001), the plate was mixed and centrifuged for 3 min at 1.450 g. The PCR reaction was performed in a 7900HT Fast Real-Time PCR System (Applied Biosystems) and consisted of 1 cycle: 10 minutes/ 95°C followed by 40 cycles: 3 seconds/95°C; 30 seconds/60°C. The data was acquired and analyzed using the software provided by Applied Biosystems. In accordance with Applied Biosystems guidelines, Ct values bigger as 35 were considered as noise.

A.15. Quantification of miRNA and siRNA

The detection of miRNAs and siRNAs was performed in a two-step reaction. In the first step, 8 µL RT-mix containing: 5.65 µL DEPC-water, 0.15 µL 100 mM dNTPs (Applied Biosystems, #362271), 1 µL 10x PCR Buffer I (Applied Biosystems, #4379876), 1 µL 25 mM $MgCl_2$ (Roche, #12032953001), 0.1 µL 1 µM RT-primer, 0.1 µL Multiscribe (50 U/µL) (Applied Biosystems, #4319983) was added to each well of a 384-well Hard-Shell PCR Plate (Bio-Rad, #HSP3901) followed by the addition of 2 µL sample. The plate was sealed (Microseal `B´ film, Bio-Rad, #MSB1001), mixed, centrifuged and incubated for 10 minutes at 25°C followed by 5 minutes at 95°C in a 7900HT Fast Real-Time PCR System (Applied Biosystems). Before unsealing, the plate was centrifuged for 3 min at 1.450 g and 5 µL/well PCR mix was added. Subsequently, the plate was sealed (Microseal `B´ film, Bio-Rad, #MSB1001), mixed and centrifuged for 3 min at 1.450 g. The PCR mix contained: 3.325 µL DEPC-water, 0.15 µL 100 mM dNTPs (Applied Biosystems, #362271), 0.5 µL 10x PCR Buffer I (Applied Biosystems, #4379876), 0.5 µL 25 mM $MgCl_2$ (Roche, #12032953001), 0.15 µL 10 µM forward primer, 0.15 µL 10 µM reverse primer, 0.075 µL 50 µM Anti-primer, 0.15 µL Hot Start Taq Polymerase (5 U/µL) (Roche, #12032953001). The PCR reaction was performed in a 7900HT Fast Real-Time PCR System (Applied Biosystems) and consisted of 1 cycle: 10 minutes/95°C followed by 50 cycles: 3 seconds/95°C; 30 seconds/55°C. The ramping speed should not exceed 3°C/s. The data was acquired and analyzed using the software provided by Applied Biosystems. Signals that did not fall within the linear range of the standard curve were considered as noise.

A.16. Quantification of AMO-miR-16

The quantification of AMO-miR-16 was performed in a two-step reaction. In the first step, 8 µL Chemical Ligation-mix containing: 5.8 µL DEPC-water, 1 µL 10x PCR Buffer (Roche #14882500), 1 µL Poly(A) (1 µg/µL diluted in RNAse-free water/GE Healthcare, #27-4110-01), 0.1 µL 10 µM PS-Ligator (5'-TTAAACCATAGCAGCACG-PS-3'), 0.1 µL 10 µM BPS-Ligator (5'-BPS-TAAATATTGGCGAACCAGT-3') was added to each well of a 384-well Hard-Shell PCR Plate (Bio-Rad, #HSP3901) followed by the addition of 2 µL sample. Subsequently, the plate was sealed (Microseal `B´ film, Bio-Rad, #MSB1001), mixed, centrifuged for 3 minutes at 1.450 g and incubated for 30 minutes at 33°C in a 7900HT Fast Real-Time PCR System (Applied Biosystems). Before unsealing, the plate was centrifuged.

Upon completion of the chemical ligation reaction, 8 µL PCR-mix containing 6.375 µL DEPC-water, 0.15 µL 100 mM dNTPs (Applied Biosystems, #362271), 1 µL 10x PCR Buffer (Roche #14882500), 0.15 µL 10 µM forward primer, 0.15 µL 10 µM reverse primer, 0.075 µL 50 µM Anti-primer, 0.1 µL Hot Start Taq Polymerase (5 U/µL) (Roche, #12032953001) was added to each well of a new 384-well Hard-Shell PCR Plate (Bio-Rad, #HSP3901) followed by the addition of 2 µL of the Chemical Ligation-mix. Subsequently, the plate was sealed (Microseal `B´ film, Bio-Rad, #MSB1001), mixed and centrifuged for 3 min at 1.450 g. The PCR reaction was performed in a 7900HT Fast Real-Time PCR System (Applied Biosystems) and consisted of 1 cycle: 10 minutes/95°C followed by 50 cycles: 3 seconds/95°C; 30 seconds/55°C; 10 seconds/72°C. The ramping speed should not exceed 3°C/s. The data was acquired and analyzed using the software provided by Applied Biosystems. Signals that did not fall within the linear range of the standard curve were considered as noise.

A.17. Statistical analysis

The statistical relevance of the results obtained for the quantification of miR16-5p and AMO-miR-16 was tested by Mann-Whitney Rank Sum Test. A t-test was performed on the values obtained for miR-191-5p quantification.

A.18. Imaging of the WBS-PCR data

RT-qPCR data of the whole body sections was deconvoluted in Excel and converted into a TissueView™ compatible image file using an Excel to Analyze Conversion macro (http://maldi.ms). Subsequently, the RT-qPCR image data was loaded into TissueView™ (AB Sciex, Toronto) and overlaid with an image of the whole body section.

A.19. Building block synthesis for chemical ligators

All reactions were carried out under an atmosphere of argon. Solvents for extraction: technical grade from Brenntag Schweizerhalle AG. Solvents for reactions: anhydrous quality from Sigma-Aldrich. Base-protected deoxynucleosides were obtained from ChemGenes (N^6-benzoyl-2'-deoxyadenosine #PM-1101, N^4-benzoyl-2'-deoxycytidine #PM-1102, N^2-isobutyryl-2'-deoxyguanosine #PM-1103, thymidine #DN-1004). All other reagents were purchased from *Sigma-Aldrich*, highest quality available, unless stated otherwise. Flash-chromatography was performed using silica gel 60 with a particle size of 40-63 µm (*Merck*). Thin layer chromatography was performed on *Merck* silica gel 60 F_{254} plates which were visualized by UV irradiation (254 nm). NMR: *Bruker DRX-400*, deuterated solvent as indicated, δ in ppm, calibration to residual solvent peaks, ^{13}C multiplicities derived from DEPT spectra, ^{31}P calibration to external H_3PO_4 (δ = 0 ppm).

A.20. Synthesis of base protected 5'-O-biphenylsulfonyl-2'-deoxynucleosides
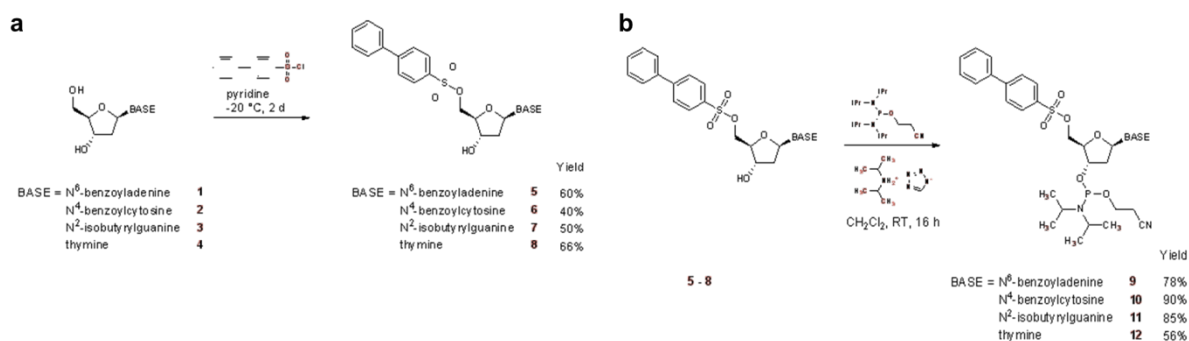
Supplementary Figure 1: *Chemical synthesis of 5'-O-biphenylsulfonyl-2'-deoxynucleosides (**a**) and of 5'-O-biphenylsulfonyl-2'-deoxynucleosides phosphoramidites (**b**)*

5 mmol of the starting base protected deoxynucleoside **1 – 4** (**Supplementary Figure 1a**) is dried by dissolving it twice in 20 mL anhydrous pyridine and evaporating the solvent. The nucleoside is redissolved in 20 mL anhydrous pyridine and cooled to -20°C (4°C for **3**) before adding 1.52 g (6.00 mmol) biphenyl-4-sulfonyl chloride. The reaction mixture is stirred for 2 days at -20°C (4°C for **3**). After completion, the reaction is quenched by the addition of 5 mL water and stirring is continued for 15 min at room temperature. The reaction mixture is then taken up in 100 mL dichloromethane and washed with saturated aqueous sodium bicarbonate solution (2 x 50 mL) and brine (50 mL). The aqueous layers are washed twice with 50 mL dichloromethane each. The combined organic phases are dried over anhydrous sodium sulfate, filtered, and evaporated. Residual pyridine is

removed by repeated co-evaporation with toluene (3 x 10 mL). The crude product is purified by flash chromatography yielding the 5'-O-biphenylsulfonyl-2'-deoxynucleoside **5** – **8** as off-white foam. Analytical data see **Supplementary Table 3**.

Compound	Yield	Analytical Data
5	60	Solvent system for flash chromatography: dichloromethane/methanol 96:4. TLC (dichloromethane/methanol 96:4): R_f = 0.07. ^{1}H NMR (400 MHz, d$_6$-DMSO) δ 11.17 (s, 1H), 8.68 (s, 1H), 8.57 (s, 1H), 8.08 – 8.03 (m, 2H), 7.88 – 7.83 (m, 4H), 7.74 – 7.70 (m, 2H), 7.68 – 7.64 (m, 1H), 7.59 – 7.54 (m, 2H), 7.51 – 7.41 (m, 3H), 6.47 (t, 1H, J = 6.7 Hz), 5.59 (s br., 1H), 4.55 – 4.50 (m br., 1H), 4.40 (dd, 1H, J$_1$ = 10.9 Hz, J$_2$ = 4.1 Hz), 4.35 (dd, 1H, J$_1$ = 11.0 Hz, J$_2$ = 6.5 Hz), 4.09 – 4.05 (m, 1H), 2.90 (p, 1H, J = 6.7 Hz), 2.40 (ddd, 1H, J$_1$ = 13.5 Hz, J$_2$ = 6.7 Hz, J$_3$ = 4.2 Hz).
6	40%	Solvent system for flash chromatography: dichloromethane/methanol 96:4. TLC (dichloromethane/methanol 96:4): R_f = 0.13. ^{1}H NMR (400 MHz, CDCl$_3$) δ 9.76 (s br., 1H), 7.96 (d, 1H, J = 7.6 Hz), 7.93 – 7.90 (m, 2H), 7.82 (d, 2H, J = 7.6 Hz), 7.75 – 7.71 (m, 2H), 7.57 – 7.52 (m, 3H), 7.46 – 7.31 (m, 6H), 6.22 (t, 1H, J = 6.3 Hz), 4.47 – 4.43 (m, 1H), 4.37 (dd, 1H, J$_1$ = 11.2 Hz, J$_2$ = 2.9 Hz), 4.33 (dd, 1H, J$_1$ = 11.4 Hz, J$_2$ = 3.1 Hz), 4.20 – 4.18 (m, 1H), 3.32 (s br., 1H), 2.65 (ddd, 1H, J$_1$ = 13.9 Hz, J$_2$ = 6.0 Hz, J$_3$ = 4.3 Hz), 2.14 (p, 1H, J = 6.7 Hz).
7	50%	Solvent system for flash chromatography: dichloromethane/acetone 4:6 to 1:9. TLC (dichloromethane/acetone 4:6): R_f = 0.23. ^{1}H NMR (400 MHz, CDCl$_3$) δ 12.20 (s, 1H), 8.89 (s, 1H), 7.81 – 7.77 (m, 3H), 7.63 – 7.60 (m, 2H), 7.49 – 7.46 (m, 2H), 7.40 – 7.31 (m, 3H), 6.13 (t, 1H, J = 6.7 Hz), 4.79 – 4.76 (m, 1H), 4.32 (dd, 1H, J$_1$ = 10.5 Hz, J$_2$ = 3.2 Hz), 4.22 (dd, 1H, J$_1$ = 10.6 Hz, J$_2$ = 4.1 Hz), 4.18 – 4.15 (m, 1H), 2.90 (p, 1H, J = 6.7 Hz), 2.73 (h, 1H, J = 6.9 Hz), 2.37 (ddd, 1H, J$_1$ = 13.2 Hz, J$_2$ = 6.1 Hz, J$_3$ = 3.0 Hz), 1.16 (d, 3H, J = 6.8 Hz), 1.15 (d, 3H, J = 6.8 Hz). ^{13}C NMR (101 MHz, CDCl$_3$) δ 180.24 (s), 155.90 (s), 148.56 (s), 147.99 (s), 147.01 (s), 139.04 (s), 138.54 (d), 133.40 (d), 129.12 (d), 128.87 (d), 128.32 (d), 127.90 (d), 127.27 (d), 121.44 (s), 85.47 (d), 84.56 (d), 71.35 (d), 70.10 (t), 39.27 (t), 36.12 (d), 19.01 (q), 18.99 (q).
8	66%	Solvent system for flash chromatography: dichloromethane/methanol 96:4. TLC (dichloromethane/methanol 9:1): R_f = 0.18. ^{1}H NMR (400 MHz, d$_6$-DMSO) δ 11.31 (s, 1H), 8.01 – 7.96 (m, 4H), 7.78 – 7.75 (m, 2H), 7.56 – 7.37 (m, 4H), 6.17 (t, 1H, J = 6.8 Hz), 5.46 (d, 1H, J = 4.3 Hz), 4.34 (dd, 1H, J$_1$ = 10.8 Hz, J$_2$ = 3.3 Hz), 4.27 (dd, 1H, J$_1$ = 10.9 Hz, J$_2$ = 5.8 Hz), 4.23 – 4.18 (m, 1H), 3.93 – 3.90 (m, 1H), 2.18 (p, 1H, J = 6.9 Hz), 2.39 (ddd, 1H, J$_1$ = 13.5 Hz, J$_2$ = 6.5 Hz, J$_3$ = 2.9 Hz). ^{13}C NMR (101 MHz, d$_6$-DMSO) δ 163.60 (s), 150.34 (s), 145.82 (s), 138.01 (s), 135.84 (d), 133.68 (s), 129.18 (d), 128.87 (d), 128.24 (d), 127.85 (d), 127.15 (d), 109.79 (s), 84.04 (d), 83.21 (d), 70.31 (t), 69.91 (d), 38.38 (t), 12.02 (q).
9	78%	Solvent system for flash chromatography: heptane/ethyl acetate 1:4 + 1% triethylamine. TLC (heptane/ethyl acetate 1:4): R_f = 0.23, 0.14. ^{1}H NMR (400 MHz, CDCl$_3$) δ 8.86 (s br., 1H), 8.66 (s, 1H), 8.11, 8.08 (2s, 1H), 7.92 – 7.89 (m, 2H), 7.86 – 7.80 (m, 2H), 7.63 – 7.27 (m, 10H), 6.40 – 6.36 (m, 1H), 4.82 – 4.74 (m, 1H), 4.37 – 4.24 (m, 3H), 3.87 – 3.78 (m, 1H), 3.74 – 3.66 (m, 1H), 3.61 – 3.36 (m, 2H), 2.98 – 2.87 (m, 1H), 2.65 – 2.51 (m, 3H), 1.24 – 1.10 (m, 12H). ^{13}C NMR (101 MHz, CDCl$_3$) δ 164.57 (s), 152.57 (d), 151.29 (s), 149.60 (s), 146.94 (s), 146.92 (s), 141.78 (d), 141.66 (d), 138.74 (s), 138.71 (s), 133.79 (s), 133.61 (s), 132.78 (d), 132.59 (d), 129.11 (d), 128.84 (d), 128.81 (d), 128.42 (d), 128.39 (d), 127.89 (d), 127.81 (d), 127.77 (d), 127.37 (d), 123.49 (s), 123.46 (s), 117.77 (s), 117.62 (s), 84.96 (d), 84.83 (d), 83.96 (d, J$_{CP}$ = 2.9 Hz), 83.68 (d, J$_{CP}$ = 6.6 Hz), 73.62 (d, J$_{CP}$ = 16.1 Hz), 73.33 (d, J$_{CP}$ = 16.1 Hz), 69.17 (t), 68.99 (t), 58.33 (t), 58.15 (t), 45.63 (d, J$_{CP}$ = 5.1 Hz), 43.36 (d, J$_{CP}$ = 12.4 Hz), 39.49 (t, J$_{CP}$ = 5.2 Hz), 38.73 (t, J$_{CP}$ = 3.7 Hz), (d), 24.67 (q), 24.61 (q), 24.54 (q), 20.46 (d, J$_{CP}$ = 7.3 Hz), 20.41 (d, J$_{CP}$ = 7.3 Hz).
10	90%	Solvent system for flash chromatography: heptane/ethyl acetate 1:4 + 1% triethylamine. TLC (heptane/ethyl acetate 14:86): R_f = 0.48, 0.39. ^{1}H NMR (400 MHz, CDCl$_3$) δ 8.56 (s br., 1H), 7.95 – 7.87 (m, 3H), 7.82 – 7.78 (m, 2H), 7.76 – 7.71 (m, 2H), 7.57 – 7.52 (m, 3H), 7.46 – 7.30 (m, 6H), 6.21 – 6.17 (m, 1H), 4.52 – 4.44 (m, 1H), 4.40 – 4.22 (m, 3H), 3.87 – 3.37 (m, 4H), 2.73 – 2.52 (m, 3H), 2.16 – 2.10 (m, 1H), 1.23 – 1.07 (m, 12H). ^{13}C NMR (101 MHz, CDCl$_3$) δ 162.25 (s), 154.68 (s), 147.31 (s), 147.29 (s), 143.98 (d), 138.73 (s), 133.84 (s), 133.80 (s), 133.19 (d), 132.99 (s), 129.14 (d), 129.02 (d), 128.86 (d), 128.45 (d), 128.09 (d), 127.59 (d), 127.41 (d), 117.76 (s), 117.58 (s), 96.70 (d), 87.37 (d), 87.28 (d), 83.93 (d, J$_{CP}$ = 2.9 Hz), 83.62 (d, J$_{CP}$ = 6.6 Hz), 72.74 (d, J$_{CP}$ = 16.1 Hz), 72.61 (d, J$_{CP}$ = 16.8 Hz), 68.42 (t, 86.26 (t), 58.27 (t, J$_{CP}$ = 19.0 Hz), 58.03 (t, J$_{CP}$ = 19.0 Hz), 45.63 (d, J$_{CP}$ = 4.4 Hz), 43.36 (d, J$_{CP}$ = 12.4 Hz), 40.71 (t), 40.66 (t), (d), 24.64 (q), 24.58 (q), 24.53 (q), 24.50 (q), 20.38 (d, J$_{CP}$ = 7.3 Hz), 20.35 (d, J$_{CP}$ = 7.3 Hz). ^{31}P NMR (162 MHz, CDCl$_3$) δ 149.9, 149.1.
11	85%	Solvent system for flash chromatography: dichloromethane/acetone 4:1 + 1% triethylamine. TLC (dichloromethane/acetone 4:1): R_f = 0.19, 0.16. ^{1}H NMR (400 MHz, CDCl$_3$) δ 12.00 (s br., 1H), 9.19, 9.17 (2s br., 1H), 7.86 – 7.83 (m, 2H), 7.69 – 7.58 (m, 3H), 7.54 – 7.50 (m, 2H), 7.44 – 7.35 (m, 3H), 6.09 – 6.02 (m, 1H), 4.80 – 4.74, 4.70 – 4.65 (2m, 1H), 4.51 – 4.46, 4.42 – 4.38 (2m, 1H), 4.29 – 4.04 (m, 2H), 3.85 – 3.78 (m, 1H), 3.72 – 3.62 (m, 1H), 3.59 – 3.39 (m, 2H), 3.16 – 3.02 (m, 1H), 2.71 – 2.49, 2.39 – 2.33 (2m, 4H), 1.22 – 1.09 (m, 18H). ^{13}C NMR (101 MHz, CDCl$_3$) δ 179.33 (s), 179.19 (s), 155.60 (s), 155.53 (s), 147.86 (s), 147.79 (s), 147.51 (s), 147.49 (s), 147.34 (s), 147.21 (s), 138.76 (d), 138.62 (s), 138.40 (d), 138.57 (s), 133.45 (s), 133.35 (s), 132.82 (d), 132.60 (d), 129.20 (d), 128.96 (d), 128.36 (d), 128.34 (d), 128.05 (d), 127.90 (d), 127.35 (d), 127.31 (d), 122.90 (s), 122.62 (s), 117.92 (s), 117.72 (s), 86.21 (d), 85.89 (d), 83.64 (d), 83.58 (d), 74.16 (d, J$_{CP}$ = 16.8 Hz), 73.51 (d, J$_{CP}$ = 15.3 Hz), 69.40 (t), 68.97 (t), 57.93 (t, J$_{CP}$ = 19.0 Hz), 57.68 (t, J$_{CP}$ = 19.0 Hz), 45.31 (d, J$_{CP}$ = 6.6 Hz), 43.32 (d, J$_{CP}$ = 14.2 Hz), 38.28 (t), 38.23 (t), (d), 36.14 (d), 36.02 (d), 24.64 (q), 24.57 (q), 24.55 (q), 24.48 (q), 20.52 (d, J$_{CP}$ = 7.3 Hz), 20.11 (d, J$_{CP}$ = 6.6 Hz), 19.00 (q), 18.98 (q), 18.91 (q), 18.88 (q).
12	56%	Solvent system for flash chromatography: heptane/ethyl acetate 2:3 + 1% triethylamine. TLC (heptane/ethyl acetate 2:3): R_f = 0.23, 0.16. ^{1}H NMR (400 MHz, CDCl$_3$) δ 8.58 (s br., 1H), 7.92 – 7.88 (m, 2H), 7.72 – 7.69 (m, 2H), 7.55 – 7.52 (m, 2H), 7.45 – 7.37 (m, 3H), 7.33, 7.29 (2q, 1H, J = 1.3 Hz), 6.29 – 6.25 (m, 1H), 4.55 – 4.46 (m, 1H), 4.33 – 4.11 (m, 3H), 3.83 – 3.37 (m, 4H), 2.58 – 2.54 (m, 2H), 2.45 – 2.32 (m, 1H), 2.19 – 2.11 (m, 1H), 1.88, 1.87 (2d, 3H, J = 1.3 Hz), 1.24 – 1.06 (m, 12H). ^{13}C NMR (101 MHz, CDCl$_3$) δ 163.53 (s), 150.27 (s), 147.30 (s), 138.77 (s), 135.27 (d), 133.86 (s), 129.20 (d), 128.93 (d), 128.42 (d), 128.06 (d), 127.35 (d), 117.70 (s), 111.68 (s), 84.85 (d), 83.37 (d), 83.34 (d), 73.25 (d), 73.09 (d), 69.13 (t), 58.14 (t), 57.95 (t), 43.46 (d), 43.33 (d), 39.40 (t), 39.36 (t), 24.64 (q), 24.57 (q), 24.55 (q), 24.48 (q), 20.42 (t), 20.35 (t), 12.43 (q). ^{31}P NMR (162 MHz, CDCl$_3$) δ 149.6, 149.0.

Supplementary Table 3: *Analytical NMR data obtained for each of the compounds synthesized in **Supplementary Figure 1***

A.21. Synthesis of N-protected 5'-O-biphenylsulfonyl-2'-deoxynucleoside phosphoramidites

To a solution of 5.00 mmol of the N-protected 5'-O-biphenylsulfonyl-2'-deoxynucleoside **5** – **8** in 25 mL anhydrous dichloromethane under argon is added 1.28 g (7.50 mmol) diisopropylammonium-tetrazolide (prepared from tetrazole and diisopropylamine or from Chem-Impex, #00951). Then 2.22 mL (2.11 g, 7.00 mmol) 2-cyanoethyl N,N,N',N'-tetraisopropylphosphordiamidite (Aldrich 97%, #305995) is added and the solution stirred at room temperature overnight. The reaction mixture is taken up in 100 mL dichloromethane and extracted with aqueous bicarbonate solution (2 x 50 mL) and brine (50 mL). The aqueous phases are reextracted with 50 mL dichloromethane. The combined organic phases are dried over sodium sulfate, filtered, and evaporated. The remaining oil is chromatographed on silica to give a mixture of diastereomeric 5'-O-biphenylsulfonyl-2'-deoxynucleoside phosphoramidites **9** – **12** (**Supplementary figure 1b**) as colorless brittle foam. Analytical data see **Supplementary Table 3**.

A.22. Synthesis of oligodeoxynucleotides with 3'-terminal phosphorothioate

DNA oligonucleotides were prepared on a MerMade 192 well DNA/RNA Synthesizer (BioAutomation) on a scale of 200 nmol. TheraPure™ deoxyribonucleoside phosphoramidites were dissolved in anhydrous acetonitrile at a concentration of 0.1 M. The activator, 5ethylthiotetrazole (ChemGenes, #RN-6397), was dissolved in acetonitrile

as a 0.5 M solution. Capping solution A consisted of acetic anhydride (Fluka, #45830) and 2,6-lutidine (Aldrich, #336106) in anhydrous THF (Aldrich, #401757) at a ratio of 1:1:8 (v/v/v) and capping solution B of 16% (v/v) 1-methylimidazole (Aldrich, #336092) in anhydrous THF. The oxidation solution was prepared by dissolving iodine (Aldrich, #207772) in a 1:1:8 (v/v/v) mixture of 2,6-lutidine, water and THF for a final concentration of 0.1 M. Deblocking solution was 4% (v/v) dichloroacetic acid (Aldrich, #D54702) in dichloromethane (Aldrich, #270997). Sulfurizing reagent consisted of a 0.05 M solution of 3-((dimethylaminomethylidene)amino)-3H-1,2,4-dithiazole-3-thione (Sulfurizing Reagent II, Glen Research, #40-4037-20) in pyridine/acetonitrile 3:2 (v/v). The synthesis cycle consisted of the following steps: 1) detritylation with deblocking solution (2 x 90 µL, 10 sec each), wash with acetonitrile (2 x 100 µL); 2) coupling reaction with a 6:1 (v/v) mixture of activator and phosphoramidite solution (2 x 35 µL, 3 min each), wash with acetonitrile (2 x 100 µL); 3) capping with a 1:1 (v/v) mixture of capping solutions A and B (100 µL, 20 sec) wash with acetonitrile (2 x 100 µL); 4) oxidation with iodine solution (100 µL, 60 sec) wash with acetonitrile (2 x 100 µL). Reagents are applied to the top of the columns and allowed to react for the time indicated. For their removal a gentle vacuum is applied as per manufacturer's instructions. Oligodeoxynucleotides are synthesized without removing the 5'-terminal dimethoxytrityl group. For the preparation of DNA oligonucleotides with a 3'-terminal thiophosphate a prepacked 200 nmol synthesis column (BioAutomation) was emptied and charged with 5 mg of 3'-phosphate CPG (Glen Research, #20-2900-01) (175). The following cycle is applied in the first coupling: 1) detritylation with deblocking solution (2 x 90 µL, 10 sec each), 2) coupling reaction with a 6:1 (v/v) mixture of activator and phosphoramidite solution (2 x 35 µL, 3 min each), wash with acetonitrile (2 x 100 µL); 3) sulfurization with sulfurizing reagent II (100 µL, 60 sec) wash with acetonitrile (2 x 100 µL); 4) capping with a 1:1 (v/v) mixture of capping solutions A and B (100 µL, 20 sec) wash with acetonitrile (2 x 100 µL). The oligodeoxynucleotides were detached from solid support and deprotected by treating with concentrated ammonia (Merck, #1.05426.1000) at 55°C overnight. The ammonia solution was filtered off and the resin washed with 500 µL water. The filtrate was lyophilized and the residue redissolved in 1 mL aqueous 0.1 M triethylammonium acetate buffer pH 7.0. The crude oligodeoxynucleotide was purified on a Oasis HLB 96-well plate (30 µm particle size, Waters, #WAT058951) applying the following protocol: 1) each well used is equilibrated by washing with 500 µL acetonitrile and 1mL aqueous 0.1 M triethylammonium acetate buffer pH 7.0; 2) the oligodeoxynucleotide solution above is applied to a single well; 3) the resin is washed with 1 mL 15% acetonitrile/water (v/v); 4) the DMT group is removed by applying 1 mL 3% aqueous dichloroacetic acid; 5) wash with 2 x 1 mL aqueous 0.1 M triethylammonium acetate buffer pH 7.0; 6) column is sucked dry by applying a gentle vacuum from the bottom; 7) apply 530 µL acetonitrile/water 1:1 (v/v) and collect oligonucleotide. The oligodeoxynucleotide solutions were evaporated on a plate lyophilizer (GeneVac, HT-4x) and the residue redissolved in water for a 80 µM stock solution. Purity and identity of all oligonucleotides were verified by LC-MS analysis (Thermo Scientific Accela 600 pumps, Accela PDA detector, and LCQ Fleet MS, equipped with a PAL System HTS PAL autosampler).

A.23. Synthesis of 5'-O-biphenylsulfonyl-derivatized oligodeoxynucleotides

Oligodeoxynucleotides containing a 5'-O-biphenylsulfonyl group were synthesized at a scale of 200 nmol as described above, except that Ultramild CE phosphoramidites (http://www.glenresearch.com/Technical/TB_UltraMild_Deprotection.pdf) for regular deoxynucleosides were used and for the final coupling step phosphoramidites **9** – **12**.

Capping was performed with phenoxyacetic anhydride (Aldrich, order no. 77750) substituting acetic anhydride. For deprotection, the CPG was treated with concentrated ammonia for 4 hrs at room temperature. Purification was achieved as above on Oasis HLB reverse phase cartridges, except that steps 4) and 5) were omitted.

A.24. Oligonucleotide synthesis

Phosphoramidites for 200 – 800 µmol syntheses of fully 2'-O-methyoxyethyl-modified oligoribonucleotides were custom synthesized ([176]). Control pore glass (CPG) solid supports with preloaded 2'-O-methyoxyethyl ribonucleoside monomers were custom synthesized starting from commercially available amine modified CPG (Prime Synthesis, LCAA/CNA CPG, #CPG601N12). Ultramild CE phosphoramidites for 200 nmol syntheses of 5'-O-biphenylsulfonyl-modified oligodeoxynucleotides were purchased from Glen Research (Pac-dA-CE Phosphoramidite #10-1601-10, Ac-dC-CE Phosphoramidite #10-1015-10, iPr-Pac-dG-CE Phosphoramidite #10-1621-10,). TheraPure™ DNA phosphoramidites were purchased from Thermo Scientific (Bz-dA-CE Phosphoramidite #27-2030-00, Bz-dC-CE Phosphoramidite #27-2032-00, iBu-dG-CE Phosphoramidite #27-2034-00, dT-CE Phosphoramidite #27-2036-00). Support for DNA oligonucleotides with a 3'-thiophosphate was obtained from Glen Research (3'-Phosphate CPG #20-2900-10). Anhydrous acetonitrile for oligonucleotide synthesis was purchased either from Biosolve (#012058, <10 ppm water) or from Sigma Aldrich (#L0114000-01, <30 ppm water). Sterile water for buffers and oligonucleotide solutions was obtained from a Milli-Q Advantage A10 station (Millipore).

A.25. AMO-miR-16 synthesis

The base-protected 2'-O-methoxyethyl ribonucleoside phosphoramidites were dissolved in anhydrous acetonitrile at a concentration of 0.15 M. AMO-miR-16 synthesis was performed on an Äkta Oligopilot plus OP100 (GE Healthcare) with the help of a 12 mL column reactor (GE Healthcare, #18-1101-16) using solid-phase synthesis cyclic procedure consisting of 5 steps, based on the manufacturer's template method. First, the 4,4'-dimethoxytrityl (DMT) protecting group was removed by adding deblocking reagent (3% DCA in toluene, Merck, #BI0832). Coupling was then achieved by adding the n+1 phophoramidite solution to the column along with an equal volume of 0.5 M 5-ethylthiotetrazole (ChemGenes, #RN-6397) in acetonitrile. Coupling was followed by capping by adding Cap A (Biosolve, #036124) and Cap B, obtained by mixing equivalent amounts of Cap B1 (Biosolve, #037424) and Cap B2 (Biosolve, #037425). The oligonucleotide was subsequently oxidized by adding iodine (Biosolve, #150724). The column was washed between each step with anhydrous acetonitrile. The synthesis procedure ended with a final detritylation step in order to remove the last DMT-group and allow easier purification. After synthesis the column was placed under vacuum in order to remove all remaining acetonitrile, and the support was transferred into a glass vial. The oligonucleotide was cleaved from the support and deprotected by incubating the support with 60 mL conc. ammonia solution 32% (Merck, #105426) overnight at 50°C under agitation. The solution was subsequently filtered on a Steritop filter unit (Millipore, #SCGPT05RE) and the filter was rinsed with water. The oligonucleotide was purified on a Fineline pilot 35 column (GE Healthcare, #18-1102-02) filled with TSK Gel SuperQ-5PW ion exchange resin (Tosoh, #18546) using an ÄKTAexplorer (GE Healthcare). Fractions of appropriate purity were pooled and then desalted by tangential flow filtration (TFF) on a Minim II TFF system (Pall Corporation) using a 1K Omega Centramate T-Series filtration unit (Pall Corporation, #OS001T12). The oligonucleotide was filtered again on a Steriflip-GP filtration unit (Millipore, #SCGP00525) and the quality of the oligonucleotide verified by

HPLC and UPLC-MS. Prior to injection into animals, endotoxin levels were assessed using the Endosafe-PTS system (Charles River) and PTS cartridges (Charles River, #PTS2005).

B.   Exosomes isolation and characterization

B.1.   Cell culture

HeLa (ATCC® CCL-2™), MS1 (ATCC® CRL-2279™) and 3T3 (ATCC® CRL-1658™) were from ATCC. Cells were cultured in Dulbecco's Modified Eagle's Medium (DMEM) (GIBCO, #32430) supplemented with 10% v/v fetal calf serum (FCS) (Invitrogen, #10270106) without antibiotics. For exosomes isolation, cells were grown until confluence in T-150 flasks (TPP, #90151), at which point the medium was replaced with 30 mL fresh DMEM supplemented with 10% v/v FCS. The conditioned medium was collected 48 hours after medium exchange and subjected to exosomes isolation.

B.2.   TCEP Lysis Buffer

The TCEP lysis buffer was prepared by diluting 100 µL 0.5 M HCl (Fluka, #84435), 500 µL 100% Triton-X-100 (Roche, #10789704001) and 75 mg TCEP (Sigma Aldrich, #4706-10G) in 50 mL DEPC-water. The lysis buffer was stored at 4°C until further handling.

B.3.   Exosomes isolation with the ExoQuick exosome precipitation solution

The entire procedure was performed in a tissue culture hood. Conditioned cell culture medium was collected in sterile Falcon tubes and centrifuged at 3,000 g for 15 minutes at 4°C to remove dead cells and cell debris. The supernatant was transferred to a new sterile Falcon tube and was supplemented with ExoQuick exosome precipitation solution (SBI, #EXOQ20A-1) in a 1:1 ratio and incubated overnight at 4°C. The solution was subsequently centrifuged at 1,500 g at 4°C for 30 minutes. The supernatant was discarded and the remaining drops were collected at the bottom of the tube by centrifugation at 1,500 g at 4°C for 5 minutes. The remaining solution was discarded, without disturbing the pelleted material. The precipitated material was resuspended in 1/10 of the original volume in PBS (GIBCO, #20012019) supplemented with protease inhibitors (Roche, #11873580001), and stored at 4°C until further handling.

B.4.   Differential ultracentrifugation for exosomes isolation

The entire procedure was performed in a tissue culture hood. The cell culture supernatant was collected from three T-150-flasks in 50 mL sterile Falcon tubes and centrifuged at 3,000 g for 10 minutes at 4°C. The supernatant was collected in fresh 50 mL Falcon tubes and centrifuged again for 10 minutes at 3,000 g at 4°C, to remove dead cells and cell debris. The supernatant was collected and transferred to 3 36 mL tubes (Beckman Coulter, #344058) from the SW40 swinging bucket rotor, and centrifuged at 100,000 g for 1 hour at 4°C. The supernatants were discarded and each pellet was dissolved in 1.5 mL PBS (GIBCO, #20012019) supplemented with protease inhibitors (Roche, #11873580001). The dissolved pellets were collected in a 5 mL tube (Beckman Coulter, #328874) from the SW60Ti swinging bucket rotor and centrifuged at 100,000 g for 1 hour at 4°C. The supernatant was discarded and the pellet was dissolved in 150 µL PBS (GIBCO, #20012019) supplemented with protease inhibitors (Roche, #11873580001). A 100%

sucrose solution was prepared by dissolving 100 g of sucrose (Sigma, #S1888) in PBS (GIBCO, #20012019) supplemented with protease inhibitors (Roche, #11873580001). This 100% sucrose solution was dissolved in PBS with protease inhibitors to prepare solutions containing 10, 15, 20, 25, 30, 35, 40, 45, 50, 55, 60, 65 and 70% sucrose. The linear sucrose gradient was prepared by overlaying 1mL of each of the sucrose solutions in a 16 mL tube (Beckman Coulter, #331372) from the SW40 swinging bucket rotor. The 70% sucrose solution was added at the bottom of the tube, using a sterile 2mL Plastipak™ Luer Slip syringe (BD, #300185) and a sterile 21G 0.8 x 40 mm needle (BD, #304432). The 65% sucrose solution was added on top of the 70% sucrose fraction by applying the end of the needle on the wall of the tube, and letting the solution flow gently along the wall, so that both solutions do not mix. This procedure was repeated for all the sucrose-containing solutions. The exosomes solutions was adjusted to 10% sucrose and overlaid on the gradient using the same procedure. The gradient was subsequently centrifuged at 100,000 g for 16 hours at 4°C. After centrifugation, the 200 μL fraction on top of the gradient was discarded. 1 mL fractions were pipetted off the gradient and transferred to 5 mL tubes from the SW60Ti swinging bucket rotor. The gradient fractions were supplemented with 3 mL PBS with protease inhibitors and centrifuged at 100,000 g for 1 hour at 4°C to pellet the exosomes from each sucrose gradient fraction. The supernatant was discarded and the pellets were dissolved in 50 μL PBS with protease inhibitors. The dissolved pellets were stored at 4°C until further handling.

B.5.   Exosomes isolation by ultrafiltration

Conditioned cell culture supernatant was subjected to ultrafiltration using the 100 kDa (Pall, #OD100C36) or 300 kDa (Pall, #OD300C37) molecular weight cut-off Macrosep devices. Prior to sample treatment, the devices were pre-rinsed by adding 15 mL DEPC water to the filtration unit and centrifuging the device at 4,500 g for 30 minutes at 4°C. The water collected in the recipient unit was discarded. The devices were sanitized by adding 15 mL 70% ethanol in the filtration unit, followed by centrifugation at 4,500 g for 30 minutes at 4°C. The ethanol collected in the recipient unit was discarded and the devices were washed by adding 15 mL DEPC water to the filtration unit. The devices were centrifuged at 4,500 g for 30 minutes at 4°C and the water collected in the recipient unit was discarded. 15 mL conditioned medium were added to the filtration unit and centrifuged at 4,500 g for 30 minutes at 4°C. The flow-through, located in the recipient unit, was collected in sterile Falcon tubes and stored at 4°C. The remaining unprocessed conditioned medium was added to the filtration unit, and centrifuged at 4,500 g for 30 minutes at 4°C. The second flow-through was collected in a sterile Falcon tube and stored at 4°C. The retentate, composed of the particles retained by the membrane in the filtration unit, was washed three successive times by adding 15 mL PBS supplemented with protease inhibitors on the retentate, and subjecting the device to centrifugation at 4,500 g for 30 minutes at 4°C. The retentate was subsequently dissolved in 500 μL PBS with protease inhibitors and stored at 4°C until further handling.

B.6.   Exosomes isolation by Tangential Flow Filtration

Prior to processing of the conditioned cell culture supernatant, the Minimate™-TFF-System (Pall, #OAPMP220) mounted with a 100 kDa molecular weight cut-off membrane (GE Healthcare, #UFP-100-C-MM01A) was flushed with 100 mL DEPC water under a maximum filtrate speed of 1 mL/min and keeping the pressure below 1 bar. The system was then washed with 200 mL 100 mM NaOH (Fluka, #72082) in DEPC water. The system was washed with DEPC water until the pH of the filtrate was down to 7. The system was purged and 500 mL conditioned cell culture supernatant were added in the

sample vessel. The TFF system was kept to a circulating speed of 1 mL/min and the pressure was kept below 1 bar. 100 mL sterile PBS supplemented with Protease inhibitors was added to the system as soon as the volume in the sample vessel was just high enough to allow the solution to flow in the tubing. This step was repeated 5 times in total. The solution remaining in the sample vessel and tubing (retentate) was collected in a sterile 15 mL Falcon tube and stored at 4°C as soon as the retentate volume was too low to circulate properly in the TFF system. The system was subsequently washed with 500 mL 100 mM NaOH in DEPC water.

B.7.   Samples preparation for Triton-dependent RT-qPCR

The exosome samples were transferred to a 96-well plate and supplemented with an equivalent volume of either TCEP Lysis Buffer or PBS. The plate was then place on a shaker for 5 minutes and centrifuged for 15 seconds at 1,450 g. The samples were subsequently diluted 1 in 10 in DEPC water and stored at -20°C until further handling.

B.8.   Polybrene/CSC precipitation

After collection, the conditioned medium was centrifuged at 3,000 g for 30 minutes at 4°C to remove dead cells and cell debris. The supernatant was transferred to fresh sterile Falcon tubes and was supplemented with TrisHCl buffer pH 7.5 to a final concentration of 100 mM. Polybrene (Sigma, #107689) diluted in PBS was added to the cell culture to a final concentration of 100 µg/mL and the solution was incubated for 30 minutes at 4°C, under agitation. Chondroitin sulfate C (Sigma, #C4384) was added to the solution to a concentration ranging between 0 and 5 mg/mL. The solution was incubated for 30 minutes at 4°C under agitation and centrifuged at 3,000 g for 30 minutes at 4°C. The supernatant was discarded and the pellet was dissolved in 10 mL PBS supplemented with Protease inhibitors. The solution was centrifuged at 3,000 g for 30 minutes at 4°C and the supernatant was discarded. The pellet was resuspended in 200 µL PBS supplemented with protease inhibitors. The pellets were stored at 4°C until further handling.

B.9.   Particle size determination by Dynamic Light Scattering

The particle size distribution of the exosomes preparation was determined on a Zetasizer Nano ZS (Malvern). 20 µL exosomes solution were diluted in 380 µL PBS and transferred in a single-use cuvette. The parameters used for the measurements are the following: Materil RI: 1.45; Dispersant name: PBS; Dispersant RI: 1.335; Viscosity: 1.0200.

B.10.   Western Blotting

13 µL samples were supplemented with 5 µL 4x LDS Loading Buffer (Invitrogen, #NP0007) and 2 µL Reducing agent (Invitrogen, #NP0004) and incubated at 70°C for 10 minutes under agitation (1,000 rpm). The samples were loaded on a NuPAGE® Novex® 4-12% Bis-Tris gel (Invitrogen, #NP0322PK2). 5 µL of Protein ladder (Bio-Rad, #161-0376) and Western blot protein ladder (Bio-Rad, #161-0381) were loaded on the gel to monitor protein migration during electrophoresis and after western blotting. Protein migration was performed using MOPS SDS running buffer (Invitrogen, #NP0001) for 50 minutes at 200 V. The semi-dry transfer was performed by overlaying 2 layers of whatman paper, a nitrocellulose membrane, the gel and 2 layers of whatman paper avoiding the presence of bubbles between the various layers and adding enough transfer buffer (Invitrogen, #NP0006) to keep all layers wet. The transfer was performed at 160 mA for 2 hours. The

membrane was blocked in 5% milk (Bio-Rad, #170-6404) in TBS-Tween for 1 hour at 4°C. The primary antibody (**Supplementary Table 4**) was incubated on the membrane in 5% milk in TBS-Tween for 1 hour at room temperature or overnight at 4°C, under agitation. The membrane was washed 3 times with TBS-Tween for 5 minutes, and incubated with the secondary antibody (**Supplementary Table 4**) in 5% milk in TBS-Tween for 1 hour at room temperature.

Target	Primary antibody		Secondary antibody	
	Reference	Dilution	Reference	Dilution
CD63	sc-15363	1:1000	sc-2077	1:5000
Alix	sc-53540	1:200	sc-2096	1:5000

Supplementary Table 4: Primary and secondary antibodies used for the detection of CD63 and Alix proteins

The membrane was washed 3 times 5 minutes with TBS-Tween. The blot was revealed by incubating it with ECL+ (GE Healthcare, #RPN2132) and a picture was taken using a BioRad XRS ChemiDoc station, and analyzed with the software Quantity One.

VIII. References

1. Stephenson, M.L. and Zamecnik, P.C. (1978) Inhibition of Rous sarcoma viral RNA translation by a specific oligodeoxyribonucleotide. *Proc Natl Acad Sci U S A*, **75**, 285-288.
2. Zamecnik, P.C. and Stephenson, M.L. (1978) Inhibition of Rous sarcoma virus replication and cell transformation by a specific oligodeoxynucleotide. *Proc Natl Acad Sci U S A*, **75**, 280-284.
3. Melnikova, I. (2007) RNA-based therapies. *Nat Rev Drug Discov*, **6**, 863-864.
4. Gavrilov, K. and Saltzman, W.M. (2012) Therapeutic siRNA: principles, challenges, and strategies. *Yale J Biol Med*, **85**, 187-200.
5. Zamecnik, P.C., Goodchild, J., Taguchi, Y. and Sarin, P.S. (1986) Inhibition of Replication and Expression of Human T-Cell Lymphotropic Virus Type-Iii in Cultured-Cells by Exogenous Synthetic Oligonucleotides Complementary to Viral-Rna. *P Natl Acad Sci USA*, **83**, 4143-4146.
6. Rayner, S., Brignac, S., Bumeister, R., Belosludtsev, Y., Ward, T., Grant, O., O'Brien, K., Evans, G.A. and Garner, H.R. (1998) MerMade: An oligodeoxyribonucleotide synthesizer for high throughput oligonucleotide production in dual 96-well plates. *Genome Research*, **8**, 741-747.
7. Hovingh, K., Besseling, J. and Kastelein, J. (2013) Efficacy and safety of mipomersen sodium (Kynamro). *Expert opinion on drug safety*.
8. Matzke, M.A. and Matzke, A.J. (2004) Planting the seeds of a new paradigm. *PLoS biology*, **2**, E133.
9. Lee, R.C., Feinbaum, R.L. and Ambros, V. (1993) The C. elegans heterochronic gene lin-4 encodes small RNAs with antisense complementarity to lin-14. *Cell*, **75**, 843-854.
10. Filipowicz, W., Jaskiewicz, L., Kolb, F.A. and Pillai, R.S. (2005) Post-transcriptional gene silencing by siRNAs and miRNAs. *Current opinion in structural biology*, **15**, 331-341.
11. Gregory, R.I. and Shiekhattar, R. (2005) MicroRNA Biogenesis and Cancer. *Cancer Research*, **65**, 3509-3512.
12. Friedman, J.M. and Jones, P.A. (2009) MicroRNAs: critical mediators of differentiation, development and disease. *Swiss medical weekly*, **139**, 466-472.
13. Rutnam, Z.J. and Yang, B.B. (2012) The involvement of microRNAs in malignant transformation. *Histology and histopathology*, **27**, 1263-1270.
14. Chen, P.S., Su, J.L. and Hung, M.C. (2012) Dysregulation of microRNAs in cancer. *Journal of biomedical science*, **19**, 90.
15. Burnett, John C. and Rossi, John J. (2012) RNA-Based Therapeutics: Current Progress and Future Prospects. *Chemistry & Biology*, **19**, 60-71.
16. Fire, A., Xu, S., Montgomery, M.K., Kostas, S.A., Driver, S.E. and Mello, C.C. (1998) Potent and specific genetic interference by double-stranded RNA in Caenorhabditis elegans. *Nature*, **391**, 806-811.
17. Rudnick, S.I., Swaminathan, J., Sumaroka, M., Liebhaber, S. and Gewirtz, A.M. (2008) Effects of local mRNA structure on posttranscriptional gene silencing. *Proc Natl Acad Sci U S A*, **105**, 13787-13792.
18. Farazi, T.A., Juranek, S.A. and Tuschl, T. (2008) The growing catalog of small RNAs and their association with distinct Argonaute/Piwi family members. *Development*, **135**, 1201-1214.

19. Grimm, D., Streetz, K.L., Jopling, C.L., Storm, T.A., Pandey, K., Davis, C.R., Marion, P., Salazar, F. and Kay, M.A. (2006) Fatality in mice due to oversaturation of cellular microRNA/short hairpin RNA pathways. *Nature*, **441**, 537-541.
20. Haussecker, D. (2012) The Business of RNAi Therapeutics in 2012. *Molecular therapy. Nucleic acids*, **1**, e8.
21. Ogris, M. and Schaffert, D. (2011) SiRNA therapeutics: chances, pitfalls and future potential. *Ther Deliv*, **2**, 1101-1104.
22. Li, C.X., Parker, A., Menocal, E., Xiang, S., Borodyansky, L. and Fruehauf, J.H. (2006) Delivery of RNA interference. *Cell Cycle*, **5**, 2103-2109.
23. Morin, A., Gallou-Kabani, C., Mathieu, J.R. and Cabon, F. (2009) Systemic delivery and quantification of unformulated interfering RNAs in vivo. *Curr Top Med Chem*, **9**, 1117-1129.
24. Stenvang, J., Petri, A., Lindow, M., Obad, S. and Kauppinen, S. (2012) Inhibition of microRNA function by antimiR oligonucleotides. *Silence*, **3**, 1.
25. Davidson, B.L. and McCray, P.B., Jr. (2011) Current prospects for RNA interference-based therapies. *Nat Rev Genet*, **12**, 329-340.
26. Vaishnaw, A.K., Gollob, J., Gamba-Vitalo, C., Hutabarat, R., Sah, D., Meyers, R., de Fougerolles, T. and Maraganore, J. (2010) A status report on RNAi therapeutics. *Silence*, **1**, 14.
27. Gleave, M.E. and Monia, B.P. (2005) Antisense therapy for cancer. *Nat Rev Cancer*, **5**, 468-479.
28. Martinez, T., Wright, N., Lopez-Fraga, M., Jimenez, A.I. and Paneda, C. (2013) Silencing human genetic diseases with oligonucleotide-based therapies. *Human genetics*, **132**, 481-493.
29. Daka, A. and Peer, D. (2012) RNAi-based nanomedicines for targeted personalized therapy. *Adv Drug Deliv Rev*, **64**, 1508-1521.
30. Davis, M.E., Zuckerman, J.E., Choi, C.H., Seligson, D., Tolcher, A., Alabi, C.A., Yen, Y., Heidel, J.D. and Ribas, A. (2010) Evidence of RNAi in humans from systemically administered siRNA via targeted nanoparticles. *Nature*, **464**, 1067-1070.
31. Miele, E., Spinelli, G.P., Di Fabrizio, E., Ferretti, E., Tomao, S. and Gulino, A. (2012) Nanoparticle-based delivery of small interfering RNA: challenges for cancer therapy. *International journal of nanomedicine*, **7**, 3637-3657.
32. Yan, M., Liang, M., Wen, J., Liu, Y., Lu, Y. and Chen, I.S. (2012) Single siRNA nanocapsules for enhanced RNAi delivery. *J Am Chem Soc*, **134**, 13542-13545.
33. Zimmermann, T.S., Lee, A.C., Akinc, A., Bramlage, B., Bumcrot, D., Fedoruk, M.N., Harborth, J., Heyes, J.A., Jeffs, L.B., John, M. *et al.* (2006) RNAi-mediated gene silencing in non-human primates. *Nature*, **441**, 111-114.
34. Tao, W., Mao, X., Davide, J.P., Ng, B., Cai, M., Burke, P.A., Sachs, A.B. and Sepp-Lorenzino, L. (2011) Mechanistically Probing Lipid-siRNA Nanoparticle-associated Toxicities Identifies Jak Inhibitors Effective in Mitigating Multifaceted Toxic Responses. *Mol Ther*, **19**, 567-575.
35. Barros, S.A. and Gollob, J.A. (2012) Safety profile of RNAi nanomedicines. *Adv Drug Deliv Rev*, **64**, 1730-1737.
36. Tabernero, J., Shapiro, G.I., Lorusso, P.M., Cervantes, A., Schwartz, G.K., Weiss, G.J., Paz-Ares, L., Cho, D.C., Infante, J.R., Alsina, M. *et al.* (2013) First-in-Humans Trial of an RNA Interference Therapeutic Targeting VEGF and KSP in Cancer Patients with Liver Involvement. *Cancer discovery*, **3**, 406-417.
37. Semple, S.C., Akinc, A., Chen, J., Sandhu, A.P., Mui, B.L., Cho, C.K., Sah, D.W., Stebbing, D., Crosley, E.J., Yaworski, E. *et al.* (2010) Rational design of cationic lipids for siRNA delivery. *Nat Biotechnol*, **28**, 172-176.

38. Tao, W., Davide, J.P., Cai, M., Zhang, G.J., South, V.J., Matter, A., Ng, B., Zhang, Y. and Sepp-Lorenzino, L. (2010) Noninvasive imaging of lipid nanoparticle-mediated systemic delivery of small-interfering RNA to the liver. *Mol Ther*, **18**, 1657-1666.

39. Leachman, S.A., Hickerson, R.P., Schwartz, M.E., Bullough, E.E., Hutcherson, S.L., Boucher, K.M., Hansen, C.D., Eliason, M.J., Srivatsa, G.S., Kornbrust, D.J. *et al.* (2010) First-in-human mutation-targeted siRNA phase Ib trial of an inherited skin disorder. *Mol Ther*, **18**, 442-446.

40. Gao, S., Dagnaes-Hansen, F., Nielsen, E.J., Wengel, J., Besenbacher, F., Howard, K.A. and Kjems, J. (2009) The effect of chemical modification and nanoparticle formulation on stability and biodistribution of siRNA in mice. *Mol Ther*, **17**, 1225-1233.

41. Fernando, G.J.P., Chen, X., Primiero, C.A., Yukiko, S.R., Fairmaid, E.J., Corbett, H.J., Frazer, I.H., Brown, L.E. and Kendall, M.A.F. (2012) Nanopatch targeted delivery of both antigen and adjuvant to skin synergistically drives enhanced antibody responses. *Journal of Controlled Release*, **159**, 215-221.

42. Wooddell, C.I., Rozema, D.B., Hossbach, M., John, M., Hamilton, H.L., Chu, Q., Hegge, J.O., Klein, J.J., Wakefield, D.H., Oropeza, C.E. *et al.* (2013) Hepatocyte-targeted RNAi Therapeutics for the Treatment of Chronic Hepatitis B Virus Infection. *Mol Ther*.

43. Jarver, P., Coursindel, T., Andaloussi, S.E., Godfrey, C., Wood, M.J. and Gait, M.J. (2012) Peptide-mediated Cell and In Vivo Delivery of Antisense Oligonucleotides and siRNA. *Molecular therapy. Nucleic acids*, **1**, e27.

44. Korrapati, A.B., Swaminathan, G., Singh, A., Khanna, N. and Swaminathan, S. (2012) Adenovirus delivered short hairpin RNA targeting a conserved site in the 5' non-translated region inhibits all four serotypes of dengue viruses. *PLoS neglected tropical diseases*, **6**, e1735.

45. Abbas-Terki, T., Blanco-Bose, W., Deglon, N., Pralong, W. and Aebischer, P. (2002) Lentiviral-mediated RNA interference. *Hum Gene Ther*, **13**, 2197-2201.

46. Feng, Y., Zhang, X., Graves, P. and Zeng, Y. (2012) A comprehensive analysis of precursor microRNA cleavage by human Dicer. *RNA*, **18**, 2083-2092.

47. Ahi, Y.S., Bangari, D.S. and Mittal, S.K. (2011) Adenoviral vector immunity: its implications and circumvention strategies. *Current gene therapy*, **11**, 307-320.

48. Koppers-Lalic, D., Hogenboom, M.M., Middeldorp, J.M. and Pegtel, D.M. (2013) Virus-modified exosomes for targeted RNA delivery; A new approach in nanomedicine. *Adv Drug Deliv Rev*, **65**, 348-356.

49. Hata, T., Murakami, K., Nakatani, H., Yamamoto, Y., Matsuda, T. and Aoki, N. (2010) Isolation of bovine milk-derived microvesicles carrying mRNAs and microRNAs. *Biochem Biophys Res Commun*, **396**, 528-533.

50. Pegtel, D.M., Cosmopoulos, K., Thorley-Lawson, D.A., van Eijndhoven, M.A., Hopmans, E.S., Lindenberg, J.L., de Gruijl, T.D., Wurdinger, T. and Middeldorp, J.M. (2010) Functional delivery of viral miRNAs via exosomes. *Proc Natl Acad Sci U S A*, **107**, 6328-6333.

51. Alvarez-Erviti, L., Seow, Y., Yin, H., Betts, C., Lakhal, S. and Wood, M.J. (2011) Delivery of siRNA to the mouse brain by systemic injection of targeted exosomes. *Nat Biotechnol*, **29**, 341-345.

52. Chen, C., Ridzon, D.A., Broomer, A.J., Zhou, Z., Lee, D.H., Nguyen, J.T., Barbisin, M., Xu, N.L., Mahuvakar, V.R., Andersen, M.R. *et al.* (2005) Real-time quantification of microRNAs by stem-loop RT-PCR. *Nucleic Acids Res*, **33**, e179.

53. Kauppinen, S. and Havelda, Z. (2008) Detection of siRNAs and miRNAs. *Methods Mol Biol*, **451**, 217-227.

54. Bahr, U., Aygun, H. and Karas, M. (2008) Detection and relative quantification of siRNA double strands by MALDI mass spectrometry. *Anal Chem*, **80**, 6280-6285.

55. Solon, E., Schweitzer, A., Stoeckli, M. and Prideaux, B. (2010) Autoradiography, MALDI-MS, and SIMS-MS Imaging in Pharmaceutical Discovery and Development. *AAPS J*, **12**, 11-26.

56. Hemsley, M., Ewles, M. and Goodwin, L. (2012) Development of a bioanalytical method for quantification of a 15-mer oligonucleotide at sub-ng/ml concentrations using LC-MS/MS. *Bioanalysis*, **4**, 1457-1469.

57. Cheng, A., Li, M., Liang, Y., Wang, Y., Wong, L., Chen, C., Vlassov, A.V. and Magdaleno, S. (2009) Stem-loop RT-PCR quantification of siRNAs in vitro and in vivo. *Oligonucleotides*, **19**, 203-208.

58. Chen, A., Dogdas, B., Mehta, S., Haskell, K., Ng, B., Keough, E., Howell, B., Meacham, D.A., Aslamkhan, A.G., Davide, J. *et al.* (2012) Quantification of Cy-5 siRNA signal in the intra-vital multi-photon microscopy images. *Conf Proc IEEE Eng Med Biol Soc*, **2012**, 3712-3715.

59. Yoo, H. and Juliano, R.L. (2000) Enhanced delivery of antisense oligonucleotides with fluorophore-conjugated PAMAM dendrimers. *Nucleic Acids Res*, **28**, 4225-4231.

60. Coe, R.A. (2000) Quantitative whole-body autoradiography. *Regul Toxicol Pharmacol*, **31**, S1-3.

61. Boos, J.A., Kirk, D.W., Piccolotto, M.-L., Zuercher, W., Gfeller, S., Neuner, P., Dattler, A., Wishart, W.L., Von Arx, F., Beverly, M. *et al.* (2013) Whole-body scanning PCR; a highly sensitive method to study the biodistribution of mRNAs, noncoding RNAs and therapeutic oligonucleotides. *Nucleic acids research*.

62. Gallo, M., Montserrat, J.M. and Iribarren, A.M. (2003) Design and applications of modified oligonucleotides. *Braz J Med Biol Res*, **36**, 143-151.

63. Kurreck, J. (2003) Antisense technologies. Improvement through novel chemical modifications. *Eur J Biochem*, **270**, 1628-1644.

64. Mraz, M., Malinova, K., Mayer, J. and Pospisilova, S. (2009) MicroRNA isolation and stability in stored RNA samples. *Biochem Biophys Res Commun*, **390**, 1-4.

65. Kanno, J., Aisaki, K., Igarashi, K., Nakatsu, N., Ono, A., Kodama, Y. and Nagao, T. (2006) "Per cell" normalization method for mRNA measurement by quantitative PCR and microarrays. *BMC Genomics*, **7**, 64.

66. Crissey, M.A., Leu, J.I., DeAngelis, R.A., Greenbaum, L.E., Scearce, L.M., Kovalovich, K. and Taub, R. (1999) Liver-specific and proliferation-induced deoxyribonuclease I hypersensitive sites in the mouse insulin-like growth factor binding protein-1 gene. *Hepatology*, **30**, 1187-1197.

67. Ng, W.A., Grupp, I.L., Subramaniam, A. and Robbins, J. (1991) Cardiac Myosin Heavy-Chain Messenger-Rna Expression and Myocardial-Function in the Mouse Heart. *Circ Res*, **68**, 1742-1750.

68. Boggs, J.M. (2006) Myelin basic protein: a multifunctional protein. *Cell Mol Life Sci*, **63**, 1945-1961.

69. Rohner, T.C., Staab, D. and Stoeckli, M. (2005) MALDI mass spectrometric imaging of biological tissue sections. *Mechanisms of Ageing and Development*, **126**, 177-185.

70. Stoeckli, M., Staab, D. and Schweitzer, A. (2007) Compound and metabolite distribution measured by MALDI mass spectrometric imaging in whole-body tissue sections. *International Journal of Mass Spectrometry*, **260**, 195-202.

90

71.   Kim, B.R., Nam, H.Y., Kim, S.U., Kim, S.I. and Chang, Y.J. (2003) Normalization of reverse transcription quantitative-PCR with housekeeping genes in rice. *Biotechnol Lett*, **25**, 1869-1872.

72.   Zhang, G., Zhao, M., Song, C., Luo, A., Bai, J. and Guo, S. (2012) Characterization of reference genes for quantitative real-time PCR analysis in various tissues of Anoectochilus roxburghii. *Mol Biol Rep*, **39**, 5905-5912.

73.   Vandesompele, J., De Preter, K., Pattyn, F., Poppe, B., Van Roy, N., De Paepe, A. and Speleman, F. (2002) Accurate normalization of real-time quantitative RT-PCR data by geometric averaging of multiple internal control genes. *Genome Biol*, **3**, RESEARCH0034.

74.   Thellin, O., Zorzi, W., Lakaye, B., De Borman, B., Coumans, B., Hennen, G., Grisar, T., Igout, A. and Heinen, E. (1999) Housekeeping genes as internal standards: use and limits. *J Biotechnol*, **75**, 291-295.

75.   Shimada, H., Obayashi, T., Takahashi, N., Matsui, M. and Sakamoto, A. (2010) Normalization using ploidy and genomic DNA copy number allows absolute quantification of transcripts, proteins and metabolites in cells. *Plant Methods*, **6**, 29.

76.   Raymond, C.K., Roberts, B.S., Garrett-Engele, P., Lim, L.P. and Johnson, J.M. (2005) Simple, quantitative primer-extension PCR assay for direct monitoring of microRNAs and short-interfering RNAs. *RNA*, **11**, 1737-1744.

77.   Li, J. and Makrigiorgos, G.M. (2007) Anti-primer quenching-based real-time PCR for simplex or multiplex DNA quantification and single-nucleotide polymorphism genotyping. *Nat Protoc*, **2**, 50-58.

78.   Wu, D.Y., Ugozzoli, L., Pal, B.K., Qian, J. and Wallace, R.B. (1991) The Effect of Temperature and Oligonucleotide Primer Length on the Specificity and Efficiency of Amplification by the Polymerase Chain-Reaction. *DNA Cell Biol*, **10**, 233-238.

79.   Jensen, S.G., Lamy, P., Rasmussen, M.H., Ostenfeld, M.S., Dyrskjot, L., Orntoft, T.F. and Andersen, C.L. (2011) Evaluation of two commercial global miRNA expression profiling platforms for detection of less abundant miRNAs. *BMC Genomics*, **12**, 435.

80.   Lagos-Quintana, M., Rauhut, R., Yalcin, A., Meyer, J., Lendeckel, W. and Tuschl, T. (2002) Identification of tissue-specific microRNAs from mouse. *Curr Biol*, **12**, 735-739.

81.   Landgraf, P., Rusu, M., Sheridan, R., Sewer, A., Iovino, N., Aravin, A., Pfeffer, S., Rice, A., Kamphorst, A.O., Landthaler, M. *et al.* (2007) A mammalian microRNA expression atlas based on small RNA library sequencing. *Cell*, **129**, 1401-1414.

82.   Sempere, L.F., Freemantle, S., Pitha-Rowe, I., Moss, E., Dmitrovsky, E. and Ambros, V. (2004) Expression profiling of mammalian microRNAs uncovers a subset of brain-expressed microRNAs with possible roles in murine and human neuronal differentiation. *Genome Biology*, **5**.

83.   Park, C.W., Zeng, Y., Zhang, X., Subramanian, S. and Steer, C.J. (2010) Mature microRNAs identified in highly purified nuclei from HCT116 colon cancer cells. *RNA Biol*, **7**, 606-614.

84.   Berezikov, E., van Tetering, G., Verheul, M., van de Belt, J., van Laake, L., Vos, J., Verloop, R., van de Wetering, M., Guryev, V., Takada, S. *et al.* (2006) Many novel mammalian microRNA candidates identified by extensive cloning and RAKE analysis. *Genome Res*, **16**, 1289-1298.

85.   Zhou, J., Zhou, Y., Yin, B., Hao, W., Zhao, L., Ju, W. and Bai, C. (2010) 5-Fluorouracil and oxaliplatin modify the expression profiles of microRNAs in human colon cancer cells in vitro. *Oncol Rep*, **23**, 121-128.

86.   Christensen, J., Natt, F., Hunziker, J., Krauser, J., Andres, H. and Swart, P. (2012) Tritium labeling of full-length small interfering RNAs. *Journal of Labelled Compounds and Radiopharmaceuticals*, **55**, 189-196.

87.   Weiler, J., Hunziker, J. and Hall, J. (2005) Anti-miRNA oligonucleotides (AMOs): ammunition to target miRNAs implicated in human disease? *Gene therapy*, **13**, 496-502.

88.   Park, J.K., Kogure, T., Nuovo, G.J., Jiang, J., He, L., Kim, J.H., Phelps, M.A., Papenfuss, T.L., Croce, C.M., Patel, T. *et al.* (2011) miR-221 silencing blocks hepatocellular carcinoma and promotes survival. *Cancer Res*, **71**, 7608-7616.

89.   Xu, Y., Karalkar, N.B. and Kool, E.T. (2001) Nonenzymatic autoligation in direct three-color detection of RNA and DNA point mutations. *Nat Biotech*, **19**, 148-152.

90.   Silverman, A.P. and Kool, E.T. (2006) Detecting RNA and DNA with templated chemical reactions. *Chem Rev*, **106**, 3775-3789.

91.   Xu, Y. and Kool, E.T. (1997) A Novel 5'-Iodonucleoside Allows Efficient Nonenzymatic Ligation of Single-stranded and Duplex DNAs. *Tetrahedron Lett*, **38**, 5595-5598.

92.   Sando, S. and Kool, E.T. (2002) Quencher as leaving group: efficient detection of DNA-joining reactions. *J Am Chem Soc*, **124**, 2096-2097.

93.   Geary, R.S., Watanabe, T.A., Truong, L., Freier, S., Lesnik, E.A., Sioufi, N.B., Sasmor, H., Manoharan, M. and Levin, A.A. (2001) Pharmacokinetic properties of 2'-O-(2-methoxyethyl)-modified oligonucleotide analogs in rats. *J Pharmacol Exp Ther*, **296**, 890-897.

94.   Pinheiro, V.B., Taylor, A.I., Cozens, C., Abramov, M., Renders, M., Zhang, S., Chaput, J.C., Wengel, J., Peak-Chew, S.Y., McLaughlin, S.H. *et al.* (2012) Synthetic genetic polymers capable of heredity and evolution. *Science*, **336**, 341-344.

95.   Harcourt, E.M. and Kool, E.T. (2012) Amplified microRNA detection by templated chemistry. *Nucleic Acids Res*, **40**, e65.

96.   Armani, M., Tangrea, M.A., Shapiro, B., Emmert-Buck, M.R. and Smela, E. (2011) Quantifying mRNA levels across tissue sections with 2D-RT-qPCR. *Anal Bioanal Chem*, **400**, 3383-3393.

97.   Prakash, S., Malhotra, M. and Rengaswamy, V. (2010) Nonviral siRNA delivery for gene silencing in neurodegenerative diseases. *Methods Mol Biol*, **623**, 211-229.

98.   Oh, Y.K. and Park, T.G. (2009) siRNA delivery systems for cancer treatment. *Adv Drug Deliv Rev*, **61**, 850-862.

99.   Lai, R.C., Yeo, R.W., Tan, K.H. and Lim, S.K. (2012) Exosomes for drug delivery - a novel application for the mesenchymal stem cell. *Biotechnology advances*.

100.   Johnstone, R.M., Adam, M., Hammond, J.R., Orr, L. and Turbide, C. (1987) Vesicle formation during reticulocyte maturation. Association of plasma membrane activities with released vesicles (exosomes). *J Biol Chem*, **262**, 9412-9420.

101.   Johnstone, R.M., Bianchini, A. and Teng, K. (1989) Reticulocyte maturation and exosome release: transferrin receptor containing exosomes shows multiple plasma membrane functions. *Blood*, **74**, 1844-1851.

102.   Clayton, A., Court, J., Navabi, H., Adams, M., Mason, M.D., Hobot, J.A., Newman, G.R. and Jasani, B. (2001) Analysis of antigen presenting cell derived exosomes, based on immuno-magnetic isolation and flow cytometry. *J Immunol Methods*, **247**, 163-174.

103.   Johnstone, R.M., Mathew, A., Mason, A.B. and Teng, K. (1991) Exosome formation during maturation of mammalian and avian reticulocytes: evidence that exosome release is a major route for externalization of obsolete membrane proteins. *Journal of cellular physiology*, **147**, 27-36.

104. Mobius, W., van Donselaar, E., Ohno-Iwashita, Y., Shimada, Y., Heijnen, H.F., Slot, J.W. and Geuze, H.J. (2003) Recycling compartments and the internal vesicles of multivesicular bodies harbor most of the cholesterol found in the endocytic pathway. *Traffic*, **4**, 222-231.

105. Skokos, D., Botros, H.G., Demeure, C., Morin, J., Peronet, R., Birkenmeier, G., Boudaly, S. and Mecheri, S. (2003) Mast cell-derived exosomes induce phenotypic and functional maturation of dendritic cells and elicit specific immune responses in vivo. *J Immunol*, **170**, 3037-3045.

106. Skokos, D., Goubran-Botros, H., Roa, M. and Mecheri, S. (2002) Immunoregulatory properties of mast cell-derived exosomes. *Molecular immunology*, **38**, 1359-1362.

107. Skokos, D., Le Panse, S., Villa, I., Rousselle, J.C., Peronet, R., David, B., Namane, A. and Mecheri, S. (2001) Mast cell-dependent B and T lymphocyte activation is mediated by the secretion of immunologically active exosomes. *J Immunol*, **166**, 868-876.

108. Thery, C., Duban, L., Segura, E., Veron, P., Lantz, O. and Amigorena, S. (2002) Indirect activation of naive CD4+ T cells by dendritic cell-derived exosomes. *Nature immunology*, **3**, 1156-1162.

109. Wubbolts, R., Leckie, R.S., Veenhuizen, P.T., Schwarzmann, G., Mobius, W., Hoernschemeyer, J., Slot, J.W., Geuze, H.J. and Stoorvogel, W. (2003) Proteomic and biochemical analyses of human B cell-derived exosomes. Potential implications for their function and multivesicular body formation. *J Biol Chem*, **278**, 10963-10972.

110. Mathivanan, S. and Simpson, R.J. (2009) ExoCarta: A compendium of exosomal proteins and RNA. *Proteomics*, **9**, 4997-5000.

111. Valadi, H., Ekstrom, K., Bossios, A., Sjostrand, M., Lee, J.J. and Lotvall, J.O. (2007) Exosome-mediated transfer of mRNAs and microRNAs is a novel mechanism of genetic exchange between cells. *Nature cell biology*, **9**, 654-659.

112. van der Vos, K.E., Balaj, L., Skog, J. and Breakefield, X.O. (2011) Brain tumor microvesicles: insights into intercellular communication in the nervous system. *Cellular and molecular neurobiology*, **31**, 949-959.

113. Lamparski, H.G., Metha-Damani, A., Yao, J.-Y., Patel, S., Hsu, D.-H., Ruegg, C. and Le Pecq, J.-B. (2002) Production and characterization of clinical grade exosomes derived from dendritic cells. *Journal of Immunological Methods*, **270**, 211-226.

114. Portman, O.W., Alexander, M. and Maruffo, C.A. (1967) Composition of subcellular constituents of aortic intima plus inner media isolated by differential and density gradient centrifugation. *Archives of Biochemistry and Biophysics*, **122**, 344-353.

115. Chen, T., Guo, J., Yang, M., Zhu, X. and Cao, X. (2011) Chemokine-Containing Exosomes Are Released from Heat-Stressed Tumor Cells via Lipid Raft-Dependent Pathway and Act as Efficient Tumor Vaccine. *The Journal of Immunology*, **186**, 2219-2228.

116. Johnstone, R.M. and Ahn, J. (1990) A common mechanism may be involved in the selective loss of plasma membrane functions during reticulocyte maturation. *Biomedica biochimica acta*, **49**, S70-75.

117. De la Maza, A. and Parra, J.L. (1994) Vesicle-micelle structural transition of phosphatidylcholine bilayers and Triton X-100. *The Biochemical journal*, **303 (Pt 3)**, 907-914.

118. Kesimer, M., Scull, M., Brighton, B., DeMaria, G., Burns, K., O'Neal, W., Pickles, R.J. and Sheehan, J.K. (2009) Characterization of exosome-like vesicles released

from human tracheobronchial ciliated epithelium: a possible role in innate defense. *The FASEB Journal*, **23**, 1858-1868.

119. Hunter, M.P., Ismail, N., Zhang, X., Aguda, B.D., Lee, E.J., Yu, L., Xiao, T., Schafer, J., Lee, M.L., Schmittgen, T.D. *et al.* (2008) Detection of microRNA expression in human peripheral blood microvesicles. *PLoS One*, **3**, e3694.

120. Lotvall, J. and Valadi, H. (2007) Cell to cell signalling via exosomes through esRNA. *Cell adhesion & migration*, **1**, 156-158.

121. Leung, A.K., Hafez, I.M., Baoukina, S., Belliveau, N.M., Zhigaltsev, I.V., Afshinmanesh, E., Tieleman, D.P., Hansen, C.L., Hope, M.J. and Cullis, P.R. (2012) Lipid Nanoparticles Containing siRNA Synthesized by Microfluidic Mixing Exhibit an Electron-Dense Nanostructured Core. *The journal of physical chemistry. C, Nanomaterials and interfaces*, **116**, 18440-18450.

122. Gibbings, D.J., Ciaudo, C., Erhardt, M. and Voinnet, O. (2009) Multivesicular bodies associate with components of miRNA effector complexes and modulate miRNA activity. *Nature cell biology*, **11**, 1143-1149.

123. Babst, M. (2005) A protein's final ESCRT. *Traffic*, **6**, 2-9.

124. Wollert, T., Yang, D., Ren, X., Lee, H.H., Im, Y.J. and Hurley, J.H. (2009) The ESCRT machinery at a glance. *Journal of cell science*, **122**, 2163-2166.

125. Baietti, M.F., Zhang, Z., Mortier, E., Melchior, A., Degeest, G., Geeraerts, A., Ivarsson, Y., Depoortere, F., Coomans, C., Vermeiren, E. *et al.* (2012) Syndecan-syntenin-ALIX regulates the biogenesis of exosomes. *Nature cell biology*, **14**, 677-685.

126. Hurley, J.H. and Odorizzi, G. (2012) Get on the exosome bus with ALIX. *Nature cell biology*, **14**, 654-655.

127. Sette, P., Jadwin, J.A., Dussupt, V., Bello, N.F. and Bouamr, F. (2010) The ESCRT-associated protein Alix recruits the ubiquitin ligase Nedd4-1 to facilitate HIV-1 release through the LYPXnL L domain motif. *Journal of virology*, **84**, 8181-8192.

128. Quah, B.J. and O'Neill, H.C. (2005) The immunogenicity of dendritic cell-derived exosomes. *Blood cells, molecules & diseases*, **35**, 94-110.

129. Ray, T. and Pattnaik, P. (2009) Improving liposome integrity and easing bottlenecks to production. *Pharmaceutical Technology Europe*, **21**, 24-28.

130. Khan, S., Jutzy, J.M., Aspe, J.R., McGregor, D.W., Neidigh, J.W. and Wall, N.R. (2011) Survivin is released from cancer cells via exosomes. *Apoptosis : an international journal on programmed cell death*, **16**, 1-12.

131. Morelli, A.E., Larregina, A.T., Shufesky, W.J., Sullivan, M.L., Stolz, D.B., Papworth, G.D., Zahorchak, A.F., Logar, A.J., Wang, Z., Watkins, S.C. *et al.* (2004) Endocytosis, intracellular sorting, and processing of exosomes by dendritic cells. *Blood*, **104**, 3257-3266.

132. Thery, C., Boussac, M., Veron, P., Ricciardi-Castagnoli, P., Raposo, G., Garin, J. and Amigorena, S. (2001) Proteomic analysis of dendritic cell-derived exosomes: a secreted subcellular compartment distinct from apoptotic vesicles. *J Immunol*, **166**, 7309-7318.

133. Thery, C., Regnault, A., Garin, J., Wolfers, J., Zitvogel, L., Ricciardi-Castagnoli, P., Raposo, G. and Amigorena, S. (1999) Molecular characterization of dendritic cell-derived exosomes. Selective accumulation of the heat shock protein hsc73. *The Journal of cell biology*, **147**, 599-610.

134. Jansen, B., Sama, I., Eleveld-Trancikova, D., van Hout-Kuijer, M., Jansen, J., Huynen, M. and Adema, G. (2011) MicroRNA genes preferentially expressed in dendritic cells contain sites for conserved transcription factor binding motifs in their promoters. *BMC Genomics*, **12**, 330.

135. Dalwadi, G. and Sunderland, V.B. (2007) Purification of PEGylated nanoparticles using tangential flow filtration (TFF). *Drug development and industrial pharmacy*, **33**, 1030-1039.

136. Dalwadi, G., Benson, H.A. and Chen, Y. (2005) Comparison of diafiltration and tangential flow filtration for purification of nanoparticle suspensions. *Pharm Res*, **22**, 2152-2162.

137. da Silveira, J.C., Veeramachaneni, D.N.R., Winger, Q.A., Carnevale, E.M. and Bouma, G.J. (2012) Cell-Secreted Vesicles in Equine Ovarian Follicular Fluid Contain miRNAs and Proteins: A Possible New Form of Cell Communication Within the Ovarian Follicle. *Biology of Reproduction*, **86**, 71, 71-10.

138. Gould, S.J., Booth, A.M. and Hildreth, J.E. (2003) The Trojan exosome hypothesis. *Proc Natl Acad Sci U S A*, **100**, 10592-10597.

139. Nguyen, D.G., Booth, A., Gould, S.J. and Hildreth, J.E. (2003) Evidence that HIV budding in primary macrophages occurs through the exosome release pathway. *J Biol Chem*, **278**, 52347-52354.

140. Pegtel, D.M., van de Garde, M.D. and Middeldorp, J.M. (2011) Viral miRNAs exploiting the endosomal-exosomal pathway for intercellular cross-talk and immune evasion. *Biochimica et biophysica acta*, **1809**, 715-721.

141. Krishnamoorthy, L., Bess, J.W., Jr., Preston, A.B., Nagashima, K. and Mahal, L.K. (2009) HIV-1 and microvesicles from T cells share a common glycome, arguing for a common origin. *Nature chemical biology*, **5**, 244-250.

142. Landazuri, N. and Le Doux, J.M. (2006) Complexation with chondroitin sulfate C and Polybrene rapidly purifies retrovirus from inhibitors of transduction and substantially enhances gene transfer. *Biotechnology and bioengineering*, **93**, 146-158.

143. Uchida, E., Kogi, M., Oshizawa, T., Furuta, B., Satoh, K., Iwata, A., Murata, M., Hikata, M. and Yamaguchi, T. (2007) Optimization of the virus concentration method using polyethyleneimine-conjugated magnetic beads and its application to the detection of human hepatitis A, B and C viruses. *Journal of virological methods*, **143**, 95-103.

144. von Harpe, A., Petersen, H., Li, Y. and Kissel, T. (2000) Characterization of commercially available and synthesized polyethylenimines for gene delivery. *Journal of Controlled Release*, **69**, 309-322.

145. Arroyo, J.D., Chevillet, J.R., Kroh, E.M., Ruf, I.K., Pritchard, C.C., Gibson, D.F., Mitchell, P.S., Bennett, C.F., Pogosova-Agadjanyan, E.L., Stirewalt, D.L. *et al.* (2011) Argonaute2 complexes carry a population of circulating microRNAs independent of vesicles in human plasma. *Proc Natl Acad Sci U S A*, **108**, 5003-5008.

146. Turchinovich, A., Weiz, L., Langheinz, A. and Burwinkel, B. (2011) Characterization of extracellular circulating microRNA. *Nucleic Acids Res*, **39**, 7223-7233.

147. Graner, M.W., Alzate, O., Dechkovskaia, A.M., Keene, J.D., Sampson, J.H., Mitchell, D.A. and Bigner, D.D. (2009) Proteomic and immunologic analyses of brain tumor exosomes. *The FASEB Journal*, **23**, 1541-1557.

148. Silverman, J.M., Clos, J., de'Oliveira, C.C., Shirvani, O., Fang, Y., Wang, C., Foster, L.J. and Reiner, N.E. (2010) An exosome-based secretion pathway is responsible for protein export from Leishmania and communication with macrophages. *Journal of cell science*, **123**, 842-852.

149. Katsuda, T., Tsuchiya, R., Kosaka, N., Yoshioka, Y., Takagaki, K., Oki, K., Takeshita, F., Sakai, Y., Kuroda, M. and Ochiya, T. (2013) Human adipose tissue-

derived mesenchymal stem cells secrete functional neprilysin-bound exosomes. *Sci. Rep.*, **3**.

150. Soo, C.Y., Song, Y., Zheng, Y., Campbell, E.C., Riches, A.C., Gunn-Moore, F. and Powis, S.J. (2012) Nanoparticle tracking analysis monitors microvesicle and exosome secretion from immune cells. *Immunology*, **136**, 192-197.

151. Raposo, G. and Stoorvogel, W. (2013) Extracellular vesicles: exosomes, microvesicles, and friends. *The Journal of cell biology*, **200**, 373-383.

152. Thery, C., Amigorena, S., Raposo, G. and Clayton, A. (2006) Isolation and characterization of exosomes from cell culture supernatants and biological fluids. *Current protocols in cell biology / editorial board, Juan S. Bonifacino ... [et al.]*, **Chapter 3**, Unit 3 22.

153. Chen, T.S., Lai, R.C., Lee, M.M., Choo, A.B., Lee, C.N. and Lim, S.K. (2010) Mesenchymal stem cell secretes microparticles enriched in pre-microRNAs. *Nucleic Acids Res*, **38**, 215-224.

154. Collino, F., Deregibus, M.C., Bruno, S., Sterpone, L., Aghemo, G., Viltono, L., Tetta, C. and Camussi, G. (2010) Microvesicles derived from adult human bone marrow and tissue specific mesenchymal stem cells shuttle selected pattern of miRNAs. *PLoS One*, **5**, e11803.

155. Esser, J., Gehrmann, U., D'Alexandri, F.L., Hidalgo-Estevez, A.M., Wheelock, C.E., Scheynius, A., Gabrielsson, S. and Radmark, O. (2010) Exosomes from human macrophages and dendritic cells contain enzymes for leukotriene biosynthesis and promote granulocyte migration. *The Journal of allergy and clinical immunology*, **126**, 1032-1040, 1040 e1031-1034.

156. Hong, B.S., Cho, J.H., Kim, H., Choi, E.J., Rho, S., Kim, J., Kim, J.H., Choi, D.S., Kim, Y.K., Hwang, D. *et al.* (2009) Colorectal cancer cell-derived microvesicles are enriched in cell cycle-related mRNAs that promote proliferation of endothelial cells. *BMC Genomics*, **10**, 556.

157. Merchant, M.L., Powell, D.W., Wilkey, D.W., Cummins, T.D., Deegens, J.K., Rood, I.M., McAfee, K.J., Fleischer, C., Klein, E. and Klein, J.B. (2010) Microfiltration isolation of human urinary exosomes for characterization by MS. *Proteomics. Clinical applications*, **4**, 84-96.

158. Zumaquero, E., Munoz, P., Cobo, M., Lucena, G., Pavon, E.J., Martin, A., Navarro, P., Garcia-Perez, A., Ariza-Veguillas, A., Malavasi, F. *et al.* (2010) Exosomes from human lymphoblastoid B cells express enzymatically active CD38 that is associated with signaling complexes containing CD81, Hsc-70 and Lyn. *Experimental cell research*, **316**, 2692-2706.

159. Bhatnagar, S., Shinagawa, K., Castellino, F.J. and Schorey, J.S. (2007) Exosomes released from macrophages infected with intracellular pathogens stimulate a proinflammatory response in vitro and in vivo. *Blood*, **110**, 3234-3244.

160. Kim, S.H., Bianco, N., Menon, R., Lechman, E.R., Shufesky, W.J., Morelli, A.E. and Robbins, P.D. (2006) Exosomes derived from genetically modified DC expressing FasL are anti-inflammatory and immunosuppressive. *Mol Ther*, **13**, 289-300.

161. Kim, S.H., Lechman, E.R., Bianco, N., Menon, R., Keravala, A., Nash, J., Mi, Z., Watkins, S.C., Gambotto, A. and Robbins, P.D. (2005) Exosomes derived from IL-10-treated dendritic cells can suppress inflammation and collagen-induced arthritis. *J Immunol*, **174**, 6440-6448.

162. Raposo, G., Nijman, H.W., Stoorvogel, W., Liejendekker, R., Harding, C.V., Melief, C.J. and Geuze, H.J. (1996) B lymphocytes secrete antigen-presenting vesicles. *J Exp Med*, **183**, 1161-1172.

96

163. Lenassi, M., Cagney, G., Liao, M., Vaupotic, T., Bartholomeeusen, K., Cheng, Y., Krogan, N.J., Plemenitas, A. and Peterlin, B.M. (2010) HIV Nef is secreted in exosomes and triggers apoptosis in bystander CD4+ T cells. *Traffic*, **11**, 110-122.

164. Sarkar, A., Mitra, S., Mehta, S., Raices, R. and Wewers, M.D. (2009) Monocyte derived microvesicles deliver a cell death message via encapsulated caspase-1. *PLoS One*, **4**, e7140.

165. Chaput, N., Taieb, J., Andre, F. and Zitvogel, L. (2005) The potential of exosomes in immunotherapy. *Expert opinion on biological therapy*, **5**, 737-747.

166. Chaput, N., Taieb, J., Schartz, N., Flament, C., Novault, S., Andre, F. and Zitvogel, L. (2005) The potential of exosomes in immunotherapy of cancer. *Blood cells, molecules & diseases*, **35**, 111-115.

167. Dai, S., Wei, D., Wu, Z., Zhou, X., Wei, X., Huang, H. and Li, G. (2008) Phase I clinical trial of autologous ascites-derived exosomes combined with GM-CSF for colorectal cancer. *Mol Ther*, **16**, 782-790.

168. Escudier, B., Dorval, T., Chaput, N., Andre, F., Caby, M.P., Novault, S., Flament, C., Leboulaire, C., Borg, C., Amigorena, S. *et al.* (2005) Vaccination of metastatic melanoma patients with autologous dendritic cell (DC) derived-exosomes: results of thefirst phase I clinical trial. *Journal of translational medicine*, **3**, 10.

169. Viaud, S., Thery, C., Ploix, S., Tursz, T., Lapierre, V., Lantz, O., Zitvogel, L. and Chaput, N. (2010) Dendritic cell-derived exosomes for cancer immunotherapy: what's next? *Cancer Res*, **70**, 1281-1285.

170. Duijvesz, D., Luider, T., Bangma, C.H. and Jenster, G. (2011) Exosomes as biomarker treasure chests for prostate cancer. *European urology*, **59**, 823-831.

171. Hoorn, E.J., Pisitkun, T., Zietse, R., Gross, P., Frokiaer, J., Wang, N.S., Gonzales, P.A., Star, R.A. and Knepper, M.A. (2005) Prospects for urinary proteomics: exosomes as a source of urinary biomarkers. *Nephrology (Carlton)*, **10**, 283-290.

172. Li, Y., Zhang, Y., Qiu, F. and Qiu, Z. (2011) Proteomic identification of exosomal LRG1: a potential urinary biomarker for detecting NSCLC. *Electrophoresis*, **32**, 1976-1983.

173. Miranda, K.C., Bond, D.T., McKee, M., Skog, J., Paunescu, T.G., Da Silva, N., Brown, D. and Russo, L.M. (2010) Nucleic acids within urinary exosomes/microvesicles are potential biomarkers for renal disease. *Kidney international*, **78**, 191-199.

174. Masyuk, A.I., Masyuk, T.V. and LaRusso, N.F. Exosomes in the Pathogenesis, Diagnostics and Therapeutics of Liver Diseases. *Journal of Hepatology*.

175. Horn, T. and Urdea, M.S. (1986) A chemical 5'-phosphorylation of oligodeoxyribonucleotides. *DNA*, **5**, 421-426.

176. Martin, P. (1995) A new access to 2′-O-Alkylated Ribonucleosides and properties of 2'-O-Alkylated Oligoribonucleotides. *Helvetica Chimica Acta*, **78**, 486-504.

IX.   CURRICULUM VITAE
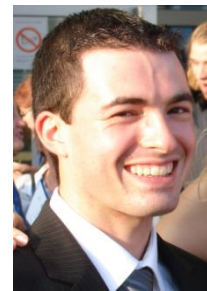
Boos Julien Alfred Jean-Paul
80, rue de Mulhouse
68300 Saint-Louis
FRANCE
Home Phone: +33 (0)3 89 69 97 60
Cell phone: +33 (0)6 13 63 32 13
e-mail: julien.boos@gmail.com, julien.boos@novartis.com

Education

2010-Present	**University of Basel** PhD in cellular biology at the Philosophisch-Naturwissen-schaftlischen Fakultät of the University of Basel
2006-2009	**University of Strasbourg (UdS), Strasbourg, France** • Engineer diploma in biotechnology from the **ESBS : Ecole Supérieure de Biotechnologie de Strasbourg** • Master's degree in Structural Genomics and Bioinformatics
2004-2006	**Lycée Jean Rostand, Strasbourg** Two years CPGE: Classes Préparatoires aux Grandes Ecoles (preparatory classes for engineering schools)
2001-2004	**Lycée Général Leclerc, Saverne, France** Three years to obtain a general Baccalauréat specialised in biology

Experience and skills

2009-Present	**RNAi Therapeutics unit in Novartis Pharma AG, Basel, Switzerland** PhD student ***Mentor:*** Dr Iwan Beuvink ***Subject:*** Development of a novel delivery method for therapeutics oligonucleotides and *in vivo* biodistribution analysis by using Whole-Body Scanning PCR • Mammalian cell culture • Fractionation techniques: differential ultracentrifugation, preparation of linear sucrose gradients • Particle size separation techniques: ultrafiltration, TFF • Development of RT-qPCR based assays for the detection of miRNAs and heavily modified oligonucleotides • Biochemistry: ELISA, Western blotting, LC-MS

samples preparation
- Successful qPCR technology transfer
- Development of a qPCR-based phage quantification assay
- Molecular biology and mutagenesis

January-August 2009

RNAi Therapeutics unit in Novartis Pharam AG, Basel, Switzerland
Eight months internship in Dr Beuvink's lab
Subject: Development of tools for high-throughput transfection, sample preparation and gene expression analysis
- Handling of mammalian cell culture
- siRNA transfections
- RT-qPCR downstream analysis

November 2008

IGBMC: Institut de Génétique et de Biologie Moléculaire et Cellulaire, Illkirch
Four weeks internship in Dr Hanauer's team, working on Coffin-Lowry syndrome
Subject: Validation of Affymetrix chips results by RT-qPCR, to identify genes differentially expressed in a mouse model for Coffin-Lowry syndrome
- Mouse dissection, RNA extraction
- RT-qPCR analysis

June 2008

ESBS, Illkirch, France
Three weeks bioinformatics project:
Subject: Modelling of the CCR5 receptor, responsible for HIV-entry in cells
- Protein sequence alignments and corrections
- Generation of 3D-models using Modeller
- Models evaluation on VMD

July 2007

IGBMC
Five weeks internship in Brigitte Kieffer's team specialized on neurobiology
Subject: Identification of an antibody specific to the delta opioid receptor
- Mouse dissection and brain sectioning
- Immunohistochemistry

September 2006-December 2008

Teacher in mathematics, biology, physics and chemistry in **Synergie-School**

Complementary skills

Basic knowledge in the use of softwares

Modeller
Jalview

VMD
                     Bioinformatics platforms
                     Protein databases
                     RT-qPCR analysis softwares: SDS1.3, SDS2.2, Viia7
                     analysis software
                     Basic office suite: Word, Excel, Power Point
                     Corel Draw
                     TissueView

Languages   French (native)
                     German (fluent)
                     English (fluent)

Other diplomas   **2008 : TOEIC,** obtained with 925 points out of 990
                     2004 : ABIBAC, composed of the french baccalauréat and
                     the german Abitur
                     2003 : ZMP (Zentrale MittelstufenPrüfung) delivered by the
                     Goethe Institut

Publications and posters

June 2013   **Manuscript published on June 13th 2013 in Nucleic Acids
                     Research:**
                     Boos JA, Kirk D., Dattler A., Piccolotto ML., Zuercher W., Gfeller S.,
                     Neuner P., Christensen J., Wishart W., Beverly M., Litherland K., Swart PJ.,
                     Faller T., Beyerbach A., Morrissey D., Hunziker J., Beuvink I.
                     ***Whole Body Scanning PCR; a highly sensitive method to
                     study the biodistribution of mRNAs, noncoding RNAs and
                     therapeutic oligonucleotides***
                     http://nar.oxfordjournals.org/content/early/2013/06/13/nar.gkt51
                     5.long

May 2012   **Poster at the 2012 Small RNA Microsymposium:**
                     Julien A Boos, David W Kirk, Mari-Luz Piccolotto, Werner Zuercher,
                     Sandro Gfeller, Philippe Neuner, André Dattler, William L Wishart, Fabian
                     Von Arx, Michael Beverly, Jesper Christensen, Karine Litherland, Esther
                     van de Kerkhof, Pieter J Swart, Thomas Faller, Armin Beyerbach, David
                     Morrissey, Juerg Hunziker, Iwan Beuvink
                     ***Whole-body scanning PCR; a highly sensitive method to
                     study the biodistribution of mRNAs, noncoding RNAs and
                     therapeutic oligonucleotides***

September 2011   **Poster at the annual FMI retreat:**
                     Julien A Boos, Iwan Beuvink
                     Purification, biomolecular characterization, and in vivo
                     biodistribution of exosomes

100

# X.	Appendix I: Published manuscript

XI. Appendix II: Proteins identified in Polybrene/CSC precipitated cell lysate

The protein list will begin on the following page.